

Structural, Spectroscopic, and Reactivity Models for the Manganese Catalases

Amy J. Wu, James E. Penner-Hahn, and Vincent L. Pecoraro*

Willard H. Dow Laboratories, Department of Chemistry, University of Michigan, Ann Arbor, Michigan 48109-1055

Received July 8, 2003

Contents

1. Introduction	903
2. Catalases in Biology	903
2.1. Oxidation States	904
2.2. Reactivity	905
2.3. Structures	905
2.4. Spectroscopy	906
2.4.1. Magnetic Resonance	906
2.4.2. Electronic Spectroscopy	907
2.4.3. Magnetism	907
3. Structural Models	907
3.1. Models with Single Oxo/Hydroxo/Alkoxo Bridges	908
3.2. Models with Bis- μ -Oxo/Hydroxo/Alkoxo Bridges	909
3.3. Carboxylate-Bridged Complexes	910
3.4. Asymmetric Ligand Complexes	913
4. Spectroscopic Models	914
4.1. X-ray Absorption Spectroscopies	914
4.2. Magnetic Studies	916
4.3. Absorption Spectroscopy	920
4.4. EPR Spectroscopy	921
5. Reactivity Models	925
5.1. Early Reactivity Models	926
5.2. Tri- and Tetranuclear Models	927
5.3. Dinuclear Models	928
6. Future Directions for Modeling the Manganese Catalases	933
6.1. Small-Molecule Models	933
6.2. Peptidic Models	933
6.3. Concluding Remarks	934
7. Acknowledgments	935
8. Glossary of Abbreviations	935
9. Note Added after ASAP Posting	935
10. References	935

1. Introduction

Given the well-defined enzymology of the manganese catalases and recent advances in the structural biology of these proteins, this is an excellent area for corroborative modeling of the active site and electronic structures of these enzymes. Additionally, there are many small molecules that display the

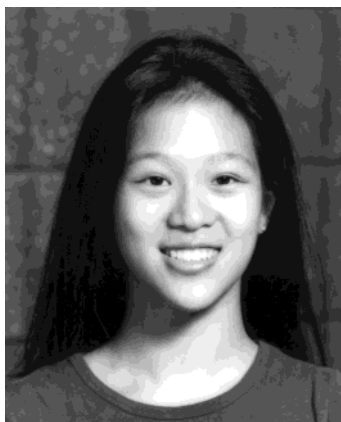
same catalytic activity as this enzyme class with rates that are approaching those reported for catalytic enzyme activity. There have been numerous excellent reviews^{1–5} that focus on the catalase enzymes themselves or speculative models (from structure to reactivity). We will focus in this review on the most relevant structural, spectroscopic, and catalytic models.

The potential relationship between the manganese catalases and the oxygen-evolving complex (OEC) of Photosystem II was an early driving force for the investigation of Mn catalase biomimetic chemistry as it was felt that the Mn catalases might provide insight into the more complex chemistry of water oxidation ($2\text{H}_2\text{O} \rightarrow \text{O}_2 + 4\text{H}^+ + 4\text{e}^-$). It is now realized that the Mn catalases are structurally more similar to Mn ribonucleotide reductases or Mn arginase (both enzymes containing two Mn ions) than the 3 + 1 organization of the OEC.⁶ Furthermore, there have been contradictory claims as to whether water oxidation occurs through a peroxide intermediate or occurs in a single, four-electron step. Thus, it is our intent to emphasize the modeling chemistry as it relates solely to manganese catalase chemistry.

2. Catalases in Biology

Hydrogen peroxide is produced in aerobes as a result of the partial reduction of O_2 . Because of the toxicity of H_2O_2 , aerobic organisms have had to develop methods for its decomposition. Most organisms utilize a heme-containing catalase to catalyze the disproportionation of H_2O_2 to H_2O and O_2 . One of the characteristics of heme catalases is that they are inhibited by low concentrations of azide and cyanide. However, it has been known since the 1960s that some catalases are insensitive to azide and cyanide,^{7–9} suggesting that they might be non-heme enzymes, and this was confirmed in 1983, with the isolation and purification of a Mn-containing catalase from *Lactobacillus plantarum*.¹⁰ Several Mn-containing catalases have now been purified and at least partially characterized, including enzymes from *Thermus thermophilus* HB-8¹¹ and *Thermoleophilum album* NM,^{12,13} *Thermus* sp. YS 8-13,¹⁴ *Salmonella enterica*,¹⁵ and most recently from the hyperthermophilic archaeon, *Pyrobaculum calidifontis* VA1.¹⁶ Sequence alignments suggest that several other organisms may contain Mn catalase. Although non-heme catalases were referred to as “pseudocatalase” in some of the early literature, Mn catalase (MnCat) is a more appropriate name,⁹ since there is nothing

* To whom correspondence should be addressed. Phone: (734) 763-1519. Fax: (734) 936-7628. E-mail: vlpec@umich.edu.



Amy Wu was born in Memphis, TN, in 1978. She received her B.A. in chemistry from the Johns Hopkins University in 2000 while working in the research group of Dr. David P. Goldberg studying biomimetic models of peptide deformylase. She attends the University of Michigan, Ann Arbor, where, as a fellow in molecular biophysics, she has completed her M.S. degree. Under the tutelage of Dr. Vincent L. Pecoraro, she is currently working toward her Ph.D. and is interested in exploring the mechanisms of manganese redox enzymes via studies of biomimetic model complexes.



James E. Penner-Hahn received a B.S. degree in chemistry from Purdue University in 1979 and a Ph.D. degree from Stanford University in 1984. At Stanford, he worked on early applications of X-ray absorption spectroscopy in biological systems. After receiving his Ph.D., he joined the staff of the Stanford Synchrotron Radiation Laboratory, where he worked for two years with Professors Keith Hodgson and Edward Solomon on polarized X-ray absorption spectroscopy. He joined the faculty of the Chemistry Department of the University of Michigan in 1985, where he is presently Professor of Chemistry and Chair of the Biophysics Research Division. His research interests focus on zinc-containing enzymes, particularly those involved in catalyzing alkyl-transfer reactions, manganese redox enzymes involved in oxygen metabolism, and on the development of new methods for using synchrotron radiation to answer biophysical questions.

“false” about their catalase activity. The Mn catalases represent a new class of biological site, and thus have provided a valuable framework for testing the ability of bioinorganic chemistry to mimic an important biological reaction. Mn catalases are relatively well characterized spectroscopically, and in recent years several MnCat crystal structures have been determined. This makes MnCat an especially attractive bioinorganic target, since one can test the ability of model compounds to mimic not only reactivity but also the spectra and the structure of the enzyme active site. This review summarizes the current state of MnCat modeling, beginning with a review of the key enzymatic properties to be modeled.

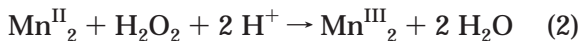
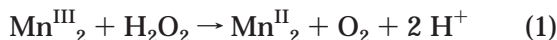


Vincent L. Pecoraro was born in Freeport, NY, on August 31, 1956. His family moved to California when he was five years old, and he completed kindergarten through his Ph.D. in that state (University of California, Los Angeles, B.S. biochemistry, 1977; University of California, Berkeley, Ph.D. with Ken Raymond, 1981). Dr. Pecoraro moved to the Midwest in 1981 as an NIH Postdoctoral Fellow with W. W. Cleland. In 1984, he joined the faculty in the Chemistry Department at the University of Michigan, Ann Arbor, and was promoted to Professor in 1992. His research has focused on bioinorganic chemistry and inorganic molecular recognition studies. He has worked for many years on the biological chemistry of manganese, especially dealing with Photosystem II and the manganese catalases. He has published extensively on vanadium coordination chemistry related to the vanadium haloperoxidases and on spectroscopic methods for studying vanadyl protein substitution. More recently, his group has focused on the de novo design of peptides capable of binding heavy metals such as Hg(II) and Cd(II). In 1989, his group first described the molecular class of metallamacrocycles that are known as metallacrowns. He has received numerous awards, including the G.D. Searle Biomedical Research Scholar, Alfred P. Sloan Fellow, and the Alexander von Humboldt Award for Senior US Scientists, and was elected a Fellow of the AAAS. He has served on numerous study sections at NIH, the editorial advisory board for ACS Books, the Advisory Board for ACS/PRF, and as an Associate Editor of *Inorganic Chemistry* since 1994. Dr. Pecoraro married Peggy Carver, a Professor in the College of Pharmacy at the University of Michigan, in 1992. They enjoy traveling, eating, and basically having a good time.

2.1. Oxidation States

Although the disproportionation of hydrogen peroxide is thermodynamically favorable, rapid reaction requires a two-electron catalyst. For heme catalases, this is accomplished by cycling between Fe^{III} and an Fe^{IV} porphyrin π -cation, and occurs at a very high rate. Manganese catalases have a turnover number of $\sim 2.0 \times 10^5 \text{ s}^{-1}$,^{17,18} approximately 1% of that for heme catalase, but still quite fast. With two Mn ions, each of which can, at least in principle, operate between Mn^{II} and Mn^{IV}, there are five possible oxidation states for MnCat. A combination of EPR, UV–visible spectroscopy, and X-ray absorption spectroscopy has shown that MnCat can exist in at least four of these: a reduced Mn^{II}₂ state, a mixed-valence Mn^{II}Mn^{III} state, an oxidized Mn^{III}₂ state, and a superoxidized Mn^{III}Mn^{IV} state.^{19,20} There is no evidence to date for a Mn^{IV}₂ state. With four known oxidation states, two different two-electron catalytic cycles are possible. However, addition of NH₂OH + H₂O₂ converts the as-isolated enzyme, which contains a mixture of all four oxidation states, to the superoxidized state, with complete loss of activity.^{21,22} The lack of reactivity for the superoxidized enzyme eliminates the possibility of a Mn^{II}Mn^{III} \leftrightarrow Mn^{III}Mn^{IV} catalytic cycle. Spectroscopic studies have shown that

H₂O₂ can both oxidize the reduced enzyme and reduce the oxidized enzyme.^{19,23} This is consistent with these being the catalytically active oxidation states (eqs 1 and 2), although it does not completely rule out the possibility of a Mn^{III}₂ ↔ Mn^{IV}₂ catalytic cycle. The



mixed-valence Mn^{II}Mn^{III} oxidation state is the least well characterized, and the *L. plantarum* enzyme has not been shown to form a stable mixed-valence Mn^{II}-Mn^{III} form. On the basis of model studies,²⁴ it has been suggested that the Mn^{II}Mn^{III} derivative is formed by one-electron reduction of the oxidized enzyme by NH₂OH and is then oxidized by H₂O₂ to form in the inactive, superoxidized Mn^{III}Mn^{IV}enzyme.

2.2. Reactivity

Activity of the *L. plantarum* and the *T. thermophilus* enzymes is nearly independent of pH from 7 to 10,^{18,22} while the *T. album* shows a narrower activity profile, with greatest activity between pH 8.0 and 9.0.¹² There are as yet no examples of intermediates in which a Mn-peroxo complex has been trapped. In lieu of such an intermediate, a great deal of effort has been devoted to studying anion binding as a surrogate for substrate binding.^{22,25,26} A variety of anions, including halides, azide, and cyanide, inhibit the enzyme. The last two are a bit surprising, since MnCat was originally identified on the basis of its azide- and cyanide-independent catalase activity. However, this simply reflects the much weaker inhibition by azide and cyanide than is seen for heme enzymes. In contrast to the pH-independent reactivity, anion binding typically shows strong pH dependence, increasing at lower pH.

For *L. plantarum* MnCat, azide inhibition is competitive,¹⁸ with $K_i = 80 \pm 4$ mM at pH 7, falling to ~5 mM at pH 5.5. Halides are also effective inhibitors of MnCat, especially at lower pH, and turnover in the presence of either fluoride or chloride traps the enzyme in the reduced state.²⁷ Two fluoride ions bind per Mn^{II}₂ active site ($K_d = 12$ and 140 μM, pH 5.5), with one H⁺ taken up per F⁻ bound.²⁸ For the oxidized enzyme, only a single fluoride binding constant was seen, and this was weaker ($K_d = 0.5$ mM, pH 5.5) than either of the binding constants for the reduced enzyme. This is not consistent with typical anion-Mn interactions, which normally increase in strength with increasing oxidation state, and may reflect a structural change such that tight anion binding is blocked for the oxidized enzyme. The higher affinity of the reduced enzyme for fluoride may explain the observation that it is the reduced enzyme that is trapped during turnover with fluoride.

2.3. Structures

Several crystal structures are now available for MnCat, including two at atomic resolution,^{29–31} these show that the Mn catalase monomer consists of a bundle of four antiparallel α-helices, with the Mn site

buried in the center of the bundle. This is a structural motif similar to that seen in a number of di-iron enzymes,³² with the first and third helices providing a glutamate or aspartate ligand, and the second and fourth containing a HXXE site, thus providing a total of two histidines and four carboxylates that could coordinate to Mn. In contrast with di-iron enzymes, one of the carboxylates in MnCat is not involved in Mn binding, with ligands coming for the two histidines, one bound to each Mn, and the other three carboxylates. For *T. thermophilus* MnCat, 1-Å crystal structures are available for the reduced and the reduced + chloride forms of the protein.²⁹ Although the structures were solved to atomic resolution, interpretation is complicated by the fact that the asymmetric unit contains two independent four-helix bundles, and each of these has two different conformations for the Mn cluster. The two conformations are present in approximately equal amounts for the native enzyme, thus giving four independent Mn cluster structures. The two conformations differ in the ligation of glutamate 36, which is bidentate chelating in one conformation and monodentate in the other (with the vacant coordination site filled by water). There is one five-coordinate Mn site and one six-coordinate Mn site, although, surprisingly, the Mn–ligand bond lengths at the five-coordinate site are slightly longer than those for three of the four six-coordinate sites (2.18 vs 2.14 Å). This is in contrast with the decrease in distance that is usually seen when coordination number decreases. The two Mn's are bridged by two solvent molecules and a bidentate carboxylate, with the bridging solvent atoms displaced by approximately 0.1 Å toward the six-coordinate Mn (Mn–O distances of 2.05 vs 2.15 Å). When chloride is added, the chlorides replace both bridging water molecules, with a Mn–Cl distance of 2.55 Å. The Mn–Mn separation is 3.13 Å in the native protein, increasing to 3.30 Å when chloride binds.

Three crystal structures have been reported for oxidized MnCat, two for the wild-type *L. plantarum* enzyme (native and with azide added) and one for a Y42F mutant of *L. plantarum* MnCat.^{31,33} These are at somewhat worse resolution (1.3–1.4 Å) except for the wild-type native *L. plantarum*, which was measured at room temperature and, perhaps for this reason, diffracted only to 1.8 Å. The core structure is very similar to that reported for reduced *T. thermophilus* catalase, although only the conformation with a monodentate glutamate + a third solvent molecule (conformation 2 for the reduced enzyme) is seen and Mn2 (the five-coordinate Mn in the reduced structures) has become six-coordinate in the oxidized enzyme, with conversion of a glutamate from monodentate to bidentate. Azide binds with displacement of a terminal water, but with little other change in structure. Surprisingly, the bond lengths for the two Mn's in the oxidized MnCat structures are quite different (average = 2.05 vs 2.21 Å). This would be consistent with partial X-ray photoreduction of the cluster. Although the crystals retained their pink color at the end of the measurements, photoreduction should be quite facile,²⁷ particularly for the native

structure measured at room temperature. The bridging solvent molecules for oxidized MnCat are modeled as one oxo and one hydroxo ligand. This would explain the strong Mn–Mn exchange coupling that is found in some studies (see below) but seems inconsistent with the long (1.9–2.1 Å) Mn–O distances that are seen, since Mn–oxo distances tend to be closer to 1.7 Å. The Mn–Mn distances are 3.03 Å in the native enzyme and 3.19 Å in the azide derivative, very similar to those found for the reduced enzyme.

The crystal structure for the oxidized form of the Y42F mutant of *L. plantarum* catalase³⁴ has Mn–ligand distances that are more typical of those seen in Mn^{III} model complexes, although this structure also suffers from the presence of two different Mn conformations. The Mn core structure is similar to that found for the wild-type oxidized site, with the exception that one of the bridging solvent molecules has been converted to a terminal ligand, leaving a five- and a six-coordinate Mn (or a four- and a six-coordinate Mn in the second conformation) and lengthening the Mn–Mn distance to 3.42 Å.

Given the presence of two conformations in several of the structures, the rather short Mn–ligand distances found for reduced MnCat, the unusually long Mn–ligand distances that are seen for one of the two Mn's in oxidized MnCat, and the possibility of radiation damage, it seems possible that these crystals may contain a mixture of Mn oxidation states. If so, this could make it difficult to determine accurate metric parameters for the Mn site from crystallography. Fortunately, both EPR and EXAFS spectroscopies provide complementary structural parameters. From the magnetic dipole interaction between the Mn, D_{dip} , the Mn–Mn distances in reduced *T. thermophilus* MnCat have been estimated to be 3.31, 3.51, 3.59, and 3.63–3.70 Å for the fluoride-, chloride-, phosphate-, and cyanide-bound derivatives, respectively, with a longer distance (≥ 3.7 Å) for the anion-free enzyme.^{35,36} Similar measurements for reduced *L. plantarum* MnCat gave an apparent Mn–Mn distance of 3.4 Å,²⁸ 0.2 Å shorter than for *T. thermophilus*. It is not clear whether this difference reflects differences in data analysis (the *L. plantarum* study took more careful account of zero-field splitting) or reflects a genuine difference between the proteins. All of the EPR-derived Mn–Mn^{35,37} distances are longer than the Mn–Mn distances that were found crystallographically.

The EXAFS data for reduced *L. plantarum* MnCat show two resolvable shells of nearest-neighbor N/O ligands at 2.11 and 2.27 Å.³⁸ These distances are typical of Mn^{II} with mixed oxygen/nitrogen ligation, but are somewhat shorter than the average Mn–ligand distance seen crystallographically. The EXAFS data also show evidence for outer-shell carbon scattering from the histidine imidazoles and from a Mn···Mn feature at 3.54 Å. This apparent Mn–Mn distance derived from EXAFS is close to that deduced from the EPR, but significantly longer than that found crystallographically. EXAFS data have also been measured for superoxidized MnCat, a form of the enzyme that has not been studied crystallo-

graphically. These data³⁹ also showed two resolvable shells of nearest-neighbor scattering, in this case at 1.82 and 2.08 Å, together with an intense Mn–Mn feature at 2.70 Å, consistent with a Mn^{III}(μ -oxo)₂Mn^{IV} structure.

2.4. Spectroscopy

2.4.1. Magnetic Resonance

EPR signals are seen for all four known oxidation states of MnCat, although the oxidized enzyme shows only an EPR signal at very low field.³³ In the absence of added anions, the EPR signal of reduced MnCat is extremely broad and weak.²² In the presence of a variety of anions, the signal shows four broad transitions, typical of a weakly coupled Mn^{II}₂ dimer. The intensity of this signal increases as the temperature increases, with a maximum at ~ 50 K, indicating that the signal arises from an excited spin state of an antiferromagnetically coupled Mn^{II}₂ dimer. The Heisenberg spin Hamiltonian ($H = -2JS_1 \cdot S_2$) allows for the exchange coupling, J , of *T. thermophilus* MnCat to be estimated²² at -14.4 cm^{-1} , assuming that only the $S = 1$ state contributes to the signal, or -5.6 cm^{-1} if contributions from the $S = 2$ state were included.³⁵ Analogous measurements for the *L. plantarum* enzyme, including spectra measured in both parallel and perpendicular polarization, gave a much stronger exchange interaction ($J = -20 \text{ cm}^{-1}$).²⁸ When two fluorides bind to the *L. plantarum* MnCat active site, there is a 4-fold decrease in J , to $\sim -5.25 \text{ cm}^{-1}$. This decrease, together with the stoichiometry of two fluorides/Mn dimer, led to the suggestion that reduced MnCat has a (μ -OH)₂-bridged structure and that the hydroxide bridges are replaced by fluoride bridges.²⁸ Although this model explains the stoichiometry and pH dependence of fluoride binding, it is not clear that the spectroscopically determined Mn–Mn separation of 3.5–3.7 Å is small enough to accommodate the di- μ -OH geometry. In addition, this structural picture does not provide a ready explanation for the pronounced sensitivity of the reduced MnCat EPR spectrum to the presence of anions such as phosphate or sulfate.

The mixed-valence oxidation state is characterized by an ~ 18 -line EPR signal attributed to an antiferromagnetically coupled $S = 1/2$ ground state.²² On the basis of the temperature dependence of this signal, the exchange coupling appears to be relatively weak ($J < -20 \text{ cm}^{-1}$).⁴⁰

Superoxidized MnCat has a 16-line EPR signal that is typical of strongly antiferromagnetically coupled Mn^{III}Mn^{IV} dimers. Detailed investigations of both the *L. plantarum* and the *T. thermophilus* enzymes, including measurements at S-, P-, X-, and W-bands and ultrahigh field, all give very similar results, with substantial hyperfine anisotropy for Mn^{III} but much less anisotropy for the Mn^{IV}.^{37,40,41} Six resolved pairs of D₂O-exchangeable lines were seen in the ¹H electron–nuclear double resonance (ENDOR) spectra for superoxidized *T. thermophilus* MnCat.⁴² These were attributed to a water (or possibly a hydroxide) that is hydrogen bonded to an oxygen ligand on the Mn^{IV}. Electron spin–echo

envelope modulation (ESEEM) spectra for superoxidized *T. thermophilus* MnCat show modulations from ^{14}N consistent with those expected for coordinated nitrogens; presumably these come from the histidines that are seen in the crystal structure of the lower oxidation states.³⁹ Addition of either N_3^- or CN^- results in a slight decrease in the Mn hyperfine coupling, with almost no change in the g tensor. Both anions give similar effects, and both cause modest changes in the ^{14}N ESEEM parameters. Identical spectra are seen for unlabeled and ^{15}N -labeled anions, suggesting that neither anion is coordinated directly to Mn in the superoxidized enzyme.

2.4.2. Electronic Spectroscopy

Electronic transitions within the d manifold are both spin and orbitally forbidden for Mn^{II} , and thus only the oxidized forms of MnCat have significant electronic transitions. The absorption spectrum of oxidized MnCat is distinct from those of most binuclear Mn^{III} models in that it lacks low-energy (5000–10 000 cm^{-1}) absorption bands.⁴³ This is consistent with the presence of five-coordinate Mn in oxidized MnCat. There are additional differences between the higher energy features in the absorption and MCD spectra of oxidized MnCat and oxo-bridged Mn^{III} models, suggesting that the Mn ions in MnCat may be bridged by a hydroxo or perhaps an aquo group rather than by an oxo group, which would be consistent with the weak exchange coupling seen at neutral pH. It has been suggested³³ that the MCD signal seen for oxidized MnCat comes from oxidatively damaged enzyme, and that the active enzyme is diamagnetic, although this would seem to be contradicted by magnetic susceptibility data for oxidized MnCat (see below). In a mutant of *L. plantarum* MnCat, MCD data suggest a pH-dependent conversion between paramagnetic and diamagnetic forms of the enzyme, at least in the Y42F mutant.³⁴

When azide is added to oxidized *L. plantarum* MnCat, an intense new transition is seen at 370 nm (27 000 cm^{-1}) that is assigned as an azide \rightarrow Mn charge-transfer transition.⁴³ There are only minor changes in the ligand field bands below 25 000 cm^{-1} when azide binds to oxidized MnCat, suggesting that the Mn coordination number does not change when azide binds. On the basis of the pattern of band shifts when N_3^- binds, it appears that N_3^- binding involves primarily $\text{N}_3^- \pi$ overlap with the Mn d_{xy} and d_{xz} orbitals (z is defined along the Mn-bridge direction). This would be consistent either with an end-on nonbridging geometry or with a $\mu_{1,3}$ -bridging geometry for N_3^- , and presumably also for H_2O_2 .

The MCD spectrum for superoxidized *L. plantarum* MnCat is similar to the spectra for di- μ -oxo-bridged $\text{Mn}^{\text{III}}\text{Mn}^{\text{IV}}$ dinuclear models, but with weaker oxo \rightarrow Mn charge-transfer transitions, suggesting that the $\text{Mn}_2(\mu\text{-O})_2$ core may be bent in superoxidized MnCat.⁴⁴ As in oxidized MnCat, azide and cyanide also bind to superoxidized MnCat, causing perturbations in the UV-visible and EPR spectra.^{39,44,45} The intensity of the oxo \rightarrow Mn charge-transfer transitions increases when azide binds, perhaps because azide

binding causes a slight flattening of the $\text{Mn}_2(\mu\text{-O})_2$ core. This would be consistent with the decrease in Mn hyperfine coupling seen in the EPR when azide binds.³⁹

2.4.3. Magnetism

Magnetic susceptibility measurements for reduced *T. thermophilus* MnCat gave $J = -2.4 \text{ cm}^{-1}$, with this value decreasing to -1.7 cm^{-1} when phosphate was added.⁴⁶ Subsequent reanalysis of these data suggested somewhat larger coupling in the phosphate-free enzyme (-5 cm^{-1}), with a similar value found for the *L. plantarum* enzyme.⁴⁷ These couplings are smaller than those deduced from EPR, suggesting that instead of a di- μ -OH-bridged core, the reduced enzyme might have a $\text{Mn}^{\text{II}}(\mu\text{-OH})(\mu\text{-carboxylato})\text{Mn}^{\text{II}}$ structure in the anion-free enzyme, and $\text{Mn}^{\text{II}}(\mu\text{-OH}_2)(\mu\text{-phosphato})(\mu\text{-carboxylato})\text{Mn}^{\text{II}}$ when phosphate is bound. A similar aquo-bridged structure was also suggested for the fluoride-inhibited enzyme ($J = -1.3 \text{ cm}^{-1}$),⁴⁷ in contrast with the suggestions from EPR and crystallography that halides bridge the two Mn's. Magnetic susceptibility data for oxidized *T. thermophilus* MnCat showed evidence for two different species, one weakly coupled ($J \approx -2 \text{ cm}^{-1}$) and one strongly coupled ($J \approx -100 \text{ cm}^{-1}$).⁴⁸ These were seen at neutral and basic pH values (6.5 and 9.5) and were attributed to μ -oxo, μ -carboxylato and di- μ -oxo, μ -carboxylato bridges, respectively. The pH dependence of the concentration of these species (42% strongly coupled at pH 6.5; 80% strongly coupled at pH 9.5) does not match that expected for a 1000-fold change in proton concentration, suggesting either that the samples may not have been fully equilibrated or that a paramagnetic impurity may have complicated interpretation of the data.

3. Structural Models

The earliest studies in this field used speculative modeling in an effort to assess the ligand types, metal oxidation states, and metal-metal separations for the various enzyme oxidation levels of the Mn catalases. As discussed above, instead of a heme group, the manganese catalases utilize a dinuclear active site for efficient disproportionation of hydrogen peroxide to dioxygen and water. The presence of a dinuclear core in the Mn catalase makes it of particular interest to biomimetic chemists as numerous other metalloenzymes containing iron, zinc, or copper are known that also use two metals as the active site. Crystallographic studies^{31,49,50} indicate that there are two five- or six-coordinate manganese ions that are each ligated by two histidines and two glutamates and bridged by at least one carboxylate from the protein and up to two oxo species (water, hydroxide, oxide) in the reduced enzyme. Many synthetic dinuclear complexes that are direct structural analogues for the manganese catalase active sites have been generated over the years; of particular interest are those that mimic spectroscopic and/or catalytic properties of the enzyme. Among the well-characterized dinuclear complexes, several bridging modes appear repeatedly, and each can be identified with a

Table 1. Mn–Mn Separations for Common Bridging Species

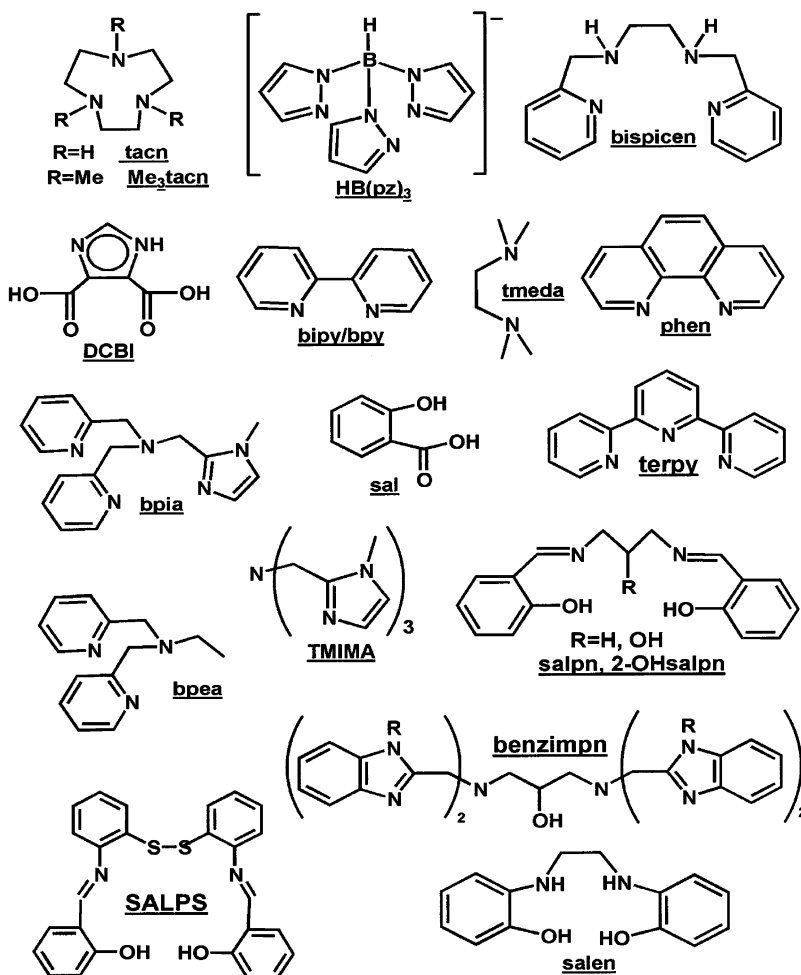
bridging species	oxidation state	Mn–Mn separation (Å)
$\text{Mn}_2(\mu\text{-O})$ linear	III/III	3.3–3.4
	IV/IV	3.5
$\text{Mn}_2(\mu\text{-O})(\mu\text{-OAc})_2$	II, III, IV	3.1–3.6
	III/III	2.8
$\text{Mn}_2(\mu\text{-O})_2$	III/IV	2.6–2.7
	IV/IV	2.6–2.7
	III/III	2.7
$\text{Mn}_2(\mu\text{-OH})_2$	III/III	3.2–3.3
	II/II	3.1–3.4
$\text{Mn}_2(\mu\text{-OR})_2$	III/III	3.1–3.2
	III/IV	3.25
	II/II	3.6
	III/III	3.3
$\text{Mn}_2(\mu_{1,3}\text{-OAc})_2(\mu\text{-OR})$	II/II	3.4–3.5
	III/III	3.5–3.6
$\text{Mn}_2(\mu\text{-OR})(\mu_{1,3}\text{-OAc})$	II/III	3.1–3.2
	III/IV	2.6

relatively invariable Mn–Mn separation (usually independent of the supporting ligands). Thus, Mn–Mn distance (Table 1) can often be used as evidence of a particular core structure when a full crystal structure is not available, as was the case until recently. It is important to note that all of the manganese complexes examined in the Mn^{II} , Mn^{III} , and Mn^{IV} oxidation levels form crystallographically valence-trapped species with distinct sites for each oxidation level.

The majority of the complexes listed in this section were speculative models for the manganese catalases. For the convenience of the reader, ligands mentioned in this section and their abbreviations are included in the glossary (section 8) and in Figure 1, respectively. This is by no means an exhaustive list, and the reader is encouraged to examine other literature^{1–5,51,52} regarding this topic.

3.1. Models with Single Oxo/Hydroxo/Alkoxo Bridges

The simplest dinuclear structures utilize a single oxo or hydroxo ligand. This bridging type is not often found in the literature because dioxo- and dihydroxo-bridged manganese dimers tend to be more thermodynamically stable than their single oxo- or hydroxo-bridged counterparts, especially if the bridging species is unsupported by the ligand framework. Therefore, of the complexes that have been characterized (Figure 2), the non-porphyrin-based ligand tpictn provides the $[\text{Mn}^{\text{II}}_2(\text{tpictn})(\mu\text{-OH})]$ complex⁵³ in which the single-bridging hydroxo is nonlinear and supported by the ligand which spans both Mn ions. The Mn–Mn separation in this structure is 3.6 Å. The $[\text{Mn}^{\text{III}}\text{-Mn}^{\text{IV}}\text{O}(\text{bpsalden})_2]^{3+}$ complex⁵⁴ has been prepared electrochemically and possesses the most linear oxo-bridge known to date, with a Mn–O–Mn angle of 178.7° and a Mn–Mn separation of 3.52 Å. Nearly linear oxo bridges can be found in two other com-

**Figure 1.** Ligands and their abbreviations.

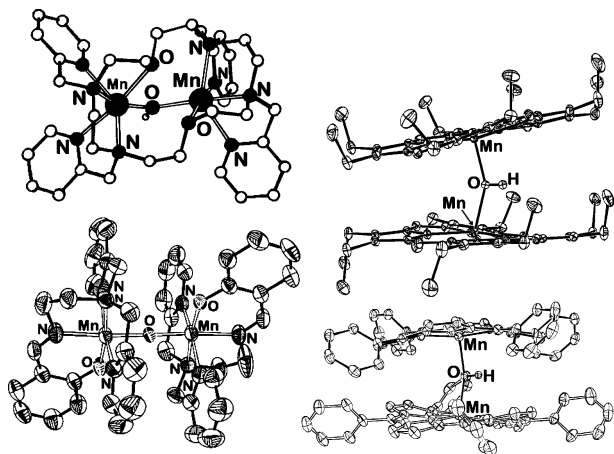


Figure 2. Complexes with single oxo-type bridges (counterclockwise from top left): $[\text{Mn}^{\text{II}}_2(\text{tpictn})(\mu\text{-OH})]$, $[\text{Mn}^{\text{III}}\text{Mn}^{\text{IV}}\text{O}(\text{bpsalden})_2]^{3+}$, $[\text{Mn}^{\text{III}}(\text{TPP})_2(\mu\text{-OH})]$, and $[\text{Mn}^{\text{III}}(\text{OEP})_2(\mu\text{-OH})]$. Reprinted with permission from refs 53–56. Copyright 1995 The Royal Society of Chemistry, and copyright 1995, 1996, and 1999 American Chemical Society.

plexes as well (Figure 2). In $[\text{Mn}^{\text{III}}(\text{OEP})_2(\mu\text{-OH})]$ and $[\text{Mn}^{\text{III}}(\text{TPP})_2(\mu\text{-OH})]$, a single hydroxo bridge links two porphyrin-bound Mn ions and is unsupported by the ligand.^{55,56} The Mn–O–Mn angles of 160.4° for the TPP complex (Figure 2c) compared to 152.7° for the OEP complex are typical of hydroxo-bridged dimers. The greater linearity of the $\mu\text{-OH}$ bridge in the TPP complex results in a greater Mn–Mn distance of 3.99 \AA . It is likely that this greater linearity is enforced by the steric demands of the four phenyl substituents on the porphyrin ring.

Analogues of the mono- $\mu\text{-OH}$ -bridged complexes include the mono- $\mu\text{-O}$ bridge and the mono- $\mu\text{-alkoxo}$ bridge. The single $\mu\text{-O}$ bridge motif is less common and can be seen in dimers that have a preference for linear Mn–O–Mn geometry; usually this preference arises from the steric demands of a hindered ligand. One such example is the $[\text{Mn}^{\text{IV}}(\text{TPP})\text{N}_3]_2(\mu\text{-O})$ complex which, like its $[\text{Mn}^{\text{III}}(\text{TPP})_2(\mu\text{-OH})]$ analogue, exhibits a nearly linear Mn–O–Mn angle.⁵⁷ Other linearly bridged manganese dimers include the $[\text{Mn}^{\text{III}}(5\text{-NO}_2\text{saldien})_2(\mu\text{-O})]$ and the $[\text{Mn}^{\text{III}}(\text{HB}(3,5\text{-}^i\text{Pr}_2\text{pz})_2(3\text{-}^i\text{PrO}-5\text{-}^i\text{Prpz}))_2(\mu\text{-O})]$ complexes.^{58,59} The Mn–Mn separations are similar, at 3.49 \AA for $[\text{Mn}^{\text{III}}(5\text{-NO}_2\text{saldien})_2(\mu\text{-O})]$ and 3.53 \AA for $[\text{Mn}^{\text{III}}(\text{HB}(3,5\text{-}^i\text{Pr}_2\text{pz})_2(3\text{-}^i\text{PrO}-5\text{-}^i\text{Prpz}))_2(\mu\text{-O})]$.

More commonly found are the $\mu\text{-alkoxo}$ -bridged dimers. These complexes have structural parameters that are quite similar to the $\mu\text{-OH}$ counterparts and are frequently found in the literature. Compounds containing a single $\mu\text{-OR}$ are not as well-known as $(\mu\text{-OR})_2$ complexes; however, several compounds have been characterized in a variety of oxidation states. The single $\mu\text{-OR}$ ligands are usually supported by the ligand scaffold as in the case of the highly supported 2-OH salpn ligand or derivatives thereof. These complexes include the mixed-valent $[\text{Mn}^{\text{III}}\text{Mn}^{\text{IV}}(2\text{-OH-(3,5-Cl}_2\text{sal)pn})_2(\text{THF})]^+$, with a Mn–O–Mn angle of 126.7° and a shortened Mn–Mn distance of 3.65 \AA from its $[\text{Mn}^{\text{III}}(2\text{-OH}(3,5\text{-Cl}_2\text{sal)pn)MeOH}]_2$ counterpart⁶⁰ (Figure 3), which has itself a Mn–Mn distance of 3.808 \AA and a Mn–O–Mn angle of 129° .

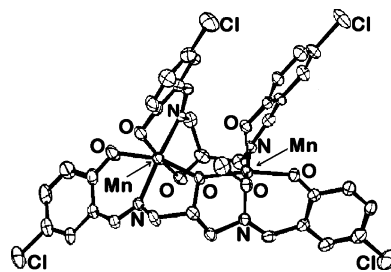


Figure 3. $[\text{Mn}^{\text{III}}(2\text{-OH}(3,5\text{-Cl}_2\text{sal)pn)MeOH}]_2$. Reprinted with permission from ref 60. Copyright 1992 American Chemical Society.

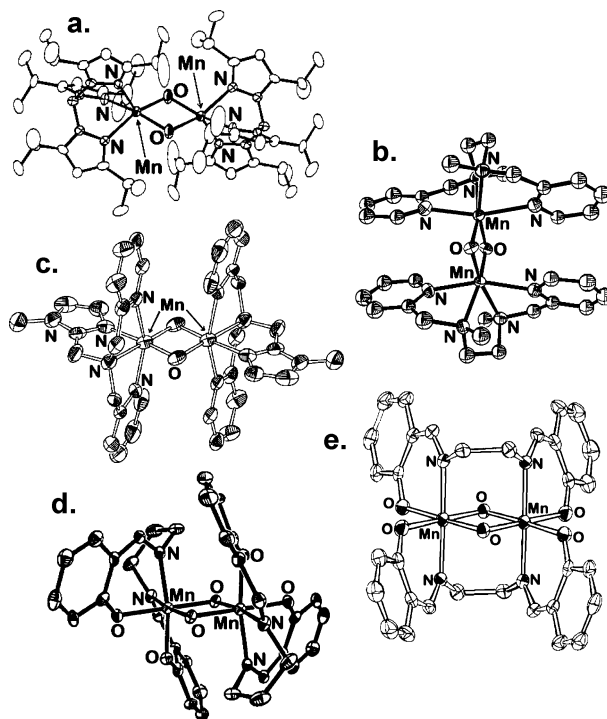


Figure 4. Complexes with unsupported $(\mu\text{-O})_2$ bridges: (a) the complex $[\text{Mn}^{\text{III}}(\text{HB}(3,5\text{-}^i\text{Pr}_2\text{pz})_3)_2(\mu\text{-O})_2]$, (b) $[\text{Mn}^{\text{III}}(\text{bispicMe}_2\text{en})_2(\mu\text{-O})_2]$, (c) the bis- $(\mu\text{-O})$ -bridged complex $[\text{Mn}^{\text{III}}\text{Mn}^{\text{IV}}(\text{bpia})_2(\mu\text{-O})_2]^{3+}$, (d) $[\text{Mn}^{\text{IV}}(\text{salpn})_2(\mu\text{-O})_2]$, and (e) salen ligand complex. Reprinted with permission from refs 61, 62, 67, 74, and 80. Copyright 1991, 1994, and 2002 American Chemical Society, and copyright 1998 Elsevier.

3.2. Models with Bis- $\mu\text{-Oxo}$ /Hydroxo/Alkoxo Bridges

A multitude of bis- $\mu\text{-oxo}$ dimanganese complexes have been synthesized and are the most prevalent dimeric form of manganese in the literature. Less frequently encountered are bis- $\mu\text{-hydroxo}$ and bis- $\mu\text{-alkoxo}$ counterparts, which demonstrate remarkable similarities in core structure to the bis- $\mu\text{-oxo}$ complexes despite having quite different ligands. An example of the bis- $\mu\text{-hydroxo}$ core is seen with the complex $[\text{Mn}^{\text{II}}(\text{HB}(3,5\text{-}^i\text{Pr}_2\text{pz})_3)_2(\mu\text{-OH})_2]$, which has a Mn–Mn separation of 3.314 \AA (Figure 4a). Oxidation of $[\text{Mn}^{\text{II}}(\text{HB}(3,5\text{-}^i\text{Pr}_2\text{pz})_3)_2(\mu\text{-OH})_2]$ by permanganate or dioxygen gives a $[\text{Mn}^{\text{III}}(\text{HB}(3,5\text{-}^i\text{Pr}_2\text{pz})_3)_2(\mu\text{-O})_2]$ complex⁶¹ with a substantially shortened Mn–Mn separation of 2.696 \AA . Another complex (Figure 4b) with nearly the same Mn–Mn distance (2.699 \AA)^{62,63} is $[\text{Mn}^{\text{III}}(\text{bispicMe}_2\text{en})_2(\mu\text{-O})_2]$. The significantly shorter metal separations in Mn(III) dimers as compared to Mn(II) dimers is a consequence of both

changes in Mn–O–Mn angles and shorter Mn–O bond distances. Typically, the average Mn^{II}–(O,N) distance is ~ 2.2 Å, whereas Mn^{III}–(O,N) distances average ~ 2.05 Å; however, these bond distances are often even further discriminated because the high-spin d⁴ Mn(III) ion is subject to a significant axial Jahn–Teller distortion. This tetragonal distortion typically elongates two bonds by ~ 0.2 Å and shortens the four equatorial bonds by ~ 0.1 – 0.15 Å. In the vast majority of dinuclear manganese complexes, the Jahn–Teller axis is perpendicular to the plane of bridging atoms (an exception is the group of dinuclear species prepared with the 2-OH-salpn ligand discussed below). There are no examples of Mn^{II}Mn^{III}, Mn^{III}₂, or Mn^{III}Mn^{IV} with (μ -O) bridges in which the elongated axis of the Mn^{III} points directly toward the bridging oxide ligand.

The (μ -O)₂ bridging core is also observed for dimers with higher oxidation states (Mn^{III}Mn^{IV} and Mn^{IV}₂). Of these dimers, several Mn^{III}Mn^{IV} complexes show valence localization in which one manganese center exhibits the axial elongation associated with isolated Mn^{III} ions and the other manganese center exhibits a more octahedral geometry. There do exist cases where valence localization is not seen; we have refrained, however, from including these in the discussion because the crystallography may not reflect the true structure (static crystallographic disorder may make the two manganese centers appear equivalent). More examples of valence localization can be found in the literature^{64–67} and include the [Mn^{III}Mn^{IV}(bpy)₄(μ -O)₂]³⁺ and [Mn^{III}Mn^{IV}(phen)₄(μ -O)₂]³⁺ complexes as well as the [Mn^{III}Mn^{IV}(bpia)₂(μ -O)₂]³⁺ structure (Figure 4c). There are several more complexes that also exhibit this characteristic. Higher valent Mn^{IV}₂(μ -O)₂ complexes have been prepared with a multitude of supporting ligands. Despite the variation in ligands, these complexes show a typical Mn–Mn separation of 2.7 ± 0.1 Å,⁶⁸ but this distance has been shown to depend on the protonation state.^{69–71} For example, one such complex is [Mn^{IV}(salpn)₂(μ -O)₂] (Figure 4d); XAS spectroscopy has shown that the Mn–Mn distance increases by 0.10 Å for each protonation of the bridge,^{72–75} yielding ~ 2.8 Å for [Mn^{IV}(salpn)₂(μ -O)(μ -OH)]⁺ and 2.9 Å for [Mn^{IV}(salpn)(μ -OH)]₂²⁺. Alkylation of the bridges results in equivalent elongation. The Mn^{IV}(μ -O)₂ complexes are too highly oxidized to be important models for the Mn catalases; however, mixed-valent cores containing Mn^{III}Mn^{IV}(μ -O)₂ are important structures for understanding the inactive, superoxidized form of the Mn catalases.

More recently, the bis- μ -oxo complex [Mn^{III}Mn^{IV}(terpy)₂(μ -O)₂(CF₃CO₂)₂]⁺ has been synthesized;⁷⁶ not only does it exhibit a (μ -O)₂ core with a Mn–Mn distance of 2.727 Å, but it also possesses two carboxylate groups that coordinate to the Mn centers in a monodentate fashion. An interesting analogue of this complex utilizes the bbml ligand to provide bis- μ -alkoxo bridges (Figure 5a); these complexes^{77,78} also exhibit terminally coordinated carboxylates at each manganese center from coordination of toluic or acetic acid, and both have Mn–Mn separations of 3.21 Å.

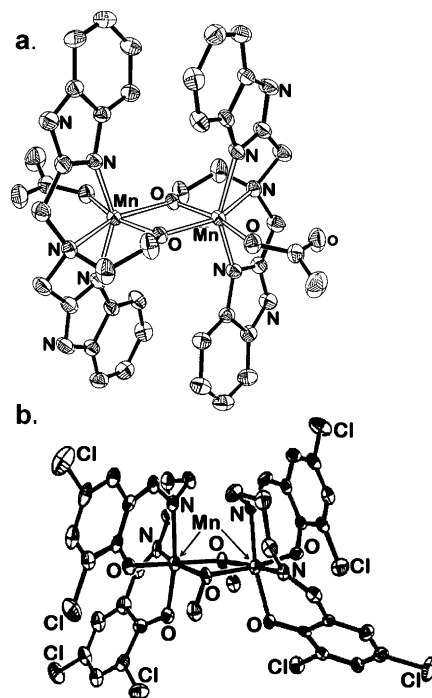


Figure 5. Bis- μ -alkoxo bridged complexes: (a) [Mn^{III}₂(ac)₂(bbml)₂](BF₄)₂ and (b) [Mn^{III}(salpn)₂(μ -OCH₃)₂] complexes. Reprinted with permission from refs 74 and 77. Copyright 1991 American Chemical Society, and copyright 2001 Elsevier.

Bis- μ -hydroxo complexes are rare by comparison to bis- μ -oxo and bis- μ -alkoxo complexes. Only a very few have been structurally characterized to date. Bis- μ -alkoxo complexes are much more prevalent in the literature. The bis- μ -alkoxo complexes based upon the salpn ligand provide for an interesting series of structural comparisons. They have been characterized with both homovalent and mixed-valent metal ions as well as with (μ -OCH₃)₂ cores and with (μ -OR)₂ cores supported by the ligand. With a core analogous to that of a (μ -OH)₂ complex, [Mn^{III}(salpn)₂(μ -OCH₃)₂] has been structurally characterized⁷⁴ and exhibits a 3.192 Å Mn–Mn separation and characteristic Jahn–Teller elongation axes which include the bridging alkoxide ligands (Figure 5b). By comparison, the supported ligand structure, [Mn^{III}(2-OHsalpn)₂], possesses two alkoxide bridges but shows a longer Mn–Mn separation. The bis- μ -alkoxo-bridged mixed-valent [Mn^{III}Mn^{IV}(2-OHsalpn)₂]⁺ is also known⁷⁹ and shows a Mn–Mn separation of 3.3 Å, a value that is significantly larger than for analogous bis- μ -O complexes in the same oxidation state. A similar Schiff-base ligand, salen, provides an interesting comparison to the salpn complexes.⁸⁰ The salen ligand bridges two manganese ligands but allows for unsupported (μ -O)₂ bridging and a Mn–Mn distance of 2.706 Å (Figure 4e).

3.3. Carboxylate-Bridged Complexes

MCD data collected on the Mn catalase enzymes^{47,48,81} suggest coordination of at least one bridging carboxylate, and X-ray structure data^{31,33} corroborate the presence of Glu70 near the dimanganese active site in *T. thermophilus* and, similarly, Glu66 in *L. plantarum*. While there exist models in

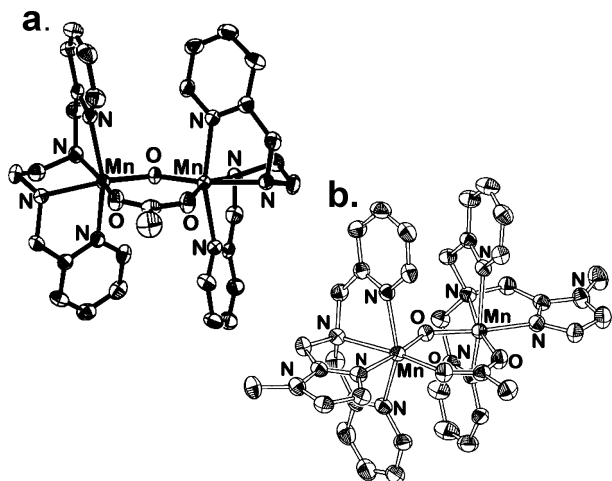


Figure 6. (a) $\{[\text{Mn}(\text{bispicen})]_2(\mu\text{-O})(\mu\text{-OAc})\}^{3+}$ complex and (b) $\{[\text{Mn}^{\text{III}}(\text{bpia})]_2(\mu\text{-O},\mu\text{-OAc})\}^{3+}$. Reprinted with permission from refs 67 and 82. Copyright 1993 and 2002 American Chemical Society.

which the bound Mn ions are exclusively $\mu_{1,3}$ -carboxylate-bridged, there are many more synthetic complexes exhibiting more than one type of bridging species that are of greater relevance to catalase active sites (which may have multiple oxo-type as well as carboxylate bridges). Therefore, the most appropriate synthetic model for the active site of the pseudocatalases must also include carboxylate ligation. The largest and most important class of synthetic complexes is those with (mono- or di- $\mu\text{-O},\mu\text{-carboxylato}$) cores.

Among the simplest complexes are those with $\text{Mn}_2(\mu\text{-O},\mu\text{-carboxylato})$ cores. One such example (Figure 6a) is $\{[\text{Mn}(\text{bispicen})]_2(\mu\text{-O})(\mu\text{-OAc})\}^{3+}$: the Mn^{III} centers maintain a roughly octahedral geometry and are separated by 3.276 Å.⁸² This particular core has been characterized only in the dimanganese(III) oxidation state. Although none of the complexes with $\text{Mn}^{\text{III}}_2(\mu\text{-OH})(\mu\text{-OAc})$ have been crystallographically characterized, comparisons can be made to $\text{Mn}_2(\mu\text{-OR})(\mu\text{-OAc})$ cores such as those found in $\text{Mn}^{\text{III}}_2(\text{salampn})(\mu\text{-OAc})$ and $\text{Mn}^{\text{II}}_2(2\text{-OHbenzimpn})(\mu\text{-OAc})$ (Figure 7).^{83,84} Despite having different oxidation states for the Mn centers, the Mn–Mn separations in these complexes are nearly identical, at 3.55 Å for the former and 3.54 Å for the latter. The benzimpn complex is noteworthy because it may accommodate a variety of different bridges (which have been proposed on the basis of its catalytic activity and which will be discussed later); only the $(\mu\text{-OR},\mu\text{-OAc})$ core,⁸⁴ however, has been structurally characterized.

Analogous to the $\{[\text{Mn}(\text{bispicen})]_2(\mu\text{-O})(\mu\text{-OAc})\}^{3+}$ complex are the $\{[\text{Mn}(\text{TMIMA})]_2(\mu\text{-O})(\mu\text{-OAc})\}^{2+}$ and $\{[\text{Mn}^{\text{III}}(\text{bpia})]_2(\mu\text{-O},\mu\text{-OAc})\}^{3+}$ complexes (Figure 6b),^{67,85} in which the Mn ions bear a separation distance of about 3.250 Å. However, for these complexes the coordination environment about the manganese centers is considerably more distorted than is seen in the case of $\{[\text{Mn}(\text{bispicen})]_2(\mu\text{-O})(\mu\text{-OAc})\}^{3+}$ due to the constraining nature of the tridentate capping ligands. These distorted geometries can be observed with other tridentate capping ligands as well; the most widely recognized of these ligands include tacn, HB(pz)₃, and TMIP. These ligands and their derivatives

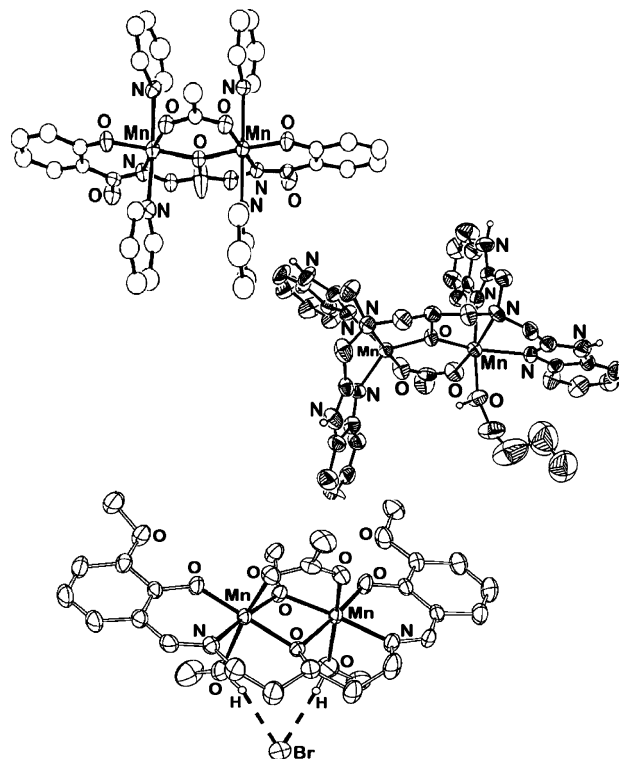


Figure 7. $\text{Mn}^{\text{III}}_2(\text{salampn})(\mu\text{-OAc})$, $\text{Mn}^{\text{II}}_2(2\text{-OHbenzimpn})(\mu\text{-OAc})$, and $[\text{Mn}_2(3\text{-MeO-salpentO})(\mu\text{-OMe})(\mu\text{-OAc})(\text{MeOH})_2]\text{-Br}$ complexes. Reprinted with permission from refs 83, 84, and 94. Copyright 2002 The Royal Society of Chemistry, copyright 1990 Elsevier, and copyright 1994 American Chemical Society.

have yielded a multitude of complexes^{86–88} bearing structural similarities to Mn catalase. Some typical examples of these complexes^{87,89,90} are $[\text{Mn}^{\text{III}}\text{Mn}^{\text{IV}}(\mu\text{-O})_2(\mu\text{-OAc})(\text{tacn})(\text{OAc})_2]$ (Figure 8a), $[\text{Mn}^{\text{III}}_2(\mu\text{-O})(\mu\text{-OAc})_2(\text{HB}(\text{pz})_3)_2]\text{CH}_3\text{CN}$ (Figure 8b), and $\text{Mn}^{\text{III}}[\text{HB}(3,5\text{-}^i\text{Pr}_2\text{pz})_3](3,5\text{-}^i\text{Pr}_2\text{pzH})(\eta^2\text{-O}_2^{2-})$, with core topologies that will be discussed later in this section.

More widely known are the triply bridged $(\mu\text{-O},\text{bis-}\mu\text{-carboxylato})\text{Mn}_2$ complexes. A multitude of these types of structure cores can be found in the literature. Typical $\text{Mn}^{\text{II}}\text{–Mn}^{\text{II}}$ distances for these cores are in the 3.15–3.18 Å range. The difference in Mn–Mn distance of the doubly bridged $(\mu\text{-O})\text{mono-}\mu\text{-carboxylato}$ as opposed to the triply bridged $(\mu\text{-O})\text{-bis-}\mu\text{-carboxylato}$ cores is to be expected because of more constrained bridge structures in the latter case. The $(\mu\text{-O})\text{bis-}\mu\text{-carboxylato}$ core topology is particularly interesting since metrical data have been obtained for $\text{Mn}_2(\mu\text{-OAc})_2(\mu\text{-O})$, $\text{Mn}_2(\mu\text{-OAc})_2(\mu\text{-OH})$, and $\text{Mn}_2(\mu\text{-OAc})_2(\mu\text{-OH}_2)$ structures. Each protonation of the oxo bridge decreases its donor ability, and this would favor longer bond lengths as well as stabilizing lower oxidation states of the metal centers. These observations are consistent with protonation of the $[\text{Mn}^{\text{IV}}(\text{salpn})]_2(\mu\text{-O})_2$ as described above. Not only does a decrease in oxidation state accompany each protonation, but also the Mn–Mn separation in these complexes increases from 3.1 to 3.4 to 3.6–3.8 Å.

The bis- $\mu\text{-oxo},\mu\text{-carboxylato}$ structure types have shortened Mn–Mn distances on the order of 2.64 Å as seen in the $[\text{Mn}^{\text{IV}}(\text{bpy})(\text{H}_2\text{O})]_2(\mu\text{-O})_2(\mu\text{-OAc})$ complex.⁹¹ The carboxylate bridge induces a bend in the

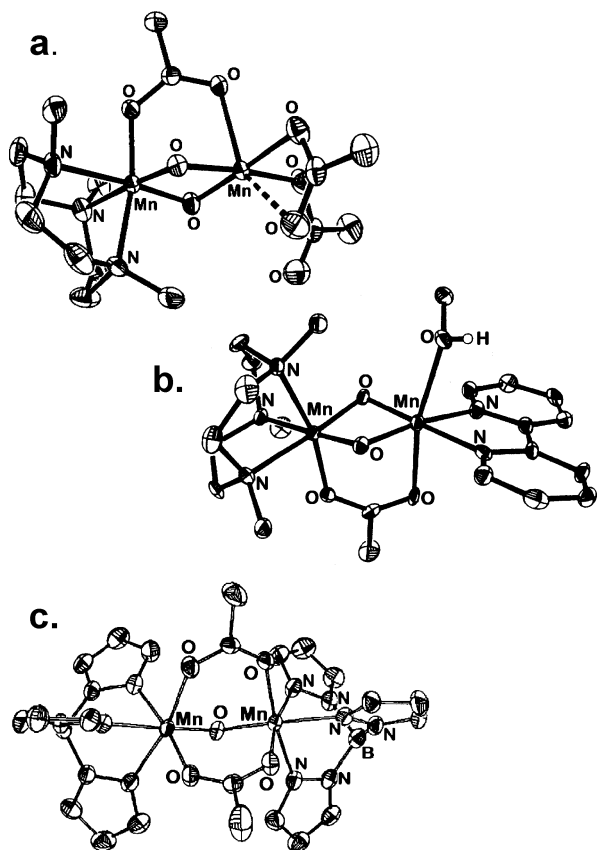


Figure 8. (a) $[\text{Mn}^{\text{III}}\text{Mn}^{\text{IV}}(\mu\text{-O})_2(\mu\text{-OAc})(\text{tacn})(\text{OAc})_2]$, (b) $[\text{Mn}^{\text{III}}_2(\mu\text{-O})(\text{OAc})_2(\text{HB}(\text{pz})_3)_2]\text{CH}_3\text{CN}$, and (c) $[\text{Mn}^{\text{III}}\text{Mn}^{\text{IV}}(\mu\text{-O})_2(\mu\text{-OAc})(\text{tacn})(\text{bipy})(\text{MeOH})]^{2+}$. Reprinted with permission from refs 87, 90, and 93. Copyright 1987 and 1994 American Chemical Society, and copyright 1992 The Royal Society of Chemistry.

$\text{Mn}(\mu\text{-O})\text{Mn}$ bridges, resulting in shortened Mn–Mn distances for these $\text{Mn}_2(\mu\text{-O})_2(\mu\text{-OAc})$ cores. Reduced derivatives such as $[\text{Mn}^{\text{III}}\text{Mn}^{\text{IV}}(\mu\text{-O})_2(\mu\text{-O}_2\text{CCH}_3)(\text{bpea})_2]^{2+}$, $[\text{Mn}^{\text{III}}\text{Mn}^{\text{IV}}(\mu\text{-O})_2(\mu\text{-OAc})(\text{tacn})(\text{OAc})_2]$ (Figure 8a), and $[\text{Mn}^{\text{III}}\text{Mn}^{\text{IV}}(\mu\text{-O})_2(\mu\text{-OAc})(\text{tacn})(\text{bipy})(\text{MeOH})]^{2+}$ (Figure 8c) possess similar structural parameters.^{92,93} While a comparison to $\text{Mn}_2(\mu\text{-OH},\mu\text{-carboxylato})$ cores would be useful, no such complexes have been isolated or structurally characterized. There are known examples of $\text{Mn}^{\text{III}}_2(\mu\text{-OR})_2(\mu_{1,3}\text{-OAc})$ complexes which have a characteristic Mn–Mn separation of about 2.9 Å. This is seen for the $[\text{Mn}^{\text{III}}_2(2\text{-OHsalpn})(\text{MeOH})_2(\mu\text{-OMe})(\mu_{1,3}\text{-OAc})]$ complex as well as for⁹⁴ the $[\text{Mn}_2(3\text{-MeO-salpentO})(\mu\text{-OMe})(\mu\text{-OAc})(\text{MeOH})_2]\text{Br}$ complex (Figure 7c).

A number of μ -phenoxide-bridged dimanganese complexes are structurally similar to their alkoxide-bridged counterparts. However, in such cases it has been shown that the donor ability of the phenolate oxygen is dependent upon the relative orientation of the aromatic phenyl ring with respect to the metal centers. When the metals are oriented perpendicularly to the aromatic plane, the phenolate oxygen is a weaker donor and allows an increase in Mn–Mn distance from about 3.26 to 3.42 Å. Thus, structurally, these types of ligands^{95,96} are of limited structural relevance.

In both small-molecule and protein complexes, carboxylates may bind in a variety of manners. One

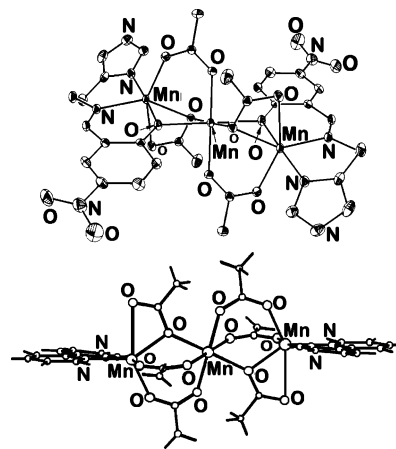


Figure 9. Trinuclear manganese complexes $\text{Mn}_3(5\text{-NO}_2\text{-salimH})_2(\text{OAc})_4$ and $\text{Mn}_3(\text{CH}_3\text{CO}_2)_6(\text{bpy})_2$. Reprinted with permission from refs 98 and 100. Copyright 1993 The Royal Society of Chemistry, and copyright 1991 American Chemical Society.

or both of the oxygens from a carboxylate group may interact with one or two metal ions, generating several different binding topologies: monodentate terminal, bidentate asymmetric, bidentate symmetric, monodentate bridging ($\mu_1\text{-O}_2\text{CR}$), and bidentate bridging ($\mu_{1,3}\text{-O}_2\text{CR}$). Evidence of all these binding modes is found in multinuclear metal sites. Thus, given the differences in preferred Mn–carboxylate binding with oxidation state of the Mn ion, the carboxylate shift first proposed by Lippard⁹⁷ in 1991 may accompany the redox changes and the metal–metal separation changes required for the $\text{Mn}^{\text{II}}_2 \leftrightarrow \text{Mn}^{\text{III}}_2$ redox cycling at the catalase active site.

There are several interesting models that exhibit more than one mode of carboxylate binding to the metal centers; most of these structures have “open” coordination sites which are occupied by solvent molecules. Structures that contain more than one type of carboxylate binding topology commonly have trinuclear manganese centers^{98–101} (Figure 9), such as $\text{Mn}_3(5\text{-NO}_2\text{salimH})_2(\text{OAc})_4$, $\text{Mn}_3(\text{CH}_3\text{CO}_2)_6(\text{phen})_2$, $\text{Mn}_3(\text{CH}_3\text{CO}_2)_6(\text{BIPhMe})_2$, $\text{Mn}_3(\text{CH}_3\text{CO}_2)_6(\text{bpy})_2$, and $\text{Mn}^{\text{II}}\text{Mn}^{\text{III}}_2(\text{saladhp})_2(\text{OAc})_4(\text{MeOH})_2$. In such structures, the Mn–Mn separation is typically about 3.6 Å and may not be as relevant to catalases as similar motifs found in dinuclear complexes. There exist some dinuclear complexes which exhibit this potentially critical characteristic. One of the complexes in which this is most obvious is $(\text{Mn}^{\text{II}}\text{tmeda})_2(\mu\text{-OAc})_2(\mu\text{-OH}_2)(\text{OAc})_2$ (Figure 10a),⁸⁸ as well as the tacn complex discussed previously (Figure 8a). In the tmeda complex, the two carboxylates are seen to adopt a syn–syn bidentate bridging mode in binding to the Mn^{II} centers. The other two acetate groups both coordinate terminally in a syn-monodentate fashion to each of the Mn ions in order to provide stability to the rarely seen $\mu\text{-OH}_2$ bridge via hydrogen-bonding interactions. The Mn–Mn separation here is also 3.6 Å and the Mn–O–Mn angle is 110°. This distance is intermediate between those typically found in tris- μ -carboxylato dimanganese cores (4.0 Å) and those found in $\mu\text{-OH},\text{bis-}\mu\text{-carboxylato}$ cores (3.35 Å). The $[\text{Mn}^{\text{II}}_2(\mu\text{-H}_2\text{O})(\mu\text{-OAc})_2(\text{Im})_4(\text{OAc})_2]$ complex (Figure 10b), which has a similar benzimidazole

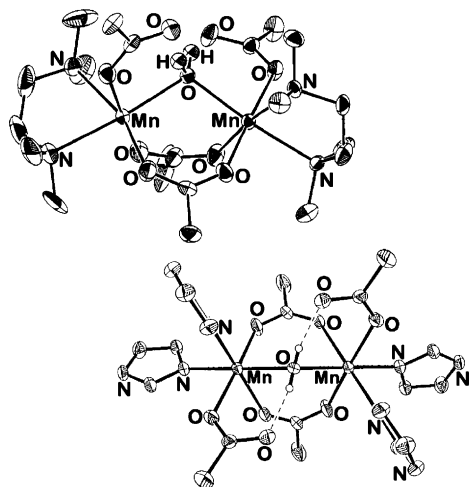


Figure 10. $(\text{Mn}^{\text{II}}\text{tmeda})_2(\text{OAc})_2(\mu_{1,3}\text{-OAc})_2(\mu\text{-OH}_2)$ and $[\text{Mn}^{\text{II}}_2(\mu\text{-H}_2\text{O})(\mu_{1,3}\text{-OAc})_2(\text{Im})_4(\text{OAc})_2]$. Reprinted with permission from refs 88 and 102. Copyright 1992 American Chemical Society, and copyright 1998 The Royal Society of Chemistry.

counterpart,¹⁰² is structurally similar to the $(\text{Mn}^{\text{II}}\text{tmeda})_2(\text{OAc})_2(\mu\text{-OAc})_2(\mu\text{-OH}_2)$ structure but has a longer Mn–Mn distance in the range of 3.7–3.8 Å and a Mn–O–Mn angle of 114°. There are additional dimanganese complexes in which more than one type of carboxylate binding mode has been proposed (usually on the basis of activity studies); these systems, however, have not been structurally characterized. Furthermore, there are even more examples of carboxylate shifts in the chemistry of diiron complexes which are structurally analogous to their dimanganese counterparts.

3.4. Asymmetric Ligand Complexes

It has been suggested from crystallographic data that the manganese catalases are structured in such a way that only one binding site is accessible to the incoming hydrogen peroxide substrate (one manganese center is six-coordinate and the other is five-coordinate). This has prompted a great deal of interest within the bioinorganic community to produce models that are asymmetric, a challenging proposition. Those seeking to make biomimetic models of manganese catalase have attempted the difficult syntheses of asymmetric ligands or their complexation with two manganese ions—complexes intended to emulate the single labile position at the manganese catalase active site.

Using the heptadentate asymmetrical phenolate ligand pichpy, three different dimanganese(II) complexes have been generated¹⁰³ (Figure 11). The variation in this series of complexes is primarily in the bridging ($\mu_{1,3}\text{-OAc}$) or ($\mu_{1,3}\text{-OBz}$) groups. All three complexes are otherwise structurally similar. It is, however, important to note that the crystal structures exhibit one open coordination site to which either a water molecule or a methanol molecule binds terminally. The Mn–Mn distances in these complexes are on the order of 3.4–3.5 Å, which is typical for these phenolate-bridged complexes. And the Mn–O–Mn angles, which range from 108 to 116°, also are within the range expected from analogous compounds reported in the literature.

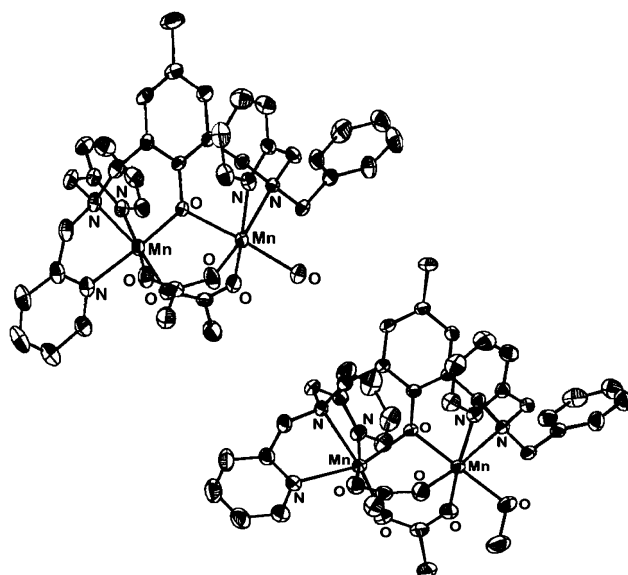


Figure 11. Dimanganese complexes of phenoxy-based ligands. Reprinted with permission from ref 103. Copyright 2003 American Chemical Society.

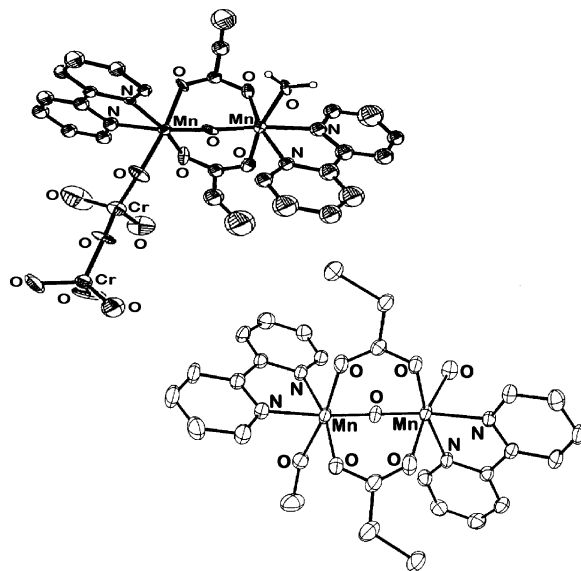


Figure 12. $[\text{Mn}_2\text{O}(\text{O}_2\text{CC}_2\text{H}_5)_2(\text{H}_2\text{O})(\text{Cr}_2\text{O}_7)(\text{bpy})_2]$ and $[\text{Mn}_2\text{O}(\text{O}_2\text{CCH}_2\text{Cl})_2(\text{H}_2\text{O})(\text{CH}_3\text{OH})(\text{bpy})_2]^{2+}$ complexes. Reprinted with permission from ref 104. Copyright 1998 Elsevier.

Simple complexes that may be analogous to the substrate-bound active site have been generated. Of particular interest are anion-bound complexes since the biological enzyme is inhibited by the presence of anions, especially halides. For example, the complexes $[\text{Mn}_2\text{O}(\text{O}_2\text{CC}_2\text{H}_5)_2(\text{H}_2\text{O})(\text{Cr}_2\text{O}_7)(\text{bpy})_2]$ and $[\text{Mn}_2\text{O}(\text{O}_2\text{CCH}_2\text{Cl})_2(\text{H}_2\text{O})(\text{CH}_3\text{OH})(\text{bpy})_2]^{2+}$ mimic end-on substrate and/or inhibitor coordination¹⁰⁴ to only one site on one manganese atom (Figure 12). These complexes have been characterized in the oxidized Mn^{III}_2 and superoxidized $\text{Mn}^{\text{III}}\text{Mn}^{\text{IV}}$ forms and contain a triply bridged $\mu\text{-O}$, bis- μ -carboxylato core. These complexes show a Mn–Mn separation of 3.1–3.2 Å. Another manganese(II) complex uses a heptadentate ligand¹⁰⁵ and has shown that the one labile position can be occupied by chloride or water; the crystal structure, unlike the previous complex, was intended

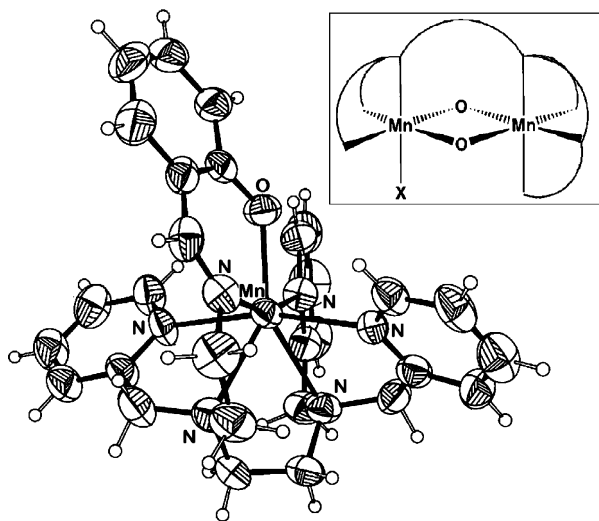


Figure 13. Asymmetric ligand design for a dimanganese complex (inset). ORTEP of the mononuclear complex obtained with this asymmetric ligand. Reprinted with permission from ref 105. Copyright 1999 Elsevier.

to contain a $Mn_2(\mu-O)_2$ core structure but no carboxylate bridges (Figure 13). Unfortunately, the target complex was not found, but a heptadentate Mn complex was generated which does indeed bind chloride and water at the one open site. This mononuclear complex is of little relevance to the catalase active site but may have relevance to manganese superoxide dismutase structure. It is conceivable, however, that access to the intended Mn_2O_2 species may still be viable with this ligand.

4. Spectroscopic Models

Structural aspects of the manganese catalase active sites have often been based on comparisons made between the spectroscopic properties of the metalloprotein and those of the synthetic model complexes. Manganese centers in metalloproteins can be studied using a variety of spectroscopic techniques, including electron paramagnetic resonance (EPR, ENDOR, and ESEEM), electronic (UV–vis), resonance Raman (RR), and X-ray absorption spectroscopies and magnetic susceptibility. UV–vis spectroscopy has been a particularly good technique for understanding the electronic structure of Mn^{III} and Mn^{IV} complexes which usually exhibit d–d and charge-transfer absorption bands in the visible region. Mn^{II}_2 , $Mn^{II}Mn^{III}$, and $Mn^{III}Mn^{IV}$ centers give characteristic EPR spectra using continuous wave X-band excitation collected with perpendicular detection methods. By examining the impact of dipolar couplings, hyperfine coupling can be related to the distance between manganese centers. Even Mn^{IV}_2 complexes with weak magnetic exchange coupling can be examined using a perpendicular detection mode for EPR. More often, however, non-Kramer ions are interrogated with parallel mode EPR spectroscopy, which recently has given new insight into enzymatic systems such as the by OEC.^{106–108}

Another important resonance approach^{109,110} is electron spin–echo envelope modification (ESEEM) spectroscopy, which is capable of extracting hyperfine

interaction parameters from systems when the continuous wave spectrum is too broad to analyze. Electron nuclear double resonance (ENDOR) spectroscopy has been applied to evaluate the nuclear quadrupole environment of coordinated ligands, which provides evidence for substrate binding to enzymes or small-molecule complexes.^{110–112} Those familiar with the chemistry of iron complexes will be disappointed to learn that Mössbauer spectroscopy is unavailable in manganese chemistry. Hence, the elegant interplay between EPR and Mössbauer used to deduce electronic structure of iron–sulfur clusters^{113–116} cannot be applied to these systems.

Magnetic susceptibility measurements allow estimation of magnetic exchange interactions that provide insight into the electronic structure of the cluster and, in certain cases, can be used to test whether a particular bridging motif is present. In this way, a range of metal–metal separations may be estimated. X-ray absorption spectroscopy may provide information about oxidation states of the manganese ions (XANES) as well as coordination environment (EXAFS). EXAFS is particularly useful when applied to systems where an X-ray structure is unavailable, as it provides metrical distances for metal–ligand bonds and metal–metal separations with high precision. Each of these methods gives limited nuclear or electronic structural information. Therefore, structural proposals rely on a combination of these techniques to provide a broader perspective on the properties of the enzymes. Essential to the interpretation of the data obtained on enzymes using these techniques is a knowledge base accumulated by collecting data on structurally well-characterized synthetic complexes.

4.1. X-ray Absorption Spectroscopies

X-rays possess wavelengths that are comparable to atomic dimensions and thus can be used to obtain precise metrical and angular information about molecules. Most commonly, X-ray diffraction of single crystalline samples provides a complete three-dimensional map of the crystal structure. Unfortunately, not all biological or chemical samples are amenable to formation of single crystals suitable for a diffraction experiment. Therefore, XAS is an attractive alternative technique for characterization of the sample in question. As is often the case, moving from one technique to another provides benefits and limitations; the shift from X-ray diffraction to X-ray spectroscopy is no exception.

The primary advantage of XAS is that it is not limited to crystalline samples. Another advantage is the ability of X-ray absorption near-edge structure (XANES) to provide oxidation state information at the same time that extended X-ray absorption fine structure (EXAFS) spectroscopy provides metrical information on the metal center. In contrast, X-ray diffraction studies must assume that photoreduction does not occur during the course of the experiment and provides no oxidation state information about the metal (except secondarily through the determination of Jahn–Teller distortions or average metal–ligand bond distances). In addition, EXAFS can extract

metal–ligand distances at much higher precision than most diffraction experiments on proteins. Thus, it is often the case that EXAFS is used to define the metal–ligand distances in a metalloprotein X-ray structure. The major limitations of XAS are that it cannot distinguish between scatterers such as oxygen or nitrogen, it usually provides no angular information regarding the ligands, and it provides average environments over all elements of the same type.¹¹⁷ Thus, a mononuclear Mn enzyme such as the MnSOD can be more straightforwardly interpreted than a dinuclear manganese site in an enzyme such as the Mn catalases. Another important issue with both XANES and EXAFS is that these techniques must be calibrated using well-defined compounds with appropriate oxidation state and structure. This limitation provides a necessity for the preparation of relevant biomimetic model compounds.

The XANES region refers to the 40 eV range about the edge, an absorption feature that occurs at the absorption threshold of a core electron. The shape and energy of the edge vary with metal ligation environment and will show systematic changes indicative of Mn oxidation state changes. The XANES region is followed by the EXAFS region of multiple decaying oscillations which extends about 1000 eV beyond the edge. The pre-edge region, occurring just before the absorption edge, often contains weakly bound transitions which can be fit in order to extrapolate geometric information about the metal environment. XANES is sensitive to all of the Mn in the sample, regardless of oxidation or spin state. This approach has proven very useful in assigning oxidation states in different Mn catalase derivatives. Mn^{II} complexes are at the lowest energy in the XANES spectra and have the most intense main peak; as the metal ion is oxidized, the peak intensity drops, its position shifts upward in energy, and the absorption feature broadens.

In all XAS experiments, care must be taken when fitting the data acquired; to obtain reliable fits from which to extract useful information, careful selection of the type and number of variable parameters and their constraints is a necessity. There are two primary methods for XANES fitting to determine edge energy: either by fitting the entire edge, or by defining the edge energy as the second inflection point. While these different fitting methods usually yield different absolute edge energy values, they usually provide the same oxidation state conclusions provided that the fitting procedure remains the same for all the data (from the model complex library as well as the experimental). There are, however, cases where different fitting procedures and parameters have yielded different oxidation state conclusions.

The Mn₂(2-OH(X-sal)pn)₂ series of complexes illustrates typical XANES spectra for a variety of oxidation state formulations (Figure 14, top) and provides a convenient method by which to determine the edge energies of these oxidation states. This library has been extended to include Kitajima's HB-(pz)₃ complexes as well. Kitajima's complexes, which vary by oxidation state as well as by bridging species, yield XANES spectra that fall within the same energy

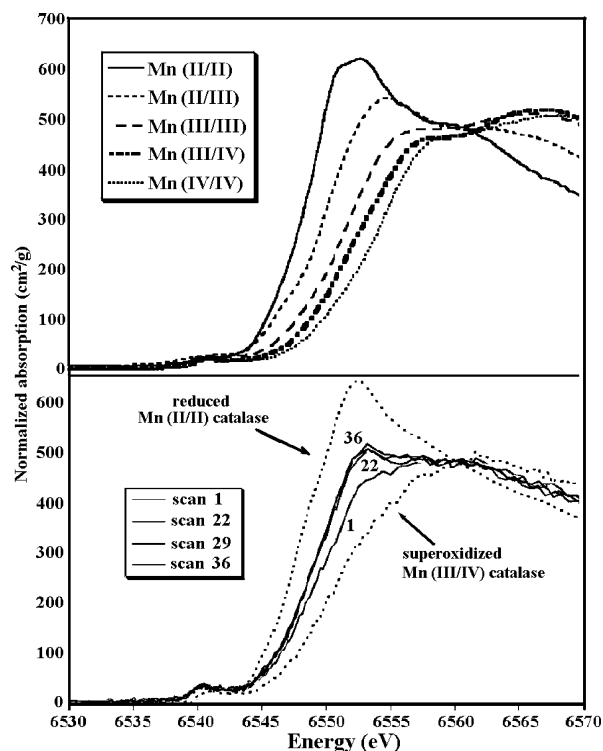


Figure 14. XANES spectra of 2-OHsalpn complexes as compared to Mn catalase. Reprinted with permission from refs 119 and 120.

range as the 2-OHsalpn set. Thus, edge shape and energy are independent of bridging ligation to a first approximation.¹¹⁸ Model complexes have indicated that the shift in edge energy is linear for lower oxidation states. Higher oxidation state changes, however, show smaller shifts in edge energy and are more difficult to fit.

Placement of the edge energies has been used to assign the various oxidation states that are exhibited by the catalases. For the catalases, the edge energies (when fit to the first inflection point) are in the range from about 6548 (Mn^{II}) to about 6551 eV (Mn^{III}Mn^{IV}); a comparison to model complexes shows that the Mn^{IV}₂ oxidation state is even higher in energy, at approximately 6553 eV. The two sets of data collected for the various oxidation states from both model complexes and enzymes are in good agreement. It is just such a comparison to the library of synthetic model complexes that has identified²¹ the active oxidized catalase as Mn^{III}₂. XANES analysis on the catalase enzymes²⁷ has confirmed the active forms of Mn catalase to be Mn^{II}₂ and Mn^{III}₂. It should be noted that, for the biological system, sample homogeneity of mixed oxidation states (especially the Mn^{II}-Mn^{III} catalase) is difficult to obtain. There are, however, ways to estimate sample composition from the XANES spectra obtained: the XANES data of the Mn catalases (Figure 14, bottom) also show distinct edge energies that are consistent with those found for model complexes.^{119,120} Despite evidence of photoreduction in the spectra for the oxidized (Mn^{III}₂) catalase sample, the rate of photoreduction can be determined and adjusted for in the fitting of the data.

It should be noted that, while oxidation state assignments are quite easily made for mononuclear

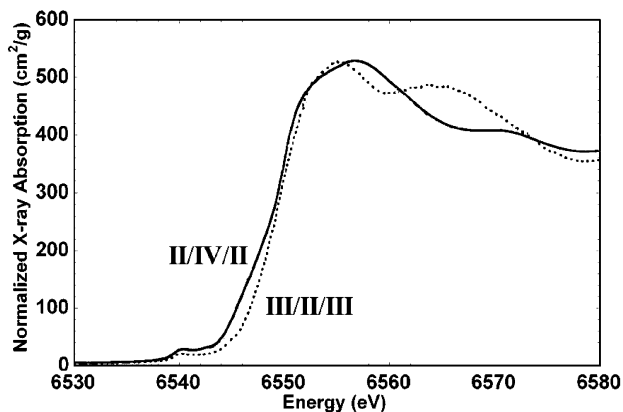


Figure 15. XANES of Mn_3 complexes with mixed II/IV/II and III/II/III oxidation states. Reprinted with permission from ref 121. Copyright 2003 American Chemical Society.

complexes, complexes with multiple metal centers are more challenging because the edge shift for the single oxidation of a dinuclear system is half of what is seen for a single oxidation of a monomer (for a trinuclear system, one-third of the monomer shift and so forth). Despite this added complexity, careful analysis of XANES spectra can positively identify mixed-valence states for complexes with up to three Mn centers. As proof of the utility of XANES in assigning oxidation state, it has been shown¹²¹ that $Mn^{II}_2Mn^{IV}$ and $Mn^{II}Mn^{III}_2$ complexes exhibit noticeably different XANES edges (Figure 15). In most of these complexes, the Mn ions are valence trapped and distinguishable; thus, this technique could be applied for identifying $Mn^{II}Mn^{IV}$ vs Mn^{III}_2 or even $Mn^{II}_3Mn^{IV}$ vs $Mn^{II}_2Mn^{III}_2$. Investigation into the latter case is currently underway.

Model complexes have yielded a wealth of information via XANES spectroscopy that has enhanced our understanding of the catalytic cycle of Mn catalases. EXAFS can aid in determination of compound structure; fitting of spectral data has been derived from the vast library of dimanganese model complexes that have been structurally characterized by X-ray crystallography. The ability of EXAFS to detect metal–metal interactions may be particularly useful for determining whether complexes remain intact in solution. There are cases, however, in which crystals cannot be readily obtained. In these types of cases, Mn–Mn distances can be determined from the EXAFS data. These are often indicative of the types of bridging atoms between the metal centers. Proper fitting of EXAFS data allows deduction of the types of donor atoms in the first coordination sphere of the metal ions.

One may be tempted to view model compounds solely as a calibrant for XAS studies on biological systems; there are cases, however, where XANES and EXAFS investigations of model compound structure are essential. As an example, the reaction of *tert*-butyl hydroperoxide with $[Mn^{III}(2-OHsalpn)]_2$ leads to vigorous evolution of dioxygen and an oxidized metal complex.¹²² Elemental analysis, UV–vis, and EPR spectroscopies supported a formulation of $\{Mn^{III}Mn^{IV}[(2-OHsalpn)_2OH]\}$ with a coordinated hydroxide ion, but single crystals of the compound could not be obtained to confirm this assignment. Crystallography

of related compounds $\{Mn^{III}Mn^{IV}(2-OHsalpn)_2\}^+$, $\{Mn^{II}Mn^{IV}(2-OH(3,5-Cl_2sal)pn)_2MeOH\}^+$, and $\{Mn^{III}Mn^{IV}(2-OH(3,5-Cl_2sal)pn)_2THF\}^+$ revealed that the presence of a coordinated exogenous ligand led to a structural rearrangement of the compound.^{60,123–125} The fully symmetric form had a Mn–Mn distance of ~ 3.34 Å while the asymmetric structure, with bound THF or methanol, contained a Mn–Mn distance on the order of 3.7 Å. EXAFS data on these dinuclear systems matched the crystallographically determined distances extremely well. XANES was used to confirm the oxidation state of $\{Mn^{III}Mn^{IV}(2-OHsalpn)_2-OH\}$, and EXAFS was used to provide supportive evidence,⁴⁴ based on the long Mn–Mn distance, that the isolated compound was the asymmetric derivative with a coordinated hydroxide. This assignment was crucial for deducing the mechanism of this reaction which was a metal-initiated, radical chain reaction that was propagated by *tert*-butoxy radical. Currently, EXAFS and stopped-flow XANES are being used to assess the production of $Mn^{IV}Mn^{IV}$ dimers vs $Mn^{IV}Mn^V$ species. This characterization of models is again an essential contribution to reactive model chemistry.

4.2. Magnetic Studies

In all biological settings, Mn^{II} is a high-spin ion which, in an octahedral ligand field, gives a 6A_1 ground state. The d^3 Mn^{IV} ion also has an orbitally singlet ground state (4A_2) in an octahedral field. Thus, no significant spin–orbit coupling may occur from these ground states (e.g., the axial zero-field-splitting component, $|D|$, is typically < 0.5 cm^{-1}). In contrast, Mn^{III} is always a high-spin d^4 ion, which forms an orbitally doublet 5E ground state in an octahedral field. As mentioned above, such systems are subject to Jahn–Teller distortions. Furthermore, 5E states possess substantial spin–orbit couplings that lead to significantly enhanced zero-field splitting; ZFS values of $|D| = 8$ cm^{-1} have been reported. In general, g values for manganese ions are only slightly lower than 2 (typically $1.97 < g_{iso} < 1.99$). Thus, in most cases, mononuclear manganese compounds deviate only slightly from the predicted spin-only values.

An understanding of the magnetic properties in systems containing more than one Mn center becomes more involved. Most studies of magnetic exchange interactions for simple dinuclear systems have used a straightforward Heisenberg spin Hamiltonian, $H = -2JS_1 \cdot S_2$. This approach works reasonably well for systems containing only Mn^{II} or Mn^{IV} ; however, adding a term to account for zero-field splitting better treats dinuclear systems that include Mn^{III} . The vast majority of dinuclear manganese compounds are antiferromagnetically coupled (i.e., $J < 0$). The general trend applies that coupling increases on going from low to high oxidation states because dinuclear Mn^{III} complexes (Mn^{III}_2 , $Mn^{II}Mn^{III}$, $Mn^{III}Mn^{IV}$) are usually strongly coupled, with $J \gg D$. In this limit, D is considered a perturbation of the spin-only energy levels, and the spin-only approach can be used to reasonably calculate J . On the other hand, in systems with extremely weak coupling ($J \ll D$), magnetism is dominated by D because J may

Table 2. Comparison of Magnetic Data for Mn₂ Complexes

compound	J (cm ⁻¹)	$ D $ (cm ⁻¹)	ref
[Mn ₂ (μ -O)(μ -OAc) ₂ (TMIP) ₂] ²⁺	< -0.2	nr ^a	188
[Mn ₂ O(OAc) ₃ (HB(pz) ₃) ₂ ·(CH ₃ CN) _x	-0.2-0.7	> 0.33	87
Mn ^{III} ₂ O(TMIMA) ₂ (OAc) ₂ ²⁺	1.33	0.40	85
[Mn ^{IV} ₂ O ₂ (tmpa) ₂] ³⁺	-137	nr	189
[Mn ^{IV} ₂ O ₂ (phen) ₄] ³⁺	-144	nr	190
Mn ₂ (μ -MeOH)(μ -OAc)(3-MeO-salpentO)(MeOH) ₂ Br	-13.7	nr	94
[Mn ₂ (μ -OAc) ₂ picphpy(OH ₂) ₂] ²⁺	-4.3	nr	103
Mn ^{II} ₂ (OH ₂)(OAc) ₄ (tmeda) ₂	-2.95	0.06	88, 191
[Mn ^{III} ₂ O(5-NO ₂ saldien) ₂]	-120	nr	58
[Mn ^{III} (tol)(bbml) ₂] ²⁺	-1.19	nr	78
[Mn(OAc)(bbml) ₂] ²⁺	-0.18	nr	77
[Mn ^{IV} ₂ (μ -O)(μ -O ₂ CH ₃)(NH ₃) ₆] ³⁺	-129	nr	192
[Mn ^{IV} ₂ (μ -O)(NH ₃) ₈] ⁴⁺	-274	nr	192
Mn ₂ (μ -Cl) ₂ (bpea) ₂ Cl ₂	-0.34	nr	164
[Mn ^{II} ₂ (μ -O ₂ CCH ₃) ₃ (bpea) ₂] ⁺	-1.3	nr	92
[Mn ^{IV} ₂ (μ -O) ₂ (μ -OAc)(bpea) ₂] ³⁺	-124	nr	193
Mn ^{III} ₂ O(μ -O ₂ CPh) ₂ (OH)(bpy) ₂ (NO ₃)	1.0	4.5	194
[Mn ^{III} ₂ (μ -O)(μ -O ₂ CPh) ₂ (N ₃) ₂ (bpy) ₂]	8.8	0.3	195
[Mn ^{III} ₂ (μ -O) ₂ (μ -OAc)Cl ₂ (bpy) ₂]	-4.1	0.07	195
[Mn ^{III} ₂ (μ -O) ₂ (μ -OAc)(H ₂ O) ₂ (bpy) ₂] ²⁺	-3.4	nr	195
[Mn ^{IV} ₂ (μ -O) ₂ (μ -OAc)Cl(H ₂ O)(bpy) ₂] ²⁺	-39.3	nr	196
[Mn ^{IV} ₂ (μ -O) ₂ (μ -OAc)(H ₂ O) ₂ (bpy) ₂] ³⁺	-43.7	nr	91
[Mn ^{IV} ₂ (μ -O) ₂ (μ -OAc)(H ₂ O) ₂ (bpy) ₂] ³⁺	-67	nr	197
[Mn ^{II} ₂ (μ -OH)(μ -OAc) ₂ (Me ₃ tacn) ₂] ⁺	-9	nr	130
[Mn ^{III} ₂ (μ -O)(μ -OAc) ₂ (Me ₃ tacn) ₂] ²⁺	9	3	130, 198
[Mn ^{III} Mn ^{IV} (μ -O)(μ -OAc) ₂ (Me ₃ tacn) ₂] ³⁺	-40	nr	130
[Mn ^{III} Mn ^{IV} (μ -O) ₂ (μ -OAc) ₂] ²⁺	-220	nr	130
[Mn ^{IV} ₂ (μ -O) ₃ (Me ₃ tacn) ₂] ²⁺	-390	nr	130
[Mn ^{III} ₂ O ₂ (bispicMe ₂ en) ₂] ²⁺	-100	nr	62
[Mn ^{III} Mn ^{IV} O ₂ (bispicen) ₂] ³⁺	-140	nr	63
[Mn ^{IV} Mn ^{IV} O ₂ (bispicen) ₂](ClO ₄) ₄ ·2CH ₃ CN	-125.6	nr	63
[Mn ^{III} ₂ (μ -O) ₂ (bispicMe ₂ en) ₂](ClO ₄) ₂ ·H ₂ O	-86.4	nr	199
[Mn ^{III} ₂ (μ -O)(μ -OAc)(bispicen) ₂](ClO ₄) ₃	19.5	4.21	82
[NaMn ₂ (2-OH-salpn) ₂ (OAc) ₄](C ₂ H ₅ O ₂) ₂ ·2H ₂ O	0	6.31	124
[Mn ₂ (2-OH-salpn) ₂ THF]	-5.5	nr	125
[Mn ^{II} (2-OH(5-NO ₂ -sal)pn) ₂] ²⁻	0.52	nr	123
(TEA)[Mn ^{II} Mn ^{III} (2-OH(5-Cl-sal)pn) ₂]	3.23	nr	123
[Mn ^{III} Mn ^{IV} (2-OH(3,5-Cl ₂ -sal)pn) ₂] ⁺	-2	nr	123
[Mn ^{III} ₂ (2-OH(5-Cl-sal)pn) ₂ (MeOH)]	-3.55	nr	124
[Mn ^{III} Mn ^{IV} (2-OH(3,5-Cl ₂ -sal)pn) ₂ (THF)] ⁺	-10	nr	60
Mn ^{II} ₂ catalase (<i>L. plantarum</i>)	-5.2	nd	47
Mn ^{II} ₂ catalase (<i>L. plantarum</i> , F ⁻)	-1.3	0.094	47
Mn ^{III} ₂ catalase (<i>T. thermophilus</i> , low pH)	-1.8	4.8/4.3	48
Mn ^{III} ₂ catalase (<i>T. thermophilus</i> , high pH)	-100	nd	48

^a nr = not reported (or not accounted for in the spin Hamiltonian).

be considered only a perturbation in the D -splitting levels. When J and D are on the same order of magnitude, treatment of temperature-dependent susceptibility is complicated by spin-orbit coupling contributions ($L \cdot S$). Assuming the same bridging motif, $|J|$ increases on going from Mn^{II}₂ to Mn^{II}Mn^{III} to Mn^{III}₂ to Mn^{III}Mn^{IV} to Mn^{IV}₂. Specific examples of the exchange couplings of dinuclear manganese compounds are given below and in Table 2, with exceptions to this trend noted as appropriate.

Mn^{II}₂ systems are weakly coupled ($J \leq 10$ cm⁻¹), and the ubiquitously observed room-temperature paramagnetism for these compounds is a result of the population of higher spin states according to the Boltzmann distribution. All known Mn^{II}₂ compounds are antiferromagnetically coupled with a diamagnetic ground state; the magnetic moment approaches zero as temperature decreases. Dinuclear Mn^{II}₂ species are known with the following bridging types: (bis- $\mu_{1,3}$ -carboxylato), (μ -O,bis- $\mu_{1,3}$ -carboxylato)₂, (bis- μ -

alkoxo), (μ -alkoxo, $\mu_{1,3}$ -carboxylato), (μ -alkoxo,bis- $\mu_{1,3}$ -carboxylato), (bis- μ -hydroxo), and (μ -aquo, $\mu_{1,3}$ -carboxylato). Given the wide range of bridging motifs—from single to multiple bridges, from water to phenolate—the exchange coupling is remarkably insensitive to structural changes. The Mn^{II}₂ form of the Mn catalase is best structurally modeled by (Mn^{II}tmeda)₂-($\mu_{1,3}$ -OAc)₂(μ -OH₂)(OAc)₂, and yet the exchange coupling for this compound is scarcely different from those of other dinuclear Mn compounds with inappropriate bridging motifs (e.g., [Mn^{II}SALPS]₂).¹²⁶ This example illustrates that magnetic exchange coupling is not an appropriate technique to deduce bridging structures for biological Mn^{II}₂ systems.

A Mn^{II}Mn^{III} form of the *T. thermophilus* Mn catalase has been reported. Unfortunately, detailed magnetic studies on this enzyme form have not been completed. However, an EPR spectrum of this mixed-valence form is known and is most consistent with an antiferromagnetically exchanged system. Exami-

nation of Table 2 illustrates that most $\text{Mn}^{\text{II}}\text{Mn}^{\text{III}}$ complexes are antiferromagnetically coupled, with J values greater than those observed for the Mn^{II}_2 counterparts. Once again, a wide range of bridging atom types and numbers provide similar exchange parameters. Notably different are compounds such as $[\text{Mn}^{\text{II}}\text{Mn}^{\text{III}}(2\text{-OH-(sal)pn})_2]^-$, which exhibits ferromagnetic exchange.¹²³ This is unusual for Mn dimer complexes, and similar $\text{Mn}^{\text{II}}\text{Mn}^{\text{III}}$ dimers¹²⁷ do not always show ferromagnetic exchange.

Many different Mn^{III}_2 dimer complexes have been synthesized with a variety of bridging types and then used to emulate the magnetic behavior seen in the active oxidized manganese catalase. Unfortunately, the system is quite complicated—the catalase has been shown to exist in two forms (one is weakly antiferromagnetically coupled, with $J \approx -1.7 \text{ cm}^{-1}$, and the other is strongly coupled, with $J \approx -100 \text{ cm}^{-1}$),⁴⁸ and the magnetic data are complicated by structural distortions (Mn^{III} is particularly susceptible to Jahn–Teller distortions). In general, ferromagnetic behavior of the dinuclear complexes ($S = 4$ ground state) is related to the degree of compression of the Mn^{III} coordination sphere and antiferromagnetism ($S = 0$ ground state) to the elongation. Thus, Mn^{III}_2 complexes show either ferromagnetic or antiferromagnetic behavior, with J values that commonly fall between ~ -100 and 50 cm^{-1} . The antiferromagnetically coupled complexes have particularly large $|J|$ values, and most of the contributions to J arise from superexchange (the delocalization between the Mn^{III} centers of excess spin electron density). These complexes are therefore particularly sensitive to bridging type.

The sensitivity to bridging type is evident in the case of the $[\text{Mn}^{\text{III}}_2(\mu\text{-O})(\mu\text{-OAc})_2(\text{Me}_3\text{tacn})_2]^{2+}$ and the $[\text{Mn}^{\text{III}}_2\text{O}(5\text{-NO}_2\text{saldien})_2]$ complexes.⁵⁸ The Me_3tacn complex has a $\text{Mn}-\text{O}-\text{Mn}$ angle of 121° and is weakly ferromagnetically exchange coupled ($J = 18 \text{ cm}^{-1}$). As the $\text{Mn}-\text{O}-\text{Mn}$ angle is increased to 168° , the more linear geometry lowers ferromagnetic contributions to the coupling, and subsequently strong ($J = -120 \text{ cm}^{-1}$) antiferromagnetic exchange coupling is evident. For the linear oxo-bridged case, the increase in exchange coupling has been attributed to better overlap between the p_x and p_z orbitals of the oxo bridge with the Mn d_{z^2} and d_{xz} orbitals, which allows for better superexchange along the $\text{Mn}(d_{xz})-\text{O}-\text{Mn}(d_{xz})$ pathway as well as along the $\text{Mn}(d_{yz})-\text{O}-\text{Mn}(d_{yz})$ path. It is possible that, for smaller $\text{Mn}-\text{O}-\text{Mn}$ bond angles, accidental orthogonality of the magnetic orbitals might also lead to an increase in the magnitude of $|J|$. This balance between antiferromagnetic and ferromagnetic contributions is typical of Mn^{III}_2 complexes, hence the broad range of possible J -values, and is seen in magnetic studies of the enzyme as well.

The orientation of the Jahn–Teller axis also influences the magnitude of $|J|$ and the type of exchange coupling that is seen in complexes. Six-coordinate Mn^{III} complexes are subject to Jahn–Teller distortions resulting from the energy lowering that occurs when degeneracy of the partially filled e_g orbitals is broken. Usually, elongation makes the bonds along

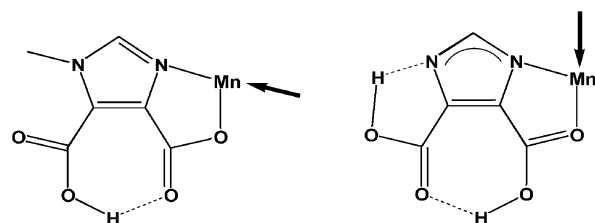


Figure 16. Jahn–Teller axes (indicated by the dark arrow) adopt various orientations with the nonbridging DCBI ligand. Reprinted with permission from ref 128. Copyright 2003 Society of Biological Inorganic Chemistry.

the Jahn–Teller axis $0.2\text{--}0.3 \text{ \AA}$ longer than the bonds equatorial to the axis, and the weakest donors are positioned on the axis. This affects not only the structural properties of the complex but also the magnetic properties. For high-spin Mn^{III} ions, the distortion results in a half-filled d_{z^2} magnetic orbital and an unfilled $d_{x^2-y^2}$ orbital that is nonmagnetic. Therefore, the orbital that forms σ bonds with strong equatorial ligands would not usually be magnetic. Within the group of $\text{Mn}_2(\text{DCBI})_x$ complexes, however,¹²⁸ the Jahn–Teller axis assumes various orientations with respect to the nonbridging DCBI ligand (Figure 16), deviating from the usual placement of weaker donors along the axis according to oxidation state of the bound Mn. The orientations of the d_{z^2} and $d_{x^2-y^2}$ orbitals are therefore realigned and may be able to introduce new magnetic exchange pathways. Thus, the rotating Jahn–Teller axis in this system can influence both magnitude and type of exchange coupling. These types of perturbations are not limited to the monomeric case. The 2-OHsalpn ligand complexes provide a good example of these perturbations in dimers.

The set of $\text{Mn}_2(2\text{-OH}(X\text{-sal)pn})_2$ dimers is interesting on two accounts. First, this series of complexes has been characterized in a variety of oxidation states¹²³ spanning the range Mn^{II}_2 to $\text{Mn}^{\text{III}}\text{Mn}^{\text{IV}}$. Second, these complexes are speciated into symmetric and antisymmetric complexes. Therefore, with very little variation in $\text{Mn}-\text{Mn}$ separation among the complexes in this series,⁷⁰ the 2-OHsalpn models provide an opportunity to study magnetic characteristics of alkoxy-bridged complexes in multiple oxidation states. The $[\text{Mn}^{\text{II}}(2\text{-OH}(5\text{-NO}_2\text{-sal)pn})_2]$ dimer has Jahn–Teller symmetric elongation axes through the bridging alkoxy atoms of the ligand. This may be compared to the Jahn–Teller-distorted $\text{Mn}-\text{alkoxide}$ bond in $[\text{Mn}^{\text{III}}_2(2\text{-OH}(5\text{-Cl}(\text{sal)pn})_2(\text{MeOH}))]$ asymmetric complex. In the latter case, lack of a second bridging ligand allows the $\text{Mn}-\text{O}-\text{Mn}$ angle to increase to 128.9° (as compared to 99.1° for the symmetric dimer). Despite shortened $\text{Mn}-\text{Mn}$ distances and addition of a second alkoxy bridge in the symmetric dimer, the asymmetric dimer is actually slightly more strongly coupled ($J = -3.55 \text{ cm}^{-1}$ vs the symmetric $J = -5 \text{ cm}^{-1}$). Here, the oxo bridge is so far from linear that orthogonal overlap of magnetic orbitals is likely occurring; this trend continues for all asymmetric vs symmetric dimers in the 2-OH(X-sal)pn series of complexes.¹²⁹ Similar magnetostructural correlations have been studied for bridging asymmetrical (μ -phenolato,bis- μ -carboxylato) complexes where the Jahn–Teller axis is oriented along

the Mn–O_{phenoxo} axis; therefore, primary influences on exchange coupling depend primarily on Mn–O bond distance. Smaller values of $-J$ are associated with shorter Mn^{III}–O_{phenoxo} distances which moves the d_z^2 orbital to higher energy and effectively reduces the crossed interactions with the d_z^2 , d_{xz} , and d_{yz} of the second Mn center.¹⁰³ Thus, a combination of Jahn–Teller orientation, orbital overlap, bridge angle and species, and Mn–Mn distance contributes to the net exchange interaction in these dimeric systems.

Probably the most thoroughly studied dinuclear manganese systems are the high-valent species containing Mn^{IV}. We will discuss both Mn^{III}Mn^{IV} and Mn^{IV}₂ complexes; the only compounds relevant to the Mn catalases, however, are the mixed-valent ones, and these compounds are only of interest for defining the superoxidized, catalytically inactive form of these enzymes. The primary interest in Mn^{IV} compounds relates to water oxidation chemistry that has been known for over 20 years to contain a mixed-valent cluster composed of Mn^{III} and Mn^{IV}. Readers interested in this chemistry are referred to a review by Armstrong et al.²³⁰

As described in the structural section of this article, the types of bridging motifs that support dinuclear Mn^{IV} compounds are more limited than for lower valent complexes. These bridges are limited primarily to oxo, hydroxo, or alkoxide cores. Occasionally carboxylate groups are also present, especially in the case of the Mn^{III}Mn^{IV} structure types. In nearly every case, these systems are strongly antiferromagnetically coupled. Typical J values are on the order of -100 cm^{-1} ; however, the range can be from as little as -10 to well over 200 cm^{-1} . Several general trends have emerged from these studies. Typically there is larger exchange coupling as the metal–metal separation decreases; however, there is no direct trend that describes this behavior.¹²⁹ Wieghardt has shown in a fascinating tri- μ_2 -oxo structure¹³⁰ that extremely large $|J|$ values can be obtained ($\sim 780\text{ cm}^{-1}$) with compounds with very short Mn–Mn separations of 2.29 \AA . The origin of the strong exchange coupling in this Mn^{IV}₂ (μ -O)₃(Me₃tacn) system is not a result of direct Mn–Mn bonding as the extremely short Mn–Mn separation might suggest; rather it appears to be a consequence of short Mn–O distances and good angular overlap between Mn and oxygen atoms for superexchange pathways. The vast majority of di- μ_2 -oxo complexes, whether Mn^{III}Mn^{IV} or Mn^{IV}₂, have $|J|$ values in the range of $75\text{--}140\text{ cm}^{-1}$. Law et al. have shown that the best trend for describing the magnitude of exchange coupling in these antiferromagnetic systems¹²⁹ is found by examining the Mn–O–Mn angle and that Mn–O distances are a smaller contributor to the magnetic exchange.

Invariably, hydroxo- or alkoxo-bridged systems have significantly reduced superexchange as compared to oxo-bridged species. Baldwin et al. demonstrated that protonation or alkylation of oxo-bridged species led to an $\sim 0.1\text{ \AA}$ increase in Mn–Mn separation per protonation,¹³¹ however, the magnetic exchange coupling dropped precipitously starting at -92 cm^{-1} for the di- μ_2 -oxo dimer, [Mn^{IV}(μ_2 -O)(salpn)]₂, moving to -48 cm^{-1} for the monoprotated

species and -6 cm^{-1} for the doubly protonated complex.⁷² Similar behavior is seen for compounds prepared solely using bridging alkoxides. In fact, the first very weakly exchange-coupled Mn^{III}Mn^{IV} and Mn^{IV}₂ di-(μ_2 -OR) dimers that were prepared, [Mn^{III}–Mn^{IV}(2-OH–(sal)pn)₂]⁺ and [Mn^{IV}(2-OH–(sal)pn)₂]²⁺, had J values on the order of -10 cm^{-1} and exhibited unique EPR signals. In these cases, the Mn–Mn separation is considerably larger than in the di-(μ_2 -O) complexes. Ferromagnetic exchange between Mn^{III}–Mn^{IV} or Mn^{IV}₂ compounds is extremely rare.

Mn^{IV}₂ dimers are known and typically exhibit fairly strong antiferromagnetic coupling; there is an example, however, of ferromagnetic coupling between Mn^{IV} centers.^{130,132} The tetramer [Mn^{IV}₄O₆(tacn)₄]⁴⁺ possesses Mn–Mn separation distances of about 3.22 \AA between the four Mn centers. These four centers occupy the corners of an idealized tetrahedron with bridging oxo groups oriented so that the [Mn₄O₆]⁴⁺ core emulates an adamantane-like structure. The facially binding tacn ligand completes the distorted octahedral environment about each Mn^{IV}. This complex has been shown to have weak ferromagnetic coupling, which is extremely rare. It should be noted that, while these complexes provide insight into the magnetic behavior of dinuclear Mn^{IV} systems, this oxidation state formulation is not relevant to the manganese catalases. (Tetranuclear Mn systems such as this have more in common with the water-splitting PS II enzyme).

Given the trend that replacing oxo bridges with alkoxides dramatically decreases antiferromagnetic exchange, one might deduce that, at the proper bridging angles, ferromagnetic exchange might prevail. Such a case has been reported¹³³ for Ba₂[Mn^{III}₂–(β -D-ManH₋₅)₂], which has a reported $J = +19\text{ cm}^{-1}$. Unfortunately, there is little experimental detail given on this compound, and we do not know its magnetization behavior or whether it is EPR active. A much better defined example of a ferromagnetic Mn^{III}Mn^{IV} occurs with [Mn^{III}Mn^{IV}salpn₂(DCBI)]. This compound has an imidazolate bridging the two Mn ions. Other imidazolate species in this series ([Mn^{III}₂–salpn₂(HDCBI)], [Mn^{III}₂salpn₂(DCBI)]⁻, and [Mn^{IV}₂–salpn₂(DCBI)]⁺) exhibited weak antiferromagnetic exchange interactions;^{134,135} this Mn^{III}Mn^{IV} compound, however, had $J = +2\text{ cm}^{-1}$. Magnetization curves confirmed the $S = 7/2$ ground state, and EPR spectra exhibited the first excited-state multiline feature from a Mn^{III}Mn^{IV} dimer. It should be noted that this compound has no direct structural or magnetic relevance to the Mn catalases; however, such bridging imidazolate motifs are known in metalloenzymes, with the CuZn superoxide dismutase being a prime example.

Solomon and co-workers have reported on the magnetic circular dichroism (MCD) of the superoxidized Mn^{III}Mn^{IV} form of the manganese catalase from *L. plantarum*.^{43,44} Evidence obtained from these experiments suggests a weakly coupled site which was attributed to five-coordinate manganese centers that were μ -hydroxo- and μ -carboxylato-bridged. These findings were disputed by Whittaker and co-workers,⁸¹ who proposed a strongly coupled active site that

was six-coordinate with μ -oxo/ μ -hydroxo and μ -carboxylato bridges; the weakly coupled species was suggested to occur due to oxidative damage. Latour and co-workers re-examined the previous data and, on the basis of their magnetic susceptibility data, concluded that both strongly and weakly coupled species exist in the manganese catalase^{48,81} and are highly dependent on pH. In fact, titration of the catalase sample in the pH range between 6.8 and 8 shows interconversion of the two forms, the magnitude of pH variation being the determinant for the percentages of strongly and weakly coupled forms present in the sample. Addition or removal of anion inhibitors⁴⁷ such as Cl^- and F^- may also result in stronger or weaker coupling.

One explanation for the pH dependence of the enzyme is that protonation/deprotonation of the bridging species plays a critical role in magnetic behavior in addition to exchange behavior exhibited by the different bridging types; for example, protonation of the bridges as discussed previously with the 2-OHsalpn complexes results in decreasing $|\mathcal{J}|$. In addition, the different bridging species themselves may affect the type and magnitude of exchange coupling in these complexes. This can be seen upon examination of the bridging species included in Table 2; in general, the presence of oxo bridges increases the magnitude of $|\mathcal{J}|$. This is clearly seen with the tacn and Me_3tacn series of complexes. Thus, it is important to examine models that exhibit both strong and weak exchange coupling as well as to address how anion inhibitors can affect coupling parameters.

4.3. Absorption Spectroscopy

Significant features in the UV–visible and MCD spectra are present only in the oxidized Mn^{III}_2 and superoxidized $\text{Mn}^{\text{III}}\text{Mn}^{\text{IV}}$ forms of the enzyme. The lower valent enzyme forms contain Mn^{II} , which has both spin- and symmetry-forbidden electronic transitions; therefore, the electronic spectra of these enzymes and complexes lack visible absorption bands. Neither are there significant charge-transfer bands observed for Mn^{III}_2 or $\text{Mn}^{\text{II}}\text{Mn}^{\text{III}}$ enzymes. The most intense bands in the visible spectroscopy of manganese complexes are d–d transitions and charge-transfer bands. The charge-transfer excitations (ligand-to-metal) are relatively insensitive to minor structural changes, so the visible spectra of polynuclear and mononuclear complexes with the same ligands are very similar. The enzymes, however, show low-energy absorption bands (5000–10 000 cm^{-1}) which are not usually seen in the model complexes. These transitions have been assigned to chromophores that are five-coordinate in a trigonal bipyramidal geometry. X-ray crystallographic analyses of the MnCat enzymes also suggest the possibility of a five-coordinate site and are in accord with these findings. Features in the absorption spectra of *T. thermophilus* catalase also include an intense absorption band at 450 nm with a shoulder at 500 nm; in the *L. plantarum* enzyme, the peak is shifted to 470 nm but retains the 500 nm shoulder and shows an additional shoulder at 398 nm.^{1,5} Anion binding affects these features significantly (Figure 17).⁴⁴

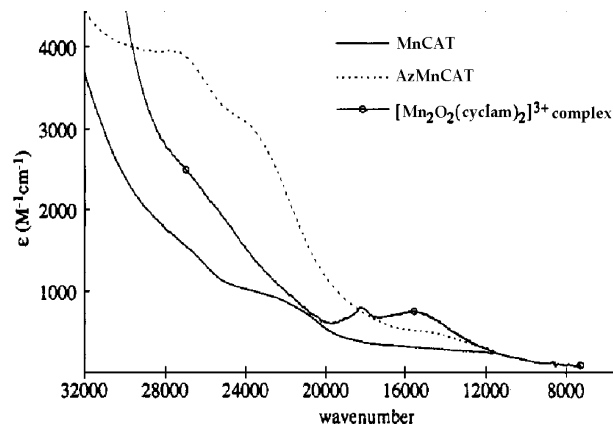


Figure 17. Room-temperature absorption spectrum for LPC and azide-bound LPC as compared to a sample model complex. Reprinted with permission from ref 44. Copyright 1994 American Chemical Society.

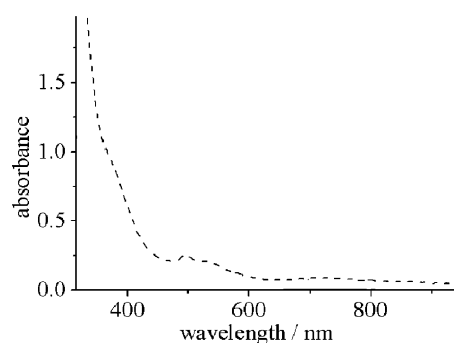


Figure 18. Absorption spectrum for the $[\text{Mn}^{\text{III}}_2(\text{bpia})_2(\mu\text{-O})(\mu\text{-OAc})](\text{ClO}_4)_3$ complex. Reprinted with permission from ref 67. Copyright 2002 American Chemical Society.

The oxo,carboxylato core is accepted as an important feature for the catalases as well as for other dinuclear manganese and iron enzymes. This core is proposed on the basis of comparisons of the electronic spectrum obtained for the *L. plantarum* enzyme to those of $[\text{Mn}^{\text{III}}_2\text{O}(\mu\text{-O}_2\text{CCH}_3)_2(\text{HB}(\text{pz})_3)_2]$ and similar complexes.^{87,89} The $[\text{Mn}^{\text{III}}_2\text{O}(\mu\text{-O}_2\text{CCH}_3)_2(\text{HB}(\text{pz})_3)_2]$ complex shows a band at 486 nm with two shoulders located at 385 and 503 nm; another band shows up at 760 nm. These features bear remarkable similarities to features seen in the oxidized catalase enzymes (with respect to location of the visible transitions as well as extinction coefficients). The tacn complex $[\text{Mn}^{\text{III}}_2(\mu\text{-O})(\mu\text{-OAc})_2\text{tacn}_2]^{2+}$ is another example that supports an oxo,carboxylato core, showing two visible absorptions at 486 and 521 nm. These absorptions have extinction coefficients $\epsilon = 337$ and $323 \text{ M}^{-1} \text{ cm}^{-1}$, respectively. Other complexes also show similar absorption features that are in good agreement with the spectrum reported for the Mn^{III}_2 form of *T. thermophilus* enzyme (which has a band at 492 nm and a broad tail that trails into the near-IR). These include $[\text{Mn}^{\text{III}}_2(\text{bpia})_2(\mu\text{-O})(\mu\text{-OAc})](\text{ClO}_4)_3 \cdot \text{CH}_3\text{CN}$, which shows d–d transitions (Figure 18) at 495 ($524 \text{ L} \cdot \text{mol}^{-1} \cdot \text{cm}^{-1}$) and 527 nm ($418 \text{ L} \cdot \text{mol}^{-1} \cdot \text{cm}^{-1}$) as well as a broad absorption feature at 711 nm ($176 \text{ L} \cdot \text{mol}^{-1} \cdot \text{cm}^{-1}$),⁶⁷ and other $\mu\text{-O}, \mu\text{-OAc}$ complexes such as $[\text{Mn}^{\text{III}}_2(\text{TMIMA})_2(\mu\text{-O})(\mu\text{-OAc})](\text{ClO}_4)_3 \cdot 2\text{CH}_3\text{CN}$ and $[\text{Mn}^{\text{III}}_2(\text{bispicen})_2(\mu\text{-O})(\mu\text{-OAc})](\text{ClO}_4)_3$.

The $\text{Mn}^{\text{III}}_2(\mu\text{-oxo})(\mu\text{-carboxylato})_2$ formulation is not the only core that might produce such spectral

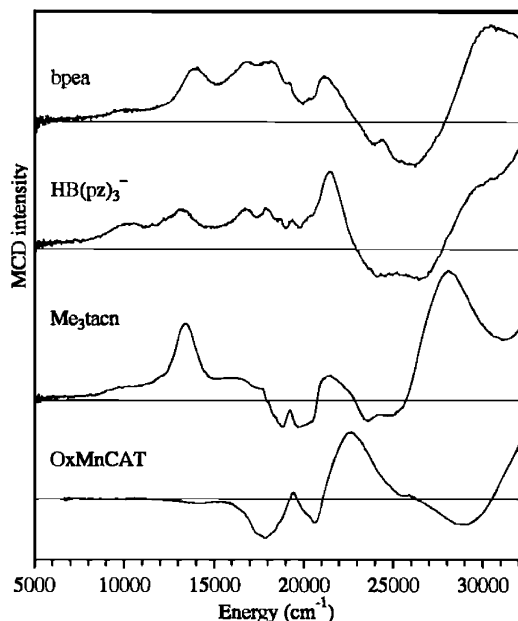


Figure 19. Comparison of the MCD spectra of oxidized MnCat and model complex. Reprinted with permission from ref 43. Copyright 1998 American Chemical Society.

absorption features, however. The electronic spectra obtained from the catalases are also a good match to complexes with $\text{Mn}^{\text{III}}\text{Mn}^{\text{IV}}(\mu\text{-oxo})(\mu\text{-carboxylato})_2$ cores. For example, $[(\text{Me}_3\text{tacn})\text{Mn}^{\text{IV}}(\mu\text{-O})_2(\mu\text{-OAc})\text{Mn}^{\text{III}}(\text{OAc})_2]$ also exhibits similar features. Therefore, these early model complexes effectively showed that the absorption bands seen in the enzyme were indicative of complexes with $\text{Mn}^{\text{III}}_2(\mu\text{-oxo})(\mu\text{-carboxylato})_2$ or $\text{Mn}^{\text{III}}\text{Mn}^{\text{IV}}(\mu\text{-oxo})_2(\mu\text{-carboxylato})$ cores. Thus, a multitude of complexes with oxo/hydroxo/aqua-bis-carboxylato, bis-oxo/hydroxo/aqua-monocarboxylato cores have been studied; some of these have been discussed in a previous section. Other spectroscopies (such as MCD) and subsequent crystallographic analyses have supported the primary bridging motifs suggested by these model complexes.

MCD spectroscopy has also been utilized to elucidate electronic as well as magnetic properties of the inorganic complexes. MCD may provide information on both excited and ground states. Room-temperature studies give excited state information and, because the selection rules for MCD and absorption spectroscopies are distinctly different, provide a complementary approach for evaluating UV-vis data. Variable-temperature MCD studies can be utilized for elucidating band assignments (assigning electronic transitions). In addition, MCD is particularly amenable to identifying electronic transitions from paramagnetic centers and for estimating g -values, spin state, zero-field-splitting parameters, and magnetic coupling constants. Therefore, use of MCD spectroscopy can enhance the information obtained from EPR experiments.

A comparison of the MCD spectra from oxidized MnCat⁴³ against those obtained for $(\mu\text{-O}, \text{di-}\mu\text{-carboxylato})$ -bridged model complexes and MnSOD (Figure 19) suggests that the OxMnCat bears structural similarities to the five-coordinate trigonal bipyramidal active site of the MnSOD. Studies of model

complexes have provided insight into the low-energy absorption bands which can provide coordination number information. The bands that appear between 5000 and 10 000 cm^{-1} are usually indicative of Mn^{III} in a six-coordinate geometry; the oxidized manganese catalase MCD spectra lack these absorption features and therefore may be formulated as two five-coordinate centers. Also of significance is the high intensity of the absorption band at 21 000 cm^{-1} in the MnCat spectra which is not indicative of an oxo bridge and is usually seen in five-coordinate Mn^{III} complexes. The striking dissimilarities in the spectra of the model complexes (bands at 10 000 and 13 000 cm^{-1} in the complexes compared to 14 500 cm^{-1} in OxMnCat) are due to the bridging O species. Thus, from MCD data alone, the active site of MnCat consists of two five-coordinate Mn^{III} ions bridged by two carboxylates and a weaker oxo bridge (such as hydroxide or water).

Closer examination of MCD saturation magnetization curves for the oxidized enzyme would suggest that the two Mn^{III} ions in the active site are ferromagnetically or weakly antiferromagnetically coupled. Analysis of model complexes with various bridging core structures has allowed exclusion of $\text{di-}\mu\text{-O}$ and $\text{di-}\mu\text{-alkoxo}$ cores which have J values of about -90 and -20 cm^{-1} , respectively. From these data, formulation of the catalase active site was proposed to be a $\text{di-}\mu\text{-O}, \mu\text{-carboxylato}$ core. This formulation is further supported by recent high-resolution crystal structures³¹ that would suggest two oxo-type bridges and one to two carboxylate bridges in the active site; the presence of five-coordinate centers (Figure 20) can also be seen (one of the Mn sites is ligated to an additional water molecule). Thus, a comparison of magnetic data from both model complexes and the enzyme has provided structural information about the enzyme active site and effectively excluded particular structural types from consideration.

4.4. EPR Spectroscopy

A comparison of the electron paramagnetic resonance (EPR) spectra of the Mn catalases and small-molecule model compounds provided the first insight into the active-site structure of these enzymes. The Mn^{II}_2 , $\text{Mn}^{\text{II}}\text{Mn}^{\text{III}}$, and $\text{Mn}^{\text{III}}\text{Mn}^{\text{IV}}$ oxidation states of the enzyme are observable at X-band frequencies (9.3 GHz), and the spectra are consistent with a dinuclear Mn center. These spectra are sufficiently different to allow the assignment of oxidation states to the manganese ions. Furthermore, one can extract precise metrical separations between the manganese ions in the fully reduced enzyme. Thus, EPR spectroscopy has been an important technique for early assessments of active-site structure and substrate binding. Crystallography subsequently proved that these assignments were correct (this is true not only for the Mn catalases but also for the structurally similar active site of arginase).

Dinuclear manganese complexes give characteristic X-band EPR spectra depending on metal oxidation states, ligation environment, and the nature of the bridging ligands, which determines the degree of exchange coupling between the metal ions. The⁵⁵⁻

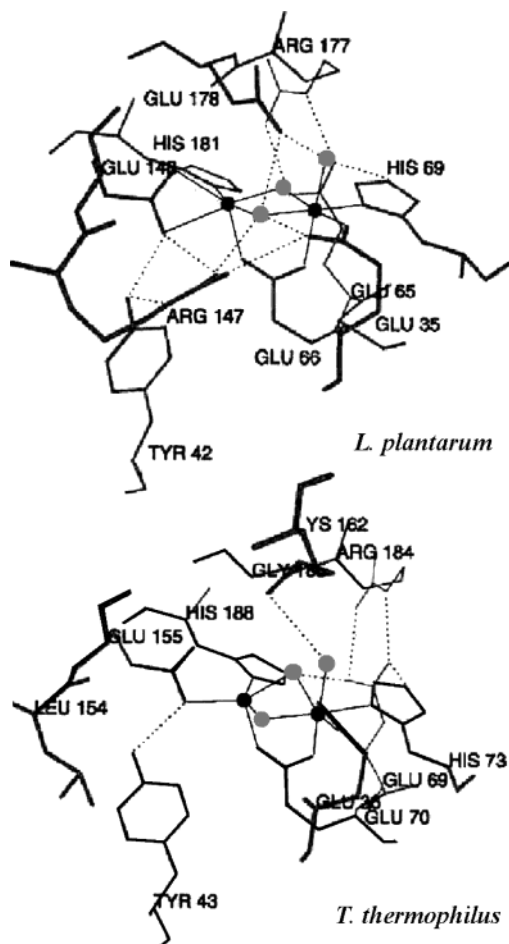


Figure 20. Active sites of LPC and TTC from a recent high-resolution crystal structure. Reprinted with permission from ref 31. Copyright 2001 Elsevier.

Mn isotope has a nuclear spin, I , of $5/2$. Mononuclear Mn^{II} compounds, which have $(2I+1)$ hyperfine lines, show a six-line spectrum centered around 3500 G ($g \approx 2$). For multinuclear systems with n Mn ions, however, as many as 6^n lines may be observed, giving rise to rich spectroscopic signatures. The magnitude of the observed hyperfine splitting is oxidation state dependent, so the width of the observed transitions, and hence the ultimate pattern of the spectrum, can be diagnostic for specific structure types. EPR is a particularly sensitive technique capable of detecting intramolecular exchange couplings as small as 0.001 cm^{-1} , as opposed to magnetic susceptibility studies which detect electronic interactions as small as a wavenumber.

Although integral spin systems are not usually seen using perpendicular mode detection, Mn^{II}_2 complexes are an exception. The manganese(II) ions are always antiferromagnetically coupled ($J < 10 \text{ cm}^{-1}$) in these systems. This leads to a spin ladder, from $S = 0$ to $S = 5$, which has small energy separations between states. Therefore, even at temperatures less than 40 K, the EPR spectra for these Mn^{II}_2 dimers can be quite complex. Often there are four broad transitions, each of which can be composed of an 11-line hyperfine structure, although usually only one or two sets of hyperfines can be resolved. One expects 11 lines from a homovalent Mn dimer on the basis of the equation $2(2)I + 1$. In addition, the measured

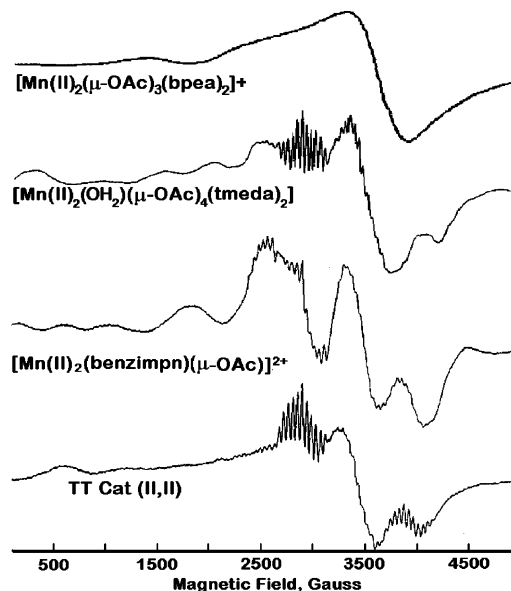


Figure 21. EPR spectra of Mn^{II}_2 complexes. Reprinted with permission from refs 45, 84, 92, and 191. Copyright 1990 Elsevier, and copyright 1994, 2000, and 2002 American Chemical Society.

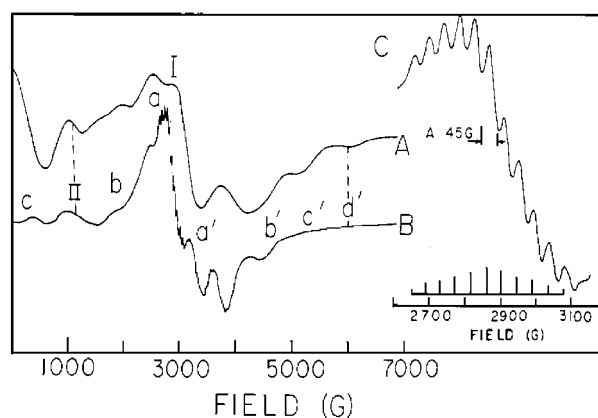


Figure 22. EPR spectra of $[Mn^{II}_2(\text{benzimpn})]$ with assigned hyperfine transitions. Reprinted with permission from ref 136. Copyright 1987 American Chemical Society.

hyperfine coupling constant is one-half of the value observed for a monovalent ion of the same oxidation state. Representative Mn^{II}_2 EPR spectra are found with the complexes $[Mn^{II}_2(2\text{-OHbenzimpn})(\mu\text{-OAc})]^{2+}$ and $[Mn^{II}_2(2\text{-OH}(5\text{-NO}_2\text{sal})\text{pn})_2]^{2+}$ as well as $[Mn_2(\mu\text{-OH}_2)(\mu\text{-OAc})_2(\text{tmeda})_2](\text{OAc})_2$ and $[Mn^{II}_2(\mu\text{-O}_2\text{CCH}_3)_3\text{-}(bpea)_2](\text{PF}_6)$. The spectral features of the model complexes may be compared favorably in some cases to the EPR spectrum of the *T. thermophilus* enzyme, shown in Figure 21, although a spectroscopic match to the enzyme has yet to be made.

Detailed interpretation of spectra from models or enzyme is complicated by the multiple excited states that are populated even at low temperatures. The EPR spectrum of $Mn^{II}_2(\text{benzimpn})$ is shown as Figure 22 with indexed hyperfine transitions.¹³⁶ Typically single-value decomposition methods are used to deconvolute each of the spectra that arise from the different paramagnetic states. Spectral simulations are achieved by preparing a Boltzmann-weighted spectrum on the basis of the J value of the complex and the extracted spectra for each paramagnetic

Table 3. X-ray Crystallographic and EPR ZFS Data for Mn^{II}₂ Centers

Mn ^{II} ₂ pair in:	<i>r</i> (Mn–Mn), Å		ref
	X-ray	ZFS	
MgO	3.06	3.07	200–203
CaO	3.32	3.31	200, 201
(CH ₃) ₄ NCdCl ₃	3.26	3.25	204
Mn ₂ (<i>μ</i> -OAc)(benzimpn)] ²⁺	3.54	3.57	35, 84, 157
Mn ₂ Cl ₃ (benzimpn)		3.63	35, 84, 157
[(HL) ₂ Mn ₂ (<i>μ</i> -OH)] ⁺	3.66 ^a	3.65	205
MnCat	3.6 ± 0.3 ^b		17
MnCat(Ph)		3.59	35
arginase (+borate)		3.50	35
arginase (–borate)		3.57	
		3.52	
		3.36	

^a L = 4,7-bis(2-hydroxybenzyl)-1-oxa-4,7-diazacyclononane, Mn–Mn distance derived from Zn-substituted complex. ^b Mn–Mn distance obtained from X-ray analysis for single crystal soaked in ammonium sulfate. Reproduced with permission from ref 35. Copyright 1995 American Chemical Society.

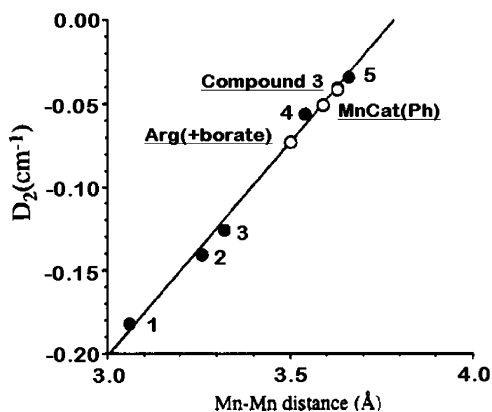


Figure 23. Correlation (solid line) between the crystallographically determined Mn–Mn distance and the EPR-determined ZFS of the quintet D_2 state for five samples. Points 1, 2, and 3 are for Mn^{II}₂ pairs in crystal lattices of MgO, (CH₃)₄NCdCl₃, and CaO, respectively. Points 4 and 5 correspond to the [Mn₂(CH₃CO₂)benzimpn](ClO₄)₂ and [Mn₂(*μ*-OH)(benzimpn)](ClO₄) compounds. Open circles indicate (Mn₂Cl₃benzimpn) compound 3, MnCat(Ph), and Arg(+borate). Reprinted with permission from ref 35. Copyright 1995 American Chemical Society.

state. Once such a simulation is achieved, the zero-field splitting for the $S = 2$ level ($D_{S=2}$) may be used to assess quantitatively the Mn–Mn separation. For the case of Mn^{II}₂(benzimpn), an estimate for the Mn–Mn separation of ≥ 3.2 Å was determined. Subsequent work examining a broader range of model compounds provided excellent determinations of the Mn–Mn separations for the Mn catalases and arginase; these are shown in Table 3.³⁵ An excellent correlation, shown in Figure 23, exists between the crystallographically determined Mn–Mn separations and the magnitude of the $D_{S=2}$. These workers further examined the relationship between the exchange integral J and structure type for 30 Mn^{II}₂ compounds (Table 4). On the basis of this analysis, a reasonable active-site structure for both Mn catalase and arginase enzymes was obtained. An alternative approach for determining Mn–Mn distances using the temperature dependence of X- and Q-band spectra has recently been reported. Additionally, one can directly

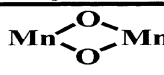
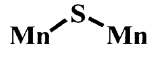
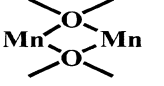
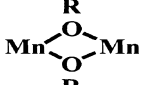


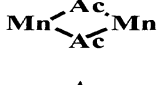
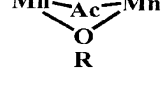
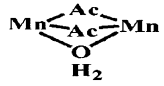


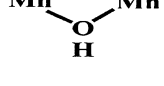
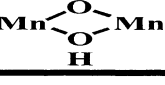
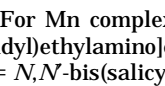
determine the sign of the zero-field-splitting parameter for each paramagnetic state in this manner.^{137,138}

Unlike the reduced Mn^{II}₂ catalases, the catalytically active high-valent Mn^{III}₂ form is typically EPR silent. However, in the presence of reductants, two other oxidation levels have been detected. The *T. thermophilus* enzyme can form a Mn^{II}Mn^{III} state while, for reasons unknown, the *L. plantarum* enzyme cannot. If the centers are antiferromagnetically coupled, they will have an $S = 1/2$ ground state which gives a characteristic EPR spectrum centered at $g = 2$. The maximum number of isotropic hyperfine lines is given as $[2(I + 1)_{\text{Mn(II)}} \cdot 2(I + 1)_{\text{Mn(III)}}]$. Unlike the case for homovalent dimers, where the a -values are equal for both ions, this mixed-valent state can exhibit between 16 and 36 hyperfine lines, depending on the relative values for $a_{\text{Mn(II)}}$ and $a_{\text{Mn(III)}}$. The EPR spectrum of the compound [Mn^{II}Mn^{III}(2-OHbenzimpn)(*μ*-OAc)]³⁺ is characteristic of antiferromagnetically coupled complexes at this oxidation level (Figure 24). One or two examples of ferromagnetically coupled compounds are known;^{123,127} the EPR spectra, however, of these complexes are quite different from those observed for the Mn catalases (e.g., having significant low-field features typical of an $S = 7/2$ state). This observation further confirms the antiferromagnetically coupled nature of catalase enzymes in the Mn^{II}-Mn^{III} oxidation level.

The antiferromagnetically coupled Mn^{II}Mn^{III} complexes usually exhibit a spectral range of about 1300–1400 G, compared to the more oxidized Mn^{III}-Mn^{IV} mixed dimers which have a spectral range of 1150 G. This decrease in spectral width is attributed to the inherent hyperfine coupling constant for Mn^{IV}, which is usually significantly less than that for Mn^{II}. The Mn^{III}Mn^{IV} compounds are, in most cases, strongly antiferromagnetically coupled, with $|J| > 100\text{cm}^{-1}$. These complexes also have an $S = 1/2$ ground state, but most excited states are too high in energy to be significantly populated at liquid helium temperatures. The Mn^{III}Mn^{IV} complexes also give distinct 16-line spectra (Figure 25); because there have been several detailed explanations of the EPR spectra for Mn^{III}Mn^{IV} with large J coupling, we will refer interested readers to these excellent articles. The EPR spectral data for the superoxidized manganese catalase are most consistent with a strongly coupled Mn^{III}Mn^{IV}(*μ*-O)₂ core.

EPR spectroscopy has long been used to identify the different manganese oxidation states.^{37,114,139} There are, however, complexes that behave differently than what is usually seen.⁸¹ For example, not all dimanganese(III/IV) complexes are necessarily strongly coupled; the 12-line spectrum of [Mn^{III}Mn^{IV}(2-OHsalpn)₂]⁺ shown as Figure 26A is unique in that no biological samples have been found that exhibit this modified multiline. More recently, EPR spectral simulations have been applied to this compound⁴⁰ in order to extract a variety of parameters to explain these complex multiline features. This approach can account for the anisotropy of hyperfine interactions, weak exchange couplings, and other properties that would affect typical Mn^{II}Mn^{III} and Mn^{III}Mn^{IV} multiline spectra.^{114,139} Another rare EPR spectrum for a

Table 4. Exchange Integrals J for Different $Mn_2(II,II)$ Dimers ($H = -2 JS_1 \cdot S_2$)^a

Compound ^b		J (cm ⁻¹)	r (Å)	M-O-M (°)	Reference
	in MgO in MnO in CaO	<u>bis(μ-O)</u>			
		-10.5	3.06		
		-6.9	3.13	90	
Mn-O-Mn	in MgO in CaO	<u>μ-O</u>			200,201
		-19.6	4.3	180	
	in MgO in CaO	<u>μ-S</u>			
		-3	4.45		
	[Mn(¹ L)Cl(CH ₃ OH)] _n	<u>μ-thiolate</u>		127.7	206
		-7.8	4.67		
	Mn ₆ O ₂ (O ₂ CPh) ₁₀ (py) ₂ (MeCN) ₂	<u>bis(μ₄-O²⁻)</u>		117.4, 119.9	207
		-2.4	3.8		
	[Mn ₂ (² L) ₂ (THF) ₂](ClO ₄) ₂ [Mn ₂ (³ L) ₂ (NCS) ₂] [Mn(⁴ L)] ₂ [Mn(⁵ L)] ₂ [Mn(⁶ L)CH ₃ CN] ₂ [Mn ₂ (⁷ L) ₂ Cl ₂] [Mn ₂ (⁸ L)Cl ₂] [Mn ₂ (⁹ L)(CH ₃ CO ₂) ₂]	<u>bis(μ-phenoxo)</u>			
		> -0.18	3.256	99.9	208
			3.422	104.1	209
		-0.63			210
		-1.88	3.3	101.2	126
			3.205	93.6	88,127
		+0.24	3.324	103.2	211
		+0.2			212
			3.34	103.6	213
			[Mn ₂ (¹⁰ L)(μ-CH ₃ CO ₂) ₃] ⁺	<u>tris(μ-carboxylato)</u>	
-1.7	4.034				
	dimanganese Concavalin A [Mn ₂ (C ₃ F ₇ CO ₂) ₄ (bipy) ₂]	<u>bis(μ-carboxylato)</u>			
		-1.8	4.25		214
	[Mn ₂ (¹¹ L)(CH ₃ CO ₂) ₂] ⁺ [Mn ₂ (¹¹ L)(PhCO ₂) ₂] ⁺ [Mn ₂ (¹² L)(CH ₃ CO ₂) ₂] ⁺ [Mn ₂ (¹³ L)(NCS)(CH ₃ CO ₂) ₂]	<u>(μ-phenoxo)bis(μ-carboxylato)</u>			
		-4.9			216,217
	[Mn ₂ (¹⁴ L)(F ₃ C ₂ CO ₂) ₄ (H ₂ O) ₃] [Mn ₂ (H ₂ O)(piv) ₄ (Me ₂ bpy) ₂ [Mn ₂ (H ₂ O)(CH ₃ CO ₂) ₄ (¹⁵ L) ₂] [Mn ₂ (¹⁶ L)(NCS)(CH ₃ CO ₂) ₂]	<u>(μ-H₂O)bis(μ-carboxylato)</u>			
		-1.65	3.739	114.6	220
	[Mn ₂ (¹⁷ L) ₂ (μ-OH)] ⁺	<u>(μ-hydroxo)bis(μ-carboxylato)</u>			
		-2.73	3.595	110.2	88
	[Mn ₂ (¹⁸ L)(m-OH)(m-CH ₃ CO ₂) ₂] ⁺	<u>(μ-alkoxo)(μ-carboxylato)(μ-phenoxo)</u>			
		-2.952	3.621	110.0	88
	[Mn ₂ (¹⁹ L) ₂ (μ-OH)] ⁺	<u>(μ-alkoxo)(μ-carboxylato)(μ-phenoxo)</u>			
		-3.8			219
	[Mn ₂ (¹⁷ L) ₂ (μ-OH)] ⁺	<u>μ-hydroxo</u>			
		-2.65			205
	[Mn ₂ (¹⁸ L) ₂ (OH) ₂]	<u>bis(m-hydroxo)</u>			
			3.314	104.8	59,61

^a For Mn complexes in Mn₂(II,III) and Mn₂(III,IV) redox states, see ref 222. ^b Ligands (ⁱL, *i* = 1, 2, 3, ...): ¹L = 2-[2-(2-(2-pyridyl)ethylamino)ethanol]; ²L = *o*-(bis(2-(1-pyrazolyl)ethyl)amino)phenol; ³L = 2-[bis(2-pyridylmethyl)aminomethyl-4-nitrophenol]; ⁴L = *N,N*-bis(salicylidene)-1,7-diamino-3-azapentane; ⁵L = *N,N'*-(1,1')dithiobis(phenylene)]bis(salicylideneaminato); ⁶L = 2-(bis(salicylideneamino)methyl)phenol; ⁷L = Schiff base of 1,3-diaminopropane and 2 mol of 2,6-diformyl-4-*tert*-butylphenol; ⁸L = Schiff base of 1,3-diaminopropane and 2 mol of 2,6-diformyl-4-methylphenol; ⁹L = Schiff base of 1,3-diamino-2-hydroxypropane and 2 mol of 2,6-diformyl-4-methylphenol; ¹⁰L = *N,N,N'*-trimethyl-1,4,7-triazacyclononane; ¹¹L = 2,6-bis[bis(2-pyridylmethyl)aminomethyl]-4-methylphenol; ¹²L = 2,6-bis[bis(2-(2-pyridyl)ethyl)amino)methyl]phenol; ¹³L = 2,6-bis[*N*-(2-pyridylethyl)iminomethyl]-4-methylphenol; ¹⁴L = 2-ethyl-4,4,5,5-tetramethyl-3-oxo-4,5-dihydro-1*H*-imidazolyl-1-oxyl; ¹⁵L = *N,N,N,N*-tetramethylethylenediamine; ¹⁶L = 2,6-bis[2-(diethylamino)ethylaminomethyl]-4-methylphenolate; ¹⁷L = 4,7-bis(2-hydroxybenzyl)-1-oxa-4,7-diazacyclononane; ¹⁸L = hydrotris(3,5-diisopropyl-1-pyrazolyl)borate. Reproduced with permission from ref 35. Copyright 1995 American Chemical Society.

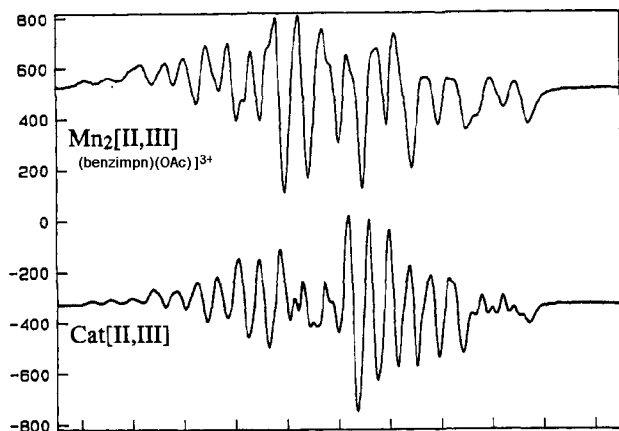


Figure 24. $\text{Mn}^{\text{II}}\text{Mn}^{\text{III}}$ EPR spectra of benzimn complex and Ttcatalase. Reprinted with permission from ref 84. Copyright 1994 American Chemical Society.

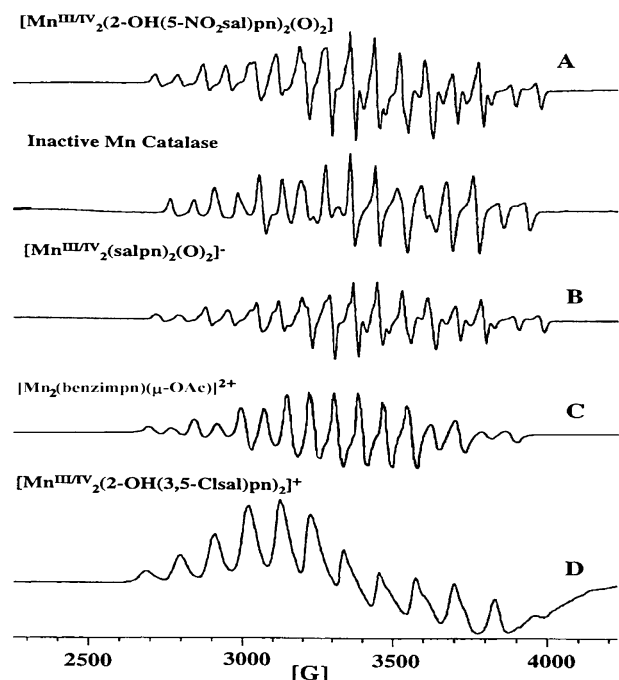


Figure 25. Comparison of EPR spectra from various $\text{Mn}^{\text{III}}\text{Mn}^{\text{IV}}$ model complexes. Adapted from refs 84 and 151. Copyright 1994 American Chemical Society.

$\text{Mn}^{\text{III}}\text{Mn}^{\text{IV}}$ complex is shown as Figure 26B for the imidazolate bridged compound $[\text{Mn}^{\text{III}}\text{Mn}^{\text{IV}}(\text{salpn})_2(\text{DCBI})]$. This compound is one of only two ferromagnetically coupled $\text{Mn}^{\text{III}}\text{Mn}^{\text{IV}}$ molecules. The most important aspects of this spectrum are the low-field features indicative of $S > 1/2$ spin systems and the appearance at higher temperature of a $g = 2$ multiline feature that is assigned to an excited-state $S = 1/2$ spin manifold. While this spectrum is not relevant to the Mn catalases or arginase, the low-field features bear a striking resemblance to the infrared-induced low-field signature of the S_2 state of the OEC. The final example that we will give on "aberrant" EPR spectra for Mn dimers is that of weakly exchange coupled Mn^{IV}_2 species. Similar to Mn^{III}_2 complexes, one expects Mn^{IV}_2 to be EPR silent because of the strong exchange coupling. However, two recent examples of Mn^{IV}_2 complexes demonstrate that weak exchange coupling can be achieved in these systems.^{119,135} The spectrum of $[\text{Mn}^{\text{IV}}_2(\text{salpn})_2(\text{DCBI})]^+$

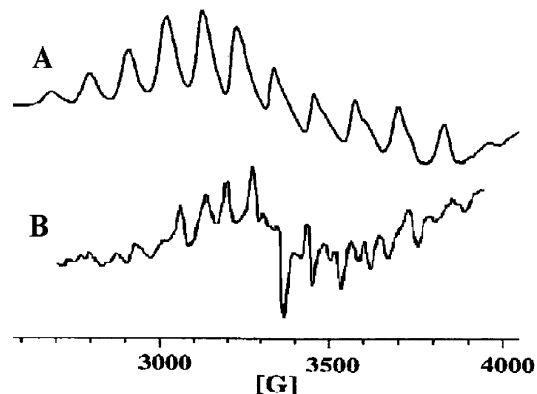


Figure 26. Unusual EPR signals given by model complexes: (A) a 12-line spectrum of $[\text{Mn}^{\text{III}}\text{Mn}^{\text{IV}}(2\text{-OH}(3,5\text{-Cl}_2)\text{-salpn})_2]^+$ and (B) X-band EPR of the $[\text{Mn}^{\text{III}}\text{Mn}^{\text{IV}}(\text{salpn})_2(\text{DCBI})]$ multiline at $g = 2$, 53 K. Reprinted with permission from refs 151 and 134. Copyright 2003 The Royal Society of Chemistry.

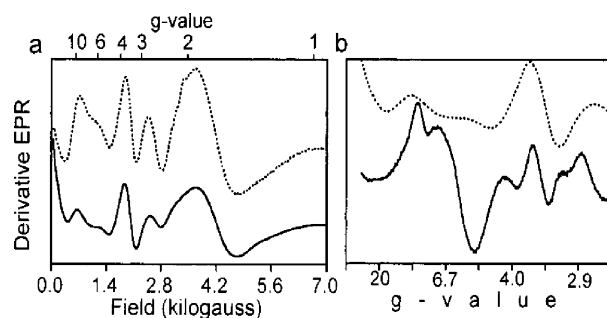


Figure 27. EPR of the $[\text{Mn}^{\text{IV}}_2(\text{salpn})_2(\text{DCBI})]^+$ complex: (a) X-band spectra of the complex at 5.5 K (solid line) and 50 K (dashed line); (b) comparison of low-field Q- (solid line) and X-band (dashed line) spectra at 5.5 K. Reprinted with permission from ref 135. Copyright 1997 American Chemical Society.

in Figure 27 is indicative of this class of compound. At first inspection, the spectral features are similar to those of the Mn^{II}_2 complexes described above and demonstrate that care needs to be taken when assigning oxidation states of dinuclear Mn compounds. Second, it may be possible to apply approaches similar to those that have been used with Mn^{II}_2 systems for discerning Mn–Mn separations in these weakly coupled Mn^{IV}_2 species.

5. Reactivity Models

Given their very efficient antioxidant capabilities (disproportionation of hydrogen peroxide occurs at or near the diffusion limit), catalases are an attractive target for not only pharmaceutical applications but, in some cases, cosmetic ones. The mechanism by which catalases reduce reactive oxygen species has not been determined. One of the most important as well as challenging aspects of model studies is mechanistic characterization of complexes that exhibit similar activity for comparison to what is observed in the biological system. Our primary interest here is to look at manganese-containing models capable of catalyzing the disproportionation of hydrogen peroxide. Although a multitude of catalase reactivity mimics have been reported, we will limit our discussion in this section to those systems with

Table 5. Comparison of Catalase-Type Activity of Various Model Systems

compound(s)	k_{cat} (s^{-1})	$k_{\text{cat}}/K_{\text{M}}$ ($\text{M}^{-1} \text{s}^{-1}$)	ref
Mn catalase (<i>T. thermophilus</i>)	2.6×10^5	3.1×10^6	17, 40, 223
Mn catalase (<i>L. plantarum</i>)	200 000	600 000	18
Mn catalase (<i>T. album</i>)	26 000	1 700 000	224
rat liver arginase	30	10.9	140
$\text{Mn}^{\text{II}}(\text{ClO}_4)_2 \cdot 6\text{H}_2\text{O}$	0.006	nr ^a	149
$\text{Mn}^{\text{II}}(\text{H}_2\text{O})_6$	0.0063	ns	24
$\text{Mn}_2(\text{edda})_2$		52 ^b	225
$[\text{Mn}_2(\text{bispicMe}_2\text{en})_2(\mu\text{-O})_2]^{3+}$		240	158
$[\text{Mn}_2(\text{bisR}_2\text{picX}_2\text{en})_2(\mu\text{-O})_2]^{3+}$ (R = Cl, X = Me)		298	158
$[\text{Mn}_2(\text{bisR}_2\text{picX}_2\text{en})_2(\mu\text{-O})_2]^{3+}$ (R = NO ₂ , X = Me)		352	158
$[\text{Mn}(\text{bpia})(\mu\text{-OAc})_2]$	1070	34 000	67
$[\text{Mn}^{\text{IV}}_2(\text{salpn})(\mu\text{-O})_2]$	250	1000	74, 165
$[\text{Mn}^{\text{III}}(2\text{-OHsalpn})_2]$	10.1	990	24
$\text{Mn}_2(\mu\text{-O})(\text{OH}_2)(\text{OAc})(\text{benzimn})^+$ with 5 equiv of ⁻ OH	2.1	700	155
$\text{Mn}_2(\mu\text{-O})(\text{OH}_2)(\text{OAc})(\text{benzimn})^+$	2.7	450	155
$\text{Mn}_2(\mu\text{-OAc})(\mu\text{-OH})(\text{benzimn})^+$	0.65	93	155, 156
$\text{Mn}_2(\text{benzimn})(\mu\text{-OAc})$	$k_{\text{bi}} = 0.23$	ns	223
$\text{Mn}^{\text{III}}(2\text{-OH}(5\text{-MeOsal})\text{pn})_2$	4.2	382	24
$\text{Na}_2[\text{Mn}^{\text{II}}(2\text{-OH}(5\text{-Clsal})\text{pn})_2]$	16	340	24, 226
$\text{Mn}^{\text{III}}(2\text{-OH}(5\text{-Clsal})\text{pn})_2$	21.9	310	24
$[\text{Mn}^{\text{III}}(2\text{-OH}(3,5\text{-Cl}_2\text{sal})\text{pn})_2]$	18.9	160	24, 226
$[\text{Mn}^{\text{II}}(2\text{-OHpicpn})_4]^{4+}$	150	70	150, 227
$[\text{Mn}^{\text{III}}\text{Mn}^{\text{IV}}(\mu\text{-O})_2(\mu\text{-OAc})(\text{tacn})(\text{bipy})(\text{OH}_2)]^{2+}$	13.2	ns	93
$[\text{Mn}^{\text{III}}\text{Mn}^{\text{IV}}(\mu\text{-O})_2(\mu\text{-OAc})(\text{tacn})(\text{OAc})_2]$	5.5	ns	93
$\text{Mn}^{\text{II}}_2\text{L}(\mu\text{-3,4-NO}_2\text{benzoate})^+$	4.4		
$\text{Mn}^{\text{II}}_2\text{L}(\mu\text{-C}_6\text{H}_5\text{CO}_2)_2(\text{NCS})$	0.79	ns	159
$[\text{Mn}^{\text{III}}\text{Mn}^{\text{IV}}(\text{bpg})_2(\mu\text{-O})_2](\text{ClO}_4)$	0.26	ns	163
$[(\text{OAc})\text{Mn}^{\text{III}}(\text{bbml})_2\text{Mn}^{\text{III}}(\text{OAc})](\text{BF}_4)_2$	0.027	ns	77
$[(\text{tol})\text{Mn}(\text{bbml})_2\text{Mn}(\text{tol})](\text{ClO}_4)_2$	0.027	ns	78
$\text{Mn}^{\text{III}}(\text{TPP})$	0.013	ns	142
$[\text{Mn}^{\text{II}}_2(\mu\text{-O}_2\text{CCH}_3)_3(\text{bpea})_2](\text{PF}_6)$		ns	
$\text{Mn}_2(\text{anthracenediporphyrin})$ complexes	1.5–6.1	ns	142
$\text{Mn}^{\text{II}}_2(\text{Hsal})_4(\text{H}_2\text{O})_4$	25.8	ns	228
$(\text{Ba}, \text{Ca})_2[\text{Mn}_4(\text{O})(\text{OH})(\text{dahpta})_2(\text{OAc})_2]$	1.04	ns	149
$[\text{Mn}_2\text{L}(\text{O}_2\text{CR})](\text{BPh}_4)_2$		14.5	
$\text{Mn}_2(\text{OMe})(\text{OAc})(3\text{-MeO-salpentO})(\text{MeOH})_2\text{Br}$	7.9	32	94

^a nr = data not reported or not available; ns = no saturation kinetics reported. ^b Active complex dissociates and increases oxidizing strength of solutions, multiple processes occurring.

the most relevance to the enzyme. These will be discussed in detail, not only with respect to their catalytic details but also, when possible, with respect to their anion-bound analogues (fluoride, azide, thiocyanide). These anion-inhibited complexes are of particular interest because, while the enzyme is known to be inhibited by anion binding, the details of how and why the inhibition occurs are not yet known.

The efficiencies of the different catalysts discussed in this section are compared to the manganese catalases in Table 5. It should also be noted that even simple Mn^{II} in aqueous solution catalyzes peroxide disproportionation, albeit slowly; therefore, in all reactivity studies appropriate controls must be completed to ensure that the model of interest is the actual catalyst. Another important distinction should be made regarding catalysts at the outset. In most cases, the structurally characterized material often presented as an ORTEP diagram is, at best, a precatalyst since ligand dissociation is required for substrate binding and subsequent reactivity. In many cases, the initial complex may begin as a dimer but dissociate during the reaction to yield a new compound that completes the catalytic cycle. Unfortunately, these details and the final disposition of the “catalyst” are often not reported.

Of the notable reactivity models (Table 5), there are only a few which exhibit catalytic rates that even begin to approach rates exhibited by the enzymes. Even in the best cases, these reactivity models are still 2–3 orders of magnitude slower than the catalase enzymes in terms of k_{cat} and $k_{\text{cat}}/K_{\text{M}}$; however, synthetic models have now met or exceeded the catalase activity of arginase.¹⁴⁰

5.1. Early Reactivity Models

Among the first reactivity models were dimers based on porphyrin-bound manganese complexes. While it was realized early in the studies of manganese catalases that the porphyrin cofactor was not present in these enzymes, such porphyrin complexes are inherently interesting since the mammalian catalases are heme enzymes. One such diporphyrinato-dimanganese(III) complex, studied by Naruta et al.,¹⁴¹ showed evidence of dioxygen evolution in aqueous media; the proposed mechanism, shown in Figure 28, was thought to involve formation of hydroxide bridges on the resulting Mn^{IV} centers. Given these promising first results, analysis of other diporphyrinato-dimanganese complexes was performed. The $[\text{Mn}^{\text{III}}(\text{TPP})]_2^{2-}$ and $[\text{Mn}^{\text{III}}(\text{OEP})]_2^{2-}$ complexes for example are stable structures which, like catalase, incorporate Mn^{III} ions in their catalytic

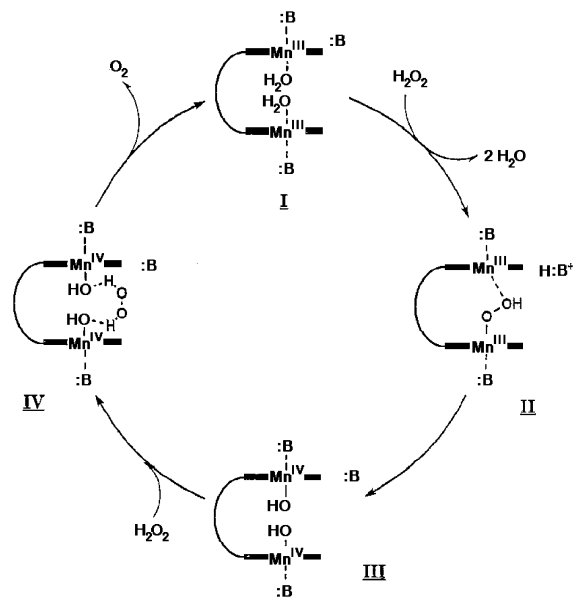


Figure 28. Proposed mechanistic cycle of the anthracene-linked diporphyrinato-dimanganese(III) complex. Reprinted with permission from ref 147. Copyright 1997 Elsevier.

cycle.¹⁴¹ During catalysis, however, the dimeric unit would dissociate. It was also found that the monomers showed evidence of oxygen evolution in the presence of hydrogen peroxide. In the case of $[\text{Mn}(\text{TPP})]^-$, initial oxygen evolution was recorded at $2.4 \times 10^{-7} \text{ mol min}^{-1}$. Mn porphyrins with rigid linkers¹⁴² such as anthracene yielded similar structures but with the added advantage that the two porphyrin units would not dissociate and could be held a fixed distance apart. The series of structures (some with bulky substituents on the porphyrin rings) showed that, while activity could be obtained for most of the complexes, O_2 evolution rates were greatly enhanced in the presence of methyl imidazole for complexes which allowed entrance of the base into the cavity. The imidazole in the H_2O_2 -Mn porphyrin systems was proposed to accelerate homolysis of the O-O bond and stabilize a $\text{Mn}^{\text{IV}}=\text{O}$ intermediate that was formed in the catalytic cycle.^{143,144} In these studies, it was shown that the dinuclear center was essential for catalysis although the catalytic cycle did not necessarily show the same oxidation states as the enzyme. Even in the best anthracenediporphyrin case, the rate of turnover was low, at about six turnovers per second compared to about 10^7 s^{-1} for *T. thermophilus* catalase.¹⁴⁵ While the intermetal distance was an important factor in this series of complexes,^{146,147} the rigid anthracene spacer in the most active complex held the metals at $\sim 4.5 \text{ \AA}$, a much larger distance than is found in the enzyme.

Although these manganese porphyrin complexes show evidence of catalase-like activity, they do not exhibit the characteristics that might make them functionally relevant models of the enzyme. For example, the catalytic cycle of these complexes employs a Mn^{IV} species, an oxidation state that has been shown to be inactive in the catalase. Saturation kinetics are not reported, and turnover is certainly much lower than desired (compared to the enzyme as well as some of the other functional models that have been reported; Table 5). First-sphere coordina-

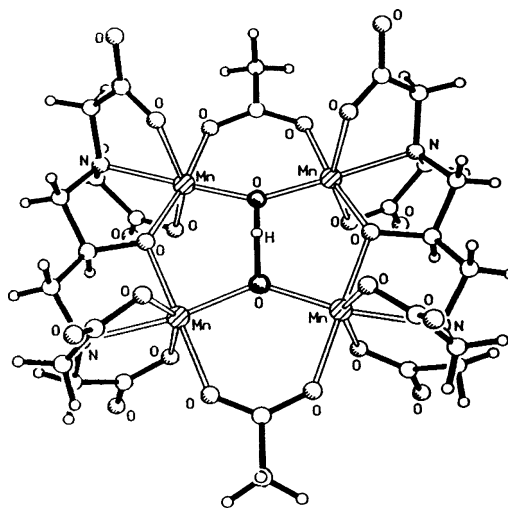


Figure 29. The unique complex by Stibrany and Gorun bearing an unusual bridging motif. Reprinted with permission from ref 149. Copyright 1990 Wiley-VCH.

tion may play a significant role in controlling properties of the catalysis at this dimanganese center, and the porphyrin ligand does not provide a good approximation for the types of ligation proposed in the active site of the enzyme. One particular porphyrin complex is worth noting. Recently, Nocera and co-workers¹⁴⁸ reported a different porphyrin derivative. Instead of utilizing two porphyrins connected by a rigid linker, they attached a rigid xanthene scaffold to the porphyrin. To this "hangman" scaffold, a functional group could be affixed in a manner that would provide a hydrogen-bonding group direction above the porphyrin-bound metal. The manganese-bound HPX- CO_2H complex and similar derivatives with dibenzofuran (HPD) are well-defined structures that have allowed the study of hydrogen-bonding influences on O-O bond activation. These hangman porphyrin complexes do indeed show increased catalase-like disproportionation of hydrogen peroxide in addition to epoxidation chemistry at rates that exceed the rates of the bare Mn-trimesitylporphyrin (i.e., without the dibenzofuran or xanthene scaffold). Despite their modest activity, they are distinguished by their use of a hydrogen-bond network to promote their enhanced catalytic oxygen activation. Few model complexes have been developed that employ hydrogen bonding in their catalytic cycle. Further mechanistic investigations of this proton-coupled dioxygen activation may provide information necessary for a more fundamental understanding of how manganese catalases so efficiently catalyze the disproportionation of hydrogen peroxide.

5.2. Tri- and Tetranuclear Models

Tri- and tetranuclear models have been synthesized that show evidence of hydrogen peroxide disproportionation activity. While these complexes may not have direct structural relevance to the enzyme, their dimeric subunits may, providing justification for examining the details of their catalysis. One of the first complexes, $(\text{Ba,Ca})_2[\text{Mn}_4(\mu\text{-O})(\mu\text{-OH})(\text{O}_2\text{-CCH}_3)_2(\text{dahpta})_2]$, was presented by Stibrany and Gorun (Figure 29) and is formulated as an $\text{Mn}^{\text{II}}\text{Mn}^{\text{III}}_3$

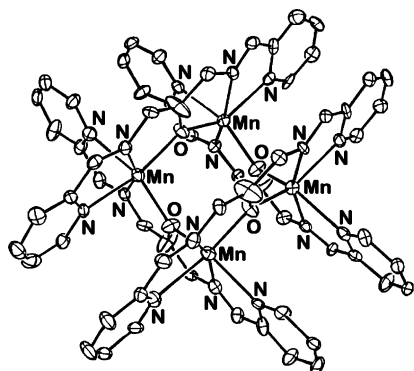


Figure 30. The first two-by-two grid complex, $[\text{Mn}^{\text{II}}(2\text{-OHpicpn})]_4^{4-}$. Reprinted with permission from ref 150. Copyright 1996 American Chemical Society.

complex¹⁴⁹ on the basis of symmetry and interatomic distances. The complex decomposes hydrogen peroxide at catalytically high rates (O_2 evolution at 4 mL s^{-1} compared to the TPP and OEP systems mentioned previously (0.05 mL s^{-1}). Unique to this complex is a bridging $(\text{O}_2\text{H})^{3-}$ which shows a strong hydrogen-bonding interaction and has been proposed as an intermediate stage in the deprotonation and coupling of two water molecules at the center of the complex.

Another important tetranuclear complex is the first two-by-two grid complex $[\text{Mn}^{\text{II}}(2\text{-OHpicpn})]_4^{4-}$ (Figure 30). This tetramer has inter-manganese distances of 3.74 \AA and disproportionates hydrogen peroxide at a significant rate.¹⁵⁰ Labeling studies reveal that the complex does not dissociate during catalysis and that both oxygen atoms in the product dioxygen originate from the same hydrogen peroxide molecule. The complex exhibits saturation kinetics ($V_{\text{max}} = 140 \pm 8 \text{ s}^{-1}$ and $K_{\text{M}} = 2.6 \pm 0.3 \text{ M}$) that proceed via cycling of oxidation states relevant to the catalase ($\text{Mn}^{\text{II}}_4 \leftrightarrow \text{Mn}^{\text{II}}_2\text{Mn}^{\text{III}}_2$). This molecule, like the $[\text{Mn}(2\text{-OH}(5\text{-ClSal})\text{pn})]_2$ complex that will be discussed later in this section, shows an H/D kinetic isotope effect, indicating that a proton-dependent step is important in the disproportionation process. The catalytic efficiency ($k_{\text{cat}}/K_{\text{M}}$) of the molecule at $55 \text{ M}^{-1} \text{ s}^{-1}$ is still lower, however, than the $300 \text{ M}^{-1} \text{ s}^{-1}$ measured for the dimeric $[\text{Mn}(2\text{-OH}(5\text{-ClSal})\text{pn})]_2$. Therefore, the picpn complex shows clearly that four Mn ions in a square arrangement can produce dioxygen from peroxide but, in this case, is less effective than some of the dimeric complexes that are even more reactive. The proposed catalytic mechanism,¹⁵¹ shown as Figure 31, suggests inner-sphere coordination of the peroxide moiety in both the reductive and oxidative halves of the redox reaction. The Weatherburn trimer¹⁵² discussed below serves as a model for a peroxide intermediate in this system.

Another tetranuclear complex worth mention is the $\text{Mn}^{\text{III}}_3\text{Mn}^{\text{IV}}$ complex $[\text{Mn}_4\text{O}_6(\text{bpea})_4]^{3+}$, an efficient hydrogen peroxide disproportionation catalyst displaying saturation kinetics at a rate of $k_{\text{cat}} = 11.1 \pm 0.9 \text{ s}^{-1}$ (vs $k_{\text{cat}} = 2.0 \times 10^5 \text{ s}^{-1}$ for *L. plantarum* enzyme).¹⁵³ The rate of disproportionation in the biomimetic system is first order in complex as well as hydrogen peroxide concentration and exhibits saturation kinetics. Isotope labeling studies reveal

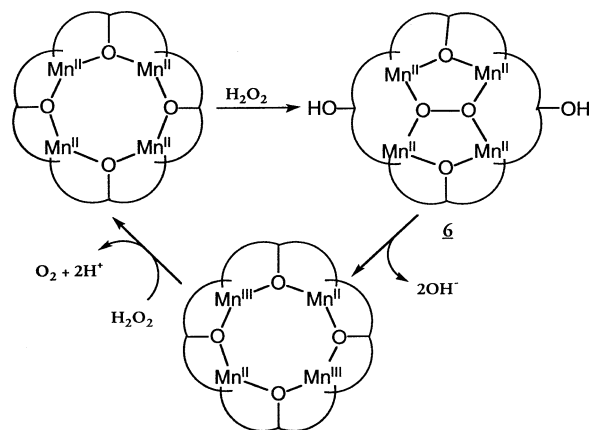


Figure 31. Proposed $[\text{Mn}^{\text{II}}(2\text{-OHpicpn})]_4^{4-}$ mechanism. Reprinted with permission from ref 151.

that both oxygen atoms of evolved dioxygen originate from one hydrogen peroxide molecule. Addition of the base $\text{Me}_3(\text{tacn})$ to the reaction solution (aqueous $\text{p}K_{\text{a}} = 11.7$) produces a deviation from Michaelis–Menten kinetics that is indicative of cooperativity in the disproportionation reaction. No oxidation state cycling is seen in this complex.¹⁵⁴

Trimeric complexes such as $\text{Mn}^{\text{II}}_3(5\text{-NO}_2\text{salim})_2(\text{OAc})_4$ and $\beta\text{-Mn}^{\text{III}}_2\text{Mn}^{\text{II}}(\text{saladhp})_2(\text{OAc})_4(\text{CH}_3\text{OH})_2$ suffer from some of the same problems as the tetrameric complexes in terms of structure, catalyst decomposition, or employing oxidation states that are not relevant to the enzyme. While these complexes show catalase-like reactivity, they too do not achieve rates that are significantly improved over the dimeric complexes that have been revealed. Probably the most important of this group is the peroxo-bridged species $\text{Mn}_3^{\text{III}}(\text{dien})_3(\mu\text{-OAc})_2(\mu_3\text{-O})(\mu\text{-O}_2)^{3+}$, prepared by Weatherburn.¹⁵² Although catalase activity was not reported for this compound, it does serve as a speculative intermediate for a hydroxide-bridged dinuclear Mn^{III} complex prior to peroxide oxidation. In fact, the complex is actually prepared by the reaction of dioxygen with the lower valent precursor.

5.3. Dinuclear Models

Dinuclear manganese complexes certainly provide a more direct structural relationship to the catalase active site than their tri- and tetrameric relatives. As structural data have become more detailed and crystal structures of the enzymes have been obtained at higher resolution, the complexity of the models has also grown. A wide variety of functional model complexes have been produced. Most of them, however, have only one or two characteristics that properly emulate the enzyme; these inherent limitations perpetuate the need for development and full characterization of improved functional models.

The first promising functional model for the manganese catalases was developed by Dismukes et al. in 1987. It was reported to catalytically disproportionate H_2O_2 and uses an N-donor-based ligand set that is biologically relevant (provided by four pendant benzimidazole groups). This septadentate ligand *N,N,N,N*-tetrakis(2-methylenebenzamidazoly)-1,3-diaminopropan-2-ol binds two Mn^{II} ions through an

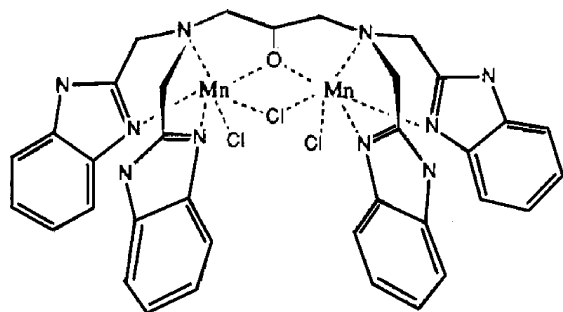


Figure 32. Halide-bound benzimpn complex. Reprinted with permission from ref 136. Copyright 1987 American Chemical Society.

alkoxide oxygen from the 2-propanol backbone. A second bridging site is occupied by either a Cl^- or $^- \text{OH}$ anion.¹³⁶ Although not structurally characterized, the complex was believed to possess a terminally bound Cl^- at each manganese ion (Figure 32); the dimanganese core was confirmed by EPR spectroscopy, and a metal–metal separation of 3.2 Å was estimated from EPR experiments (vide supra). This complex was the first of its kind to exhibit better than stoichiometric reactivity with hydrogen peroxide, disproportionating 200 mmol of peroxide per millimole of complex. Kinetic studies indicate that it uses the Mn^{II}_2 and Mn^{III}_2 oxidation states during its reaction with H_2O_2 —the same type of reactivity observed for the manganese catalases.

Dismukes has since reported^{84,155–157} analogous complexes in which the chloride bridge has been replaced with a carboxylate group (either monodentate or bidentate), generating five-coordinate Mn^{II} ions. Besides having increased solubility compared to the chloride-bound precursor, the complexes exhibited the same redox cycling as seen during the catalase reaction. It was also observed that a lag phase was present with the acetate-bridged species and that an excess of acetate inhibited the reaction, suggesting that dissociation of acetate was critical to the reaction. Without the presence of the bound anion, rate enhancement was observed and the turnover number increased from 200 to greater than 1000. Kinetic data place a second-order rate constant at $1.2 \text{ M}^{-1} \text{ s}^{-1}$, suggesting that reduction of peroxide and regeneration of the Mn^{III}_2 complex might be the rate-limiting step. The best of these complexes gives a k_{cat} of 0.2 s^{-1} but has $k_{\text{cat}}/K_{\text{M}}$ values at about $3 \text{ M}^{-1} \text{ s}^{-1}$.

The most efficient catalysts of this series do not have lag phases and are formed when 5 equiv of hydroxide is added to the system. The compounds shift from colorless to bright orange. Spectral investigation (UV–vis, NMR) suggests that this species is a dinuclear Mn^{III} complex with a terminal acetate group, a bridging μ_2 -oxo between the Mn ions, and a terminally coordinated hydroxide ion. This conversion does not change the slow step of the catalytic cycle, which is the oxidation of the Mn^{II}_2 dimer. One of the attractive features of this system is that catalysis occurs in mixed aqueous/methanol solutions whereas other models require a less polar/protic solvent for optimal rates. The catalyst generated with 5 equiv of base in a 98% methanol/2% water mixture

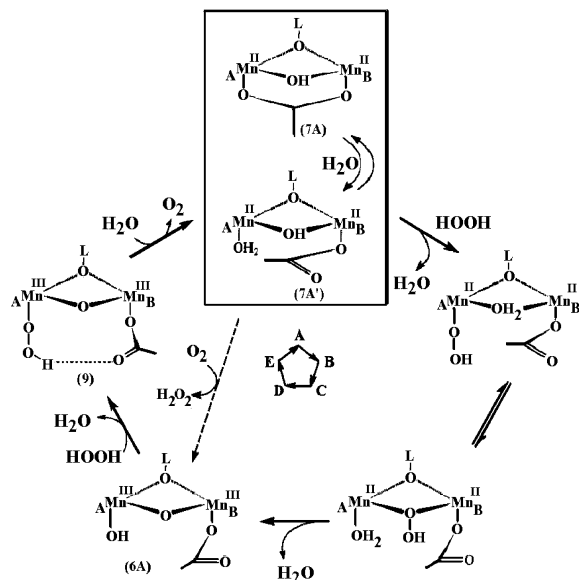


Figure 33. Proposed five-step mechanism for the catalytic benzimpn complexes. Reprinted with permission from ref 155. Copyright 2000 American Chemical Society.

exhibits a significant enhancement for k_{cat} at 2.7 s^{-1} , a $K_{\text{m}} = 6 \text{ mM}$ for peroxide, and a $k_{\text{cat}}/K_{\text{M}}$ at $450 \text{ M}^{-1} \text{ s}^{-1}$. The $k_{\text{cat}}/K_{\text{M}}$ can be raised substantially ($700 \text{ M}^{-1} \text{ s}^{-1}$) by changing the solvent to an 11% methanol/89% water mixture. The change in $k_{\text{cat}}/K_{\text{M}}$ is due not to a higher maximal rate (k_{cat} at 2.1 s^{-1}) but rather a strengthening of the substrate affinity which now has a Michaelis constant of 0.3 mM. The added hydroxide ions are thought to aid in deprotonation of metal-bound hydrogen peroxide in the proposed five-step mechanism¹⁵⁵ shown as Figure 33. This places these compounds, based on a $k_{\text{cat}}/K_{\text{M}}$ criterion, within a factor of 800–4500 of the enzymatic rates. The authors believe that the rate of catalase reactions is not critically dependent on the reduction potential of the catalysts. Instead, it is proposed that the intramolecular hydroxide, required for substrate deprotonation, is the essential component for efficient catalysis. In addition, an unobstructed substrate binding site is required for the proposed end-on hydroperoxyanion coordination. Like the Mn catalases, the $\text{Mn}^{\text{III}}\text{Mn}^{\text{IV}}$ complex of this septadentate ligand system is catalytically inactive. Given the high efficiency and many similarities to the Mn catalases, this system has been one of the most effective models for the enzymatic reaction.

The bispicen ligand is a simple system which provides four nitrogen donors (two from pyridine and two from ethylenediamine). The $\text{Mn}_2(\mu\text{-O})_2(\text{bispicX}_2\text{-en})_2$ complexes are known as both structural⁶² and functional¹⁵⁸ models. The complexes are usually two-fold symmetric and vary only in bridging species. At least eight different derivatives of these complexes are known, and catalysis proceeds to disproportionate hydrogen peroxide in neutral aqueous media. There are three critical flaws for this system, however: incorrect oxidation states are utilized in the catalytic cycle ($\text{Mn}^{\text{III}}_2 \leftrightarrow \text{Mn}^{\text{IV}}_2$), the complex is dioxygen sensitive, and the complex likely dissociates into monomers during the lower oxidation portion of the cycle. While as many as 2000 turnovers may be

achieved, the catalytic rate decreases significantly as more dioxygen is evolved in the catalysis. Thus, despite catalyzing the same disproportionation reaction, this is a less likely functional model for the catalases upon closer inspection.

The tacn ligand provides three nitrogens that bind facially and provide some steric constraints to the Mn-bound complexes. These ligands may sometimes yield slightly more distorted geometries about the metal than their more simplistic counterparts, especially if bulky alkyl substituents are added. Certainly they have already provided information regarding bridging types in the enzyme. In terms of function, complexes such as $[\text{Mn}^{\text{III}}\text{Mn}^{\text{IV}}(\mu\text{-O})_2(\mu\text{-OAc})(\text{tacn})(\text{bipy})(\text{MeOH})](\text{ClO}_4)_2$ and $[\text{Mn}^{\text{III}}\text{Mn}^{\text{IV}}(\mu\text{-O})_2(\mu\text{-OAc})(\text{tacn})(\text{OAc})_2]$ show moderate rates of catalysis and present an intermanganese distance of about 2.65 Å.⁹³ The k_{cat} values reported for these two complexes are 13.5 and 5.5 s⁻¹, respectively, although it is almost certain that these are precatalysts with reactive compounds missing acetate groups. No saturation kinetics have been reported for the tacn complexes and, as in the previous case, closer inspection shows that its oxidation state cycle during catalysis employs oxidation states that are not used in the enzyme. In particular, the redox cycling occurs between oxidation states that are known to be inactive ($\text{Mn}^{\text{II}}\text{Mn}^{\text{III}} \leftrightarrow \text{Mn}^{\text{III}}\text{Mn}^{\text{IV}}$) in the enzyme. Another disadvantage is that the compounds likely dissociate during the reaction cycle. The tacn series of complexes have been fully characterized even for inhibition complexes that are azide or SCN bound.

Other anion-bound complexes have been studied thoroughly.^{95,159} Notable among these are the phenolate-based ligands or macrocycles; these have been well-characterized but are of little interest as models due to their non-representative magnetic properties (discussed in section 3.3) as well as nonrelevant ligand set. In terms of reactivity, observed rates are on the order of 0.3–0.8 s⁻¹ for both macrocyclic and non-macrocyclic ligand complexes;^{160–162} these rates are certainly not exceptional. Catalytic cycles occur between the Mn^{III}_2 and Mn^{IV}_2 oxidation states. Additionally, while complexes with Cl⁻ bridges or bound anions have been synthesized, their presence accelerates the observed catalytic rate^{26,160}—the opposite of the inhibitory effect seen for the enzymes.

Other complexes that utilize amine-based tri- and tetrapodal ligands bear a different set of limitations but rarely fare any better with respect to reactivity. The $[\text{Mn}^{\text{III}}\text{Mn}^{\text{IV}}(\text{bpg})_2(\mu\text{-O})_2]^-$ complex also does not exhibit saturation kinetics. The advantage of this complex lies in incorporation of glycine as one of the ligand arms. This, of course, provides a biologically relevant carboxylate ligation to the manganese ion(s) and is, in this respect, a better donor set than tacn (although the pyridyl nitrogens in the bpg ligand are still electronically different from histidine). Interestingly, the activity of the complex is highly dependent on the presence of protons (a characteristic that is not unexpected and that has been seen in many other functional complexes). The value of k_{cat} is, at 0.25 s⁻¹, quite a bit lower than that for the tacn complexes just discussed.¹⁶³ The complex $[\text{Mn}^{\text{II}}_2-$

$(\mu\text{-O}_2\text{CCH}_3)_3(\text{bpea})_2]^-$ is worth mentioning at this point. Although it has the same bispicolyl framework as bpg, the glycine has been substituted for a simple alkyl group. It is indeed catalytically active,⁹² although details of the catalytic activity have not been reported. A chloride-bridged derivative has also been described¹⁶⁴ and is structurally in agreement with the mode of binding for F⁻ inhibition of the catalase that was deduced from magnetic studies.⁴⁷ Despite a large Mn–Mn separation of 3.92 Å due to the presence of three carboxylate bridges, it is notable that this complex has been observed to utilize $\text{Mn}^{\text{II}}_2 \leftrightarrow \text{Mn}^{\text{III}}_2$ cycling during catalysis.

For many years, $[\text{Mn}^{\text{IV}}_2(\text{salpn})(\mu\text{-O})_2]$ held the record for the fastest hydrogen peroxide disproportionation catalyst containing manganese. For this reason, the kinetics of this Mn^{IV} dimer has been studied extensively.^{74,165} It was first recognized that $[\text{Mn}^{\text{IV}}_2(\text{salpn})(\mu\text{-O})_2]$ could be prepared beginning with a mononuclear $\text{Mn}^{\text{III}}(\text{salpn})^+$ precursor using either dioxygen or hydrogen peroxide. The dioxygen reactivity required a basic solution and gave product in moderate to poor yields. In contrast, 2 equiv of base was sufficient to allow for the hydrogen peroxide-initiated oxidation of $\text{Mn}^{\text{III}}(\text{salpn})^+$ to the desired di- μ -oxo dimer. If this reaction was carried out in acetonitrile, quantitative yields of $[\text{Mn}^{\text{IV}}_2(\text{salpn})(\mu\text{-O})_2]$ were obtained. An identical product was obtained by the reaction of the dimeric $[\text{Mn}^{\text{III}}(\text{salpn})(\mu_2\text{-OCH}_3)_2]$ with hydrogen peroxide. If labeled peroxide was utilized ($\text{H}_2^{18}\text{O}_2$), the $[\text{Mn}^{\text{IV}}_2(\text{salpn})(\mu\text{-}^{18}\text{O})_2]$ was isolated. An unexpected change in reactivity occurred when hydrogen peroxide was reacted with $\text{Mn}^{\text{III}}(\text{salpn})^+$ in dichloromethane. While the same $[\text{Mn}^{\text{IV}}_2(\text{salpn})(\mu\text{-O})_2]$ was ultimately isolated, a strong exothermic reaction occurred with the liberation of a gas. Analysis of the gas confirmed the production of dioxygen. These observations suggested that hydrogen peroxide was catalytically decomposed by $[\text{Mn}^{\text{IV}}_2(\text{salpn})(\mu\text{-O})_2]$. The direct reaction of $[\text{Mn}^{\text{IV}}_2(\text{salpn})(\mu\text{-O})_2]$ with hydrogen peroxide in dichloromethane yielded quantitative levels of dioxygen, confirming that a catalase-like reaction was operative. The catalyst was stable for over 5000 turnovers. Reactivity and labeling studies with $\text{H}_2^{16}\text{O}_2$ and $\text{H}_2^{18}\text{O}_2$ showed that this complex yielded the same resultant isotope composition as the enzyme (i.e., both oxygens of dioxygen were derived exclusively from the same hydrogen peroxide molecule). The reaction of $\text{H}_2^{16}\text{O}_2$ with $[\text{Mn}^{\text{IV}}_2(\text{salpn})(\mu\text{-}^{18}\text{O})_2]$ or $\text{H}_2^{18}\text{O}_2$ with $[\text{Mn}^{\text{IV}}_2(\text{salpn})(\mu\text{-}^{16}\text{O})_2]$ gave $^{16}\text{O}_2$ and $^{18}\text{O}_2$, respectively. Therefore, the origin of the dioxygen was not the bridging oxygen atoms, but rather the peroxide substrate itself. If one commenced the reaction with an equimolar mixture of $[\text{Mn}^{\text{IV}}_2(\text{salpn})(\mu\text{-O})_2]$ and $[\text{Mn}^{\text{IV}}_2(\text{X-salpn})(\mu\text{-O})_2]$, the recovered product was a statistical mixture of $[\text{Mn}^{\text{IV}}_2(\text{salpn})(\mu\text{-O})_2]$, $[\text{Mn}^{\text{IV}}_2(\text{X-salpn})(\mu\text{-O})_2]$, and $[\text{Mn}^{\text{IV}}_2(\text{salpn})(\text{X-salpn})(\mu\text{-O})_2]$. This pattern showed that the dimer dissociated into monomers during the reaction cycle. However, under multiple turnover conditions with $\text{H}_2^{16}\text{O}_2$ and $\text{H}_2^{18}\text{O}_2$, the μ -oxo bridges were also converted to $[\text{Mn}^{\text{IV}}_2(\text{salpn})(\mu\text{-}^{18}\text{O})_2]$ and $[\text{Mn}^{\text{IV}}_2(\text{salpn})(\mu\text{-}^{16}\text{O})_2]$ without the presence of mixed labeled products, indicating that

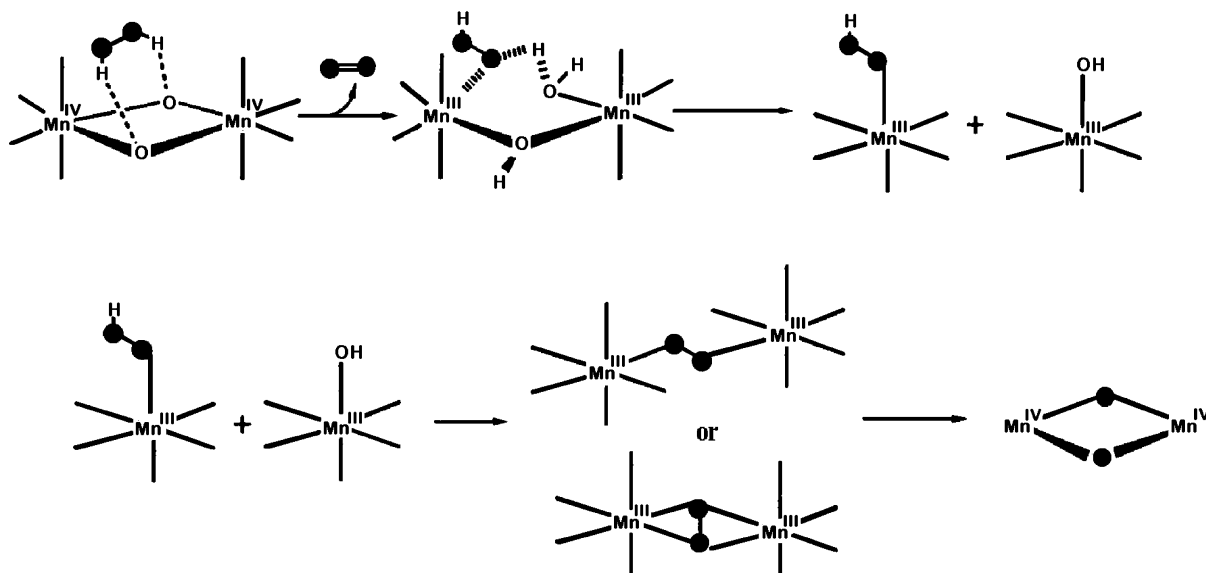


Figure 34. Proposed mechanism for the $\text{Mn}^{\text{IV}}_2\text{salpn}_2$ complex. Reprinted with permission from ref 165. Copyright 1991 American Chemical Society.

the peroxide bond breakage occurred after association of peroxide as a dimeric Mn complex. On the basis of these studies, the mechanism shown as Figure 34 was proposed.¹⁶⁵ The proposed peroxo intermediate in the mechanism is analogous to the structural determination of $[\text{Mn}^{\text{IV}}(\text{Me}_3\text{tacn})(\mu_2\text{-O})(\text{O}_2)]$ reported by Wieghardt.¹⁶⁶ A consequence of this mechanism was that the addition of 1 equiv of acid should cut the ultimate rate in half and that 2 equiv of protons would completely inhibit the reaction. This prediction was ultimately verified using both H^+ and CH_3^+ sources. To date, this catalase mimic reaction is the most thoroughly understood. However, despite its respectable observed rates of catalysis and high catalytic efficiency ($k_{\text{cat}} = 250 \text{ s}^{-1}$ and $k_{\text{cat}}/K_{\text{M}} = 1000 \text{ M}^{-1} \text{ s}^{-1}$), the complex shows Mn^{III}_2 and Mn^{IV}_2 oxidation states during catalysis. Furthermore, the dissociation into monomers ultimately limits the relevance to the catalases. Thus, this system may have more practical application to the OEC.

The salpn ligand can be modified by adding a hydroxyl group to the ligand backbone, forming the class of ligands known as 2-OH(X-sal)pn. As described in the structural section of this article, this ligand has been able to support dimeric complexes in oxidation levels ranging from Mn^{II}_2 to Mn^{IV}_2 . Of particular note is the $[\text{Mn}^{\text{III}}(2\text{-OHsalpn})_2]$ complex which exhibits saturation kinetics with respectable turnover rates when reacted with hydrogen peroxide. The EPR spectra and UV-visible spectra of the Mn^{II} dimer could be used to assess that the reaction proceeded via the lower oxidation level. Similarly, identical rates were observed when $[\text{Mn}^{\text{II}}(2\text{-OHsalpn})_2]^{2-}$ was used as the starting complex.²⁴ Thus, unlike the $[\text{Mn}^{\text{IV}}_2(\text{salpn})(\mu\text{-O})]_2$, this reaction cycles between the Mn^{II}_2 and Mn^{III}_2 oxidation levels, and there is no reactivity with either the $\text{Mn}^{\text{III}}\text{Mn}^{\text{IV}}$ or Mn^{IV}_2 species. Catalyst decomposition does not occur, and the integrity of the dimeric complex is maintained for several thousand turnovers. Isotope labeling studies were carried out on this system in order to assess whether the dimer dissociated during the catalytic

cycle and whether the product dioxygen originated from a single molecule of hydrogen peroxide, and to assess the importance of protons for the reaction scheme. It was concluded that each molecule of oxygen produced is derived solely from one molecule of peroxide substrate. The $[\text{Mn}^{\text{III}}(2\text{-OHsalpn})_2]$ does not dissociate into monomers during the course of the catalase reaction, which is another significant difference from the chemistry of salpn and most other model systems. Reactions with D_2O_2 and H_2O_2 demonstrated a significant isotope effect, indicating that a proton-dependent step was important in the reaction. Later, $[\text{Mn}^{\text{III}}(2\text{-OH(X-sal)pn})_2]$ complexes employed 3- and/or 5-substituted 2-OHsalpn ligands; the electron-withdrawing and/or -donating substituents are known to change the donor capacity, thereby influencing the redox potential of the complex substantially. Therefore, one can assess the dependence of the reaction rate on redox potential and Lewis acidity of the manganese ions. One found that there were two opposing trends to the rates: the ability of the compound to be reduced (increasing with electron-withdrawing groups) and the inability of the compound to gain a ligand (increasing with electron-donating groups). The trend with potentials is as expected; however, it was interesting to have the second trend. Fortunately, the $[\text{Mn}^{\text{III}}(2\text{-OHsalpn})_2]$ series can also be isolated as an asymmetric series of compounds in which an exogenous ligand binds to one of the two Mn^{III} ions. In the process, the bridging alkoxide bond breaks.²⁴ These symmetric ($\text{Mn}-\text{Mn} \sim 3.3 \text{ \AA}$) and asymmetric ($\text{Mn}-\text{Mn} \sim 3.7 \text{ \AA}$) complexes have been crystallographically and spectroscopically characterized in several different oxidation states. Thus, they serve as both structural and functional manganese catalase mimics. This is an example of an alkoxide shift and is analogous to what Lippard and Tolman first described as a carboxylate shift. These data provided strong evidence that such a ligand shift occurred in this model system, making this the first manganese-based system to mimic a carboxylate-like shift in an enzyme. On the basis of

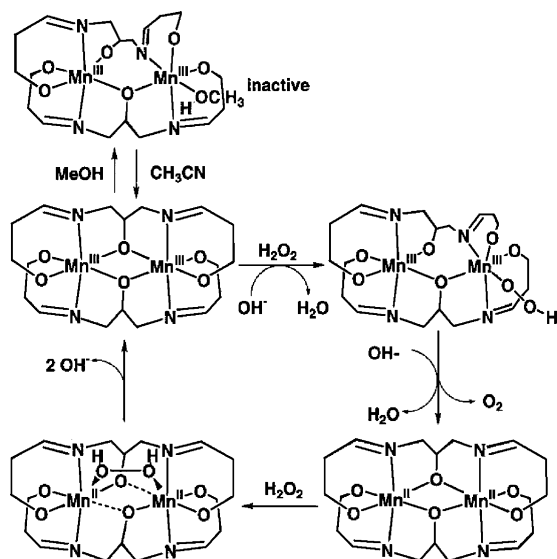


Figure 35. Mechanism of hydrogen peroxide dismutation for the $\text{Mn}^{\text{III}}_2(2\text{-OH},5\text{-Clisalpn})_2$ complex. Reprinted with permission from ref 24. Copyright 1998 American Chemical Society.

all of these results, the mechanism in Figure 35 was proposed.

For the $[\text{Mn}^{\text{III}}(2\text{-OH}(\text{X-salpn}))_2]$ series of complexes, observed rates of reaction are not as high as for the $[\text{Mn}^{\text{IV}}_2(\text{salpn})(\mu\text{-O})_2]$ case; these rates are, however, still significant. These 2-OHsalpn complexes are efficient functional models for the catalases, having k_{cat} values as high as 21.9 s^{-1} (in the case of $[\text{Mn}^{\text{III}}(2\text{-OH}(5\text{-Clisalpn}))_2]$) and $k_{\text{cat}}/K_{\text{M}}$ of up to $990 \text{ M}^{-1} \text{ s}^{-1}$ for the $[\text{Mn}^{\text{III}}(2\text{-OHsalpn})_2]$ complex. All complexes in this series give catalytic rates between 4.2 and 21.9 s^{-1} and $K_{\text{cat}}/K_{\text{M}}$ values between 160 and 990 while utilizing the same oxidation states of the enzyme for catalysis. This places the $[\text{Mn}^{\text{III}}(2\text{-OH}(\text{X-salpn}))_2]$ compounds, based on a $k_{\text{cat}}/K_{\text{M}}$ criterion, within a factor of 500–3200 of the enzymatic rates. Based on the criteria of catalytic efficiency, stability as a dimer, and cycling between the proper oxidation levels, the $[\text{Mn}^{\text{III}}(2\text{-OH}(\text{X-salpn}))_2]$ series and $\text{Mn}_2(\text{benzimpn})$ were until recently the most significant advances in manganese catalase mimicry. The $[\text{Mn}^{\text{III}}(2\text{-OH}(\text{X-salpn}))_2]$ series also has the advantage that it is a true catalyst in which all of the relevant complexes have been structurally characterized. The $[\text{Mn}^{\text{III}}\text{Mn}^{\text{IV}}(2\text{-OHsalpn})_2]^+$, which like the superoxidized form of the Mn catalases is unreactive with H_2O_2 , shows a signature EPR spectrum that is nearly identical to that of the $\text{Mn}^{\text{III}}\text{Mn}^{\text{IV}}$ catalase. In addition, under the appropriate conditions, $[\text{Mn}^{\text{III}}(2\text{-OHsalpn})_2]$ shows azide insensitivity just as the enzyme does. Likewise, treatment of this mixed-valence state with hydroxylamine will reduce this species to a catalytically active form. This observation was used to propose a mechanism, Figure 36, for the formation of the superoxidized Mn catalases in the presence of H_2O_2 and hydroxylamine.

A significant breakthrough in catalytic efficiencies of manganese catalase mimics has been made recently.⁶⁷ The complex, $[\text{Mn}^{\text{II}}(\text{bpia})(\mu\text{-OAc})_2]^{2-}$, can be considered a structural model for the catalytically active reduced form of manganese catalases because

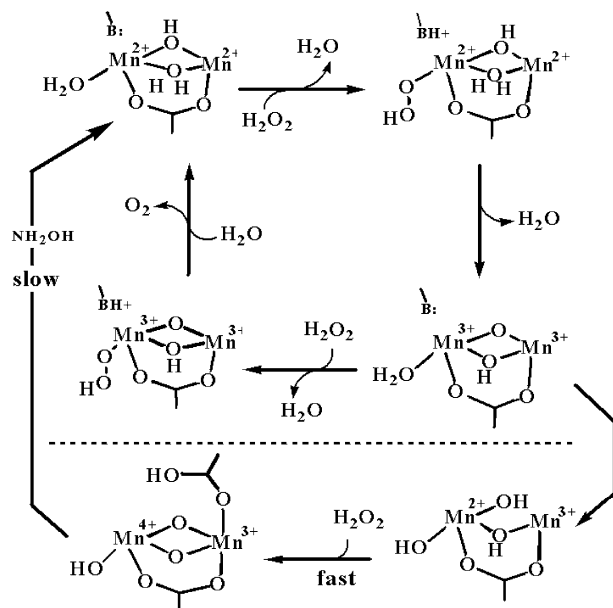


Figure 36. Proposed four-step mechanism for catalases.

of its imidazole/acetate donor set; however, the Mn–Mn distance is quite long at 4.13 \AA . Reaction of this compound with H_2O_2 in *N*-methylformamide leads to oxygen production with saturation kinetics at high substrate concentrations. The observed kinetics are truly exceptional, $k_{\text{cat}} = 1.07 \times 10^3 \text{ s}^{-1}$ and $k_{\text{cat}}/K_{\text{M}} = 3.4 \times 10^4 \text{ M}^{-1} \text{ s}^{-1}$, making this complex the most efficient catalase mimic developed to date. These values are within a factor of 17–92 in relative activity to the three characterized manganese catalases, exceeding the activity reported for arginase disproportionation of hydrogen peroxide. Possibly most impressive, the rates for $[\text{Mn}^{\text{II}}(\text{bpia})(\mu\text{-OAc})_2]^{2-}$ represent a 1.7×10^5 rate acceleration as compared to Mn^{II} . While this system is very exciting and requires further study, it does have its potential limitations. Examination of the structure would suggest that the complex dissociates during the catalytic reaction and, as already mentioned, the Mn–Mn separation is too long for a precise structural mimic of the enzyme. Furthermore, we do not know whether this compound is a catalyst or precatalyst, as detailed kinetic studies have not been completed. In fact, it has not even been confirmed that a Mn^{III} dimer is responsible for the oxidative end of the catalytic cycle. Other mono- and dinuclear compounds containing the bpia ligand did not show catalytic activity. This includes $\text{Mn}^{\text{II}}\text{Mn}^{\text{III}}$ and Mn^{III}_2 species and a monomeric Mn^{II} derivative. Thus, these complexes are eliminated as contributors to the observed activity. A chloride-bridged complex, $[\text{Mn}_2(\text{bpia})_2(\text{Cl})_2(\mu\text{-O})]^{2-}$, has also been prepared and serves as a mimic for halide-inhibited manganese catalase; it shows no catalase activity, as would be expected. Cyclic voltammetric data have suggested that the lack of activity for the inhibition complex may be due to a shift in redox potentials to more positive values, an effect that arises presumably from substitution of oxygen atoms for chloride. The $[\text{Mn}^{\text{III}}(\text{bpia})(\mu\text{-O})_2]^{2-}$ complex, in the $\text{Mn}^{\text{III}}\text{Mn}^{\text{IV}}$ oxidation level, has also been studied and is shown to be a catalase mimic. This observation is interesting because many other $\text{Mn}^{\text{III}}\text{Mn}^{\text{IV}}$ dimers and the super-

oxidized Mn catalase are catalytically incompetent. Since the b_{pia} system has not been completely characterized, further studies are required to elucidate a possible mechanism of this reaction; at that point, these complexes could be assessed as functional mimics for manganese catalases.

6. Future Directions for Modeling the Manganese Catalases

The previous sections have highlighted the developments in structural spectroscopic and reactivity modeling of the manganese catalases over the past 20 years. Clearly there have been many successes over this period, including small-molecule complexes that are nearly as efficient hydrogen peroxide disproportionation catalysts as the enzymes themselves. Despite these advances, we still strive for better models in order to understand more fully these important detoxification reactions. The present generation of models is ever improving with respect to mimicking the first coordination sphere of the manganese ions and providing bridges that are reflective of the enzyme active site.

6.1. Small-Molecule Models

Small-molecule models, in general, have several severe limitations. One of the primary limitations is that these low-molecular-weight compounds are unable to control the dielectric environment around the manganese ions. Thus, one sees catalytic activity that fluctuates greatly with solvent system; activity may be greatly pronounced in one solvent system but inactive in another. Another important limitation is that most small-molecule models are highly symmetric species because it is challenging to synthesize asymmetry into a single ligand and, in many cases, dimeric models are produced by the symmetric association of two identical monomeric units. Only recently have ligands been developed that might approximate the asymmetry of the dimanganese active site; this synthetic approach is challenging but worthy of consideration since effects of active-site asymmetry on spectroscopic and functional characteristics of dinuclear manganese sites have not been fully explored due to lack of such models for study. In addition, most small molecules cannot control hydrogen-bonding and salt-bridging effects that occur in enzyme active sites. These effects of first- and second-sphere coordination environments are now recognized as key structural features that influence the properties of metalloenzyme active sites. On an elementary level, basic first-sphere coordination can now be modeled with the appropriate synthetic ligand—although not many of these complexes employ nitrogen or oxygen donors that are identical to amino acid side chains found in biology. Second-sphere coordination with simple synthetic model complexes is virtually unknown. Most models, however, fail to approximate any second-sphere coordination about the manganese center despite the fact that the manganese catalase active site is embedded within a four-helix bundle in the enzyme. Recent advances in the area of de novo peptide design have

broached an exciting new prospect for modeling first- as well as second-sphere coordination about this active site. Using these de novo-designed peptides, one may easily be able to incorporate ligand asymmetry into the design strategy.

6.2. Peptidic Models

The tremendous advances in molecular and structural biology over the past 20 years now allow synthetic chemists the opportunity to design protein sequences using first principles (de novo design) or to redesign existing protein scaffolds in order to build metallo-binding sites in proteins. De novo-designed helical bundles can be a powerful tool for understanding not only protein structure but function as well. The goal is to design a novel peptide sequence that will associate and fold to resemble a completely native-like protein. In the case of manganese catalases, the target is a short peptide sequence that would not only assemble in a four-helix bundle but also bind two manganese ions in a manner similar to that of the native enzyme. This construct would be an extremely important model, given its potential for allowing investigation of structure–function–spectroscopy relationships.^{167,168} This new approach to modeling is, with one exception, undeveloped with respect to dinuclear metallopeptides. Historically, metal binding sites were inserted into a short protein sequence as discrete units (prefolded amino acid sequences were modified by site-directed mutagenesis to include amino acids amenable to metal binding).^{51,169} This was quickly followed by substitution of metal-binding side chains in the protein ligands so that subsequent association of three or four of these polypeptides would provide trihistidine,¹⁷⁰ hexahistidine,¹⁷¹ or tricysteine^{172,173} sites for metal binding within an α -helical bundle. Three-coordinate zinc sites have also been designed into four-helix bundle proteins,¹⁷⁴ and other sites possess a different set of side chains that emulate the binding of zinc in zinc finger enzymes,¹⁷⁵ iron (methane monooxygenase and ribonucleotide reductase),^{176,177} copper (blue copper sites),^{178,180} iron–sulfur clusters,^{181–183} and heme maquettes.^{184,185} In the latter case, metal insertion into the peptide bundles was achieved by introducing a prosthetic group such as a porphyrin or other synthetic appendages onto the peptide structure. Most of these metallopeptides are designed to bind only one metal since insertion of the charged, metal-binding side chains destabilizes the hydrophobic interior that is responsible for stable folding and bundle assembly.

Only one example of bimetallic peptides has been reported that binds both metal centers in close proximity. The peptide, DF1, is a recent development by DeGrado and co-workers and represents an idealized model for carboxylate-bridged proteins such as methane monooxygenase, the R2 subunit of ribonucleotide reductase, ferritins, and manganese catalases. The DF1 polypeptide was originally designed to form a dimeric four-helix bundle; each monomer is a helix–turn–helix such that two of these monomeric units assemble into an antiparallel four-helix bundle. The core of the four-helix bundle is lined with

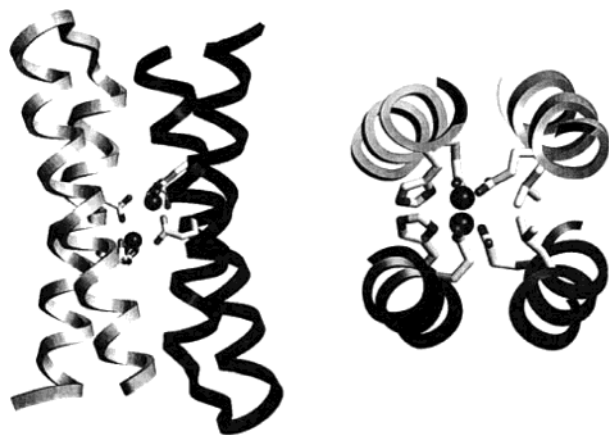


Figure 37. Crystal structure of $Zn_2(DF1)_2$. Perpendicular views of the peptide bundle showing the six chelating residues. Reprinted with permission from ref 186. Copyright 2001 The Protein Society.

hydrophobic residues, and the dimetal binding site is located near the center of the structure for greatest stability. This site has been shown to bind two iron ions or two zinc ions effectively;¹⁸⁶ both of these bimetallic peptide structures have been crystallographically confirmed with the structure of the zinc enzyme shown as Figure 37. Additional evidence supports formation of the binding site even in the apo-peptide. Although the system is promising, the DF1 peptide system has its limitations. First, the protein shows only limited solubility in aqueous solution. Second, the bundle assembles into a coherent structure that is thought to prohibit solvent access to the metals, a feature that is critical if the dinuclear metal site is to be catalytically active (substrates must be able to gain access to the active site). Despite such limitations that might hinder progress toward design of a catalytically active peptide model based on DF1, the peptide does indeed fold and assemble into the intended structure and bind two metal ions with bridging glutamates, although complexation with iron did not readily form a diferric oxo-bridged core.

A modification of DF1 is the DF2 peptide which effectively resolves the issues of its precursor. DF2 achieves better water solubility by replacing leucine residues on the exterior with side chains that would increase hydrophilicity: tyrosine, glutamine, alanine, serine, asparagine, and aspartate. The solubility of DF2 increases with pH over the range 4–7 and is soluble up to about 0.5 mM, although the hydrophobic stabilization is disturbed in this new peptide so that analytical ultracentrifugation analysis shows the presence of higher order aggregates of the apo-DF2 peptide (at near neutral pH). The aggregation is pH dependent, and the dimeric apo-DF2 peptide is favored at lower pH.

Crystal structures of dimetallic DF2 peptide have been obtained with two manganese atoms bound in the interior of the bundle. Unfortunately, binding of dinuclear manganese to DF2 does not result in one unique structure, and the presence of three crystallographically distinct manganese-bound DF2 dimers has been detected. These dimers vary in intermetal distance from 3.6 to 3.9 Å. More importantly, in the

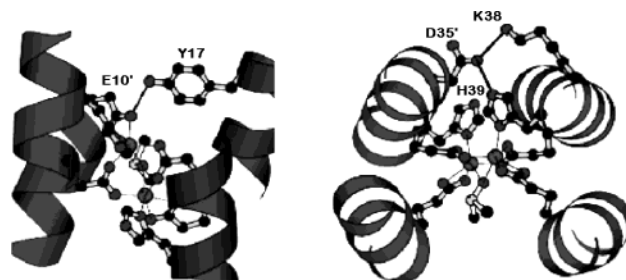


Figure 38. Tyrosine placement in the second sphere and hydrogen-bonding network that influences the bound metal. Reprinted with permission from ref 187. Copyright 2001 American Chemical Society.

DF2 system, solvent access is achieved with a leucine-to-alanine mutation, and one crystal structure shows the presence of a bridging DMSO molecule between the manganese centers. Introduction of second-sphere coordination about the metal site is achieved with a tyrosine placed at the appropriate location (Figure 38) and aids in providing for substrate access to the metals.¹⁸⁷ It is important to note that the intermetal distance achieved by the peptide is 3.66 Å for the substrate-bound manganese ions.

Further study is necessary to determine whether the $[Mn(DF2)]_2$ complex retains its overall structural configuration in solution, retains its metal-binding characteristics in solution, and can exhibit catalase-like activity and spectroscopic signatures resembling those of the enzyme. Such studies on this and subsequent Mn_2 -polypeptide complexes may facilitate a better understanding of protein folding and assembly, of first- and second-sphere influences on a bimetallic site, and of activity arising from that active site. This understanding will further elucidate the combination of structural, spectroscopic, and functional characteristics that constitute manganese catalases.

6.3. Concluding Remarks

Thus far, research with biomimetic models has provided a wealth of information that has aided the interpretation of complex spectra, like those obtained from pulsed EPR experiments or XANES. Complete characterization of series of models will allow us to probe relationships between structure and magnetic coupling or how structural modifications affect redox potentials of the bound metals. There is still much work that can be done in this ever-expanding field of study. For example, of great interest is the question of how halides, azide, and ammonium hydroxide bind to and inhibit the manganese catalases. Although inhibited catalases show particular spectroscopic features, few conclusions can be drawn as to where the binding of inhibitors occurs, what the binding mode is, and how the metal centers are perturbed. Further development and characterization of inhibition models with fluoride, azide, and ammonium hydroxide may provide answers to some of the questions. Thus far, few inhibition models have been produced. Most have not been fully characterized, and more investigation into inhibition models is required to reveal details about how these anions may inhibit the enzyme.

Structural models have progressed from the more speculative prior to high-resolution crystal structure analysis of the enzyme to the more corroborative. The corroborative modeling approach is intended to match the high-resolution data obtained for the active site of the enzyme. The first coordination sphere is accounted for by some of the simpler dimanganese ligand complexes. More recently, however, the second coordination sphere is generally accepted as being critical to tailoring properties of the metal centers. This is especially true in metalloproteins, and more complex models should eventually reflect this level of sophistication.

Spectroscopic models have thus far been used to elucidate magnetic, electronic, and structural properties of the enzyme. These models can be used to understand the reaction pathway by which the enzyme proceeds. No model system has been developed as yet that provides sufficient likeness of all features of the enzyme in all its various oxidation states. Further exploration in this area can help elucidate properties of more complicated models and deconvolute information contained in the more complex spectral features obtained from pulsed EPR for example.

Improved reactivity models are certainly a necessity. While modern structural biology has allowed us to understand in high resolution the protein structure of the Mn catalases and their active sites, there are currently no ways to characterize each independent step in such manganese systems. For this, model complexes provide a unique way of testing mechanisms in these systems. This having been said, model complexes still have their limitations. None have so far achieved rates of catalysis matching that of the enzyme. Only a handful show promising reactivity while utilizing the appropriate oxidation states during catalysis. Only one or two of those model systems, in fact, uses nitrogen donors that are similar to biological nitrogen donors. Mechanistic characteristics of the model complexes vary widely along with activity. Further discovery and characterization of reactivity models is a challenging but vital area of study. Inclusion of peptidic models and development of catalytically active peptides may prove extremely beneficial to elucidating a mechanism by which hydrogen peroxide disproportionation occurs. The final approach may allow us to satisfy the old adage that we only truly understand a system when we can build it from scratch.

7. Acknowledgments

This work was supported by the National Institutes of Health Grants GM 39406 (V.L.P.), GM 45205 (J.E.P.-H.), and GM 008270 (A.J.W.).

8. Glossary of Abbreviations

AcAc	2,4-pentadione
Acporph	2,2'-benzyl-5,5'-(1,3-diiminopropyl)-dipyrrole macrocycle
benzimpn	<i>N,N,N,N</i> -tetrakis((<i>N</i> -alkyl)benzimidazolyl)-1,3-diaminopropan-2-ol
bispicen	<i>N,N</i> -bis(2-pyridylmethyl)-1,2-ethanediamine

bpea	<i>N,N</i> -bis(2-pyridylmethyl)ethylamine
bpg	<i>N,N</i> -bis(2-pyridylmethyl)glycine
bpy, bipy	2,2'-bipyridine
Bpsalden	<i>N,N</i> -bis(2-pyridylmethyl)- <i>N</i> -salicylidene-1,2-diaminoethane
dahpta	1,3-diamino-2-hydroxypropane- <i>N,N,N,N</i> -tetraacetic acid
dpa	<i>N,N</i> -bis(2-pyridylmethyl)glycine
edda	ethylenediamine- <i>N,N</i> -diacetate
en	ethylenediamine
Hbbml	2-[bis(2-benzimidazolylmethyl)amino]-ethanol
HPX-CO ₂ H	5-[4-(5-methoxycarbonyl-2,7-di- <i>tert</i> -butyl-9,9-dimethylxanthenyl)]-10,15,20-trimesitylporphyrin
H ₂ saladhp	2-(salicylideneiminato)-2-methyl-1,3-dihydroxypropane
H ₂ salpn	1,3-bis(salicylideneiminato)propane
H ₂ [(5-Cl-sal)pn]	1,2-bis((5-chlorosalicylideneiminato)propane
H ₂ [(2-OH-sal)pn]	1,3-bis(salicylideneiminato)-2-hydroxypropane
H ₂ salen	1,2-bis(salicylideneiminato)ethane
H ₂ salps	<i>N,N</i> -[2,2'-dithiobis(phenylene)]bis(salicylideneaminato)
Manf	mannofuranose
OAc	acetate anion
OEP	octaethylporphyrin
phen	1,10-phenanthroline
Picphpy	2-(bis(2-pyridylmethyl)aminomethyl)-6-((2-pyridylmethyl)(benzyl)aminomethyl)-4-methylphenol
salimH ₂ ⁴⁻	[2-(salicylideneimine)ethyl]imidazole
salpentOH	1,5-bis(salicylideneamino)pentan-3-ol
TBA	tetra- <i>n</i> -butylammonium cation
Tmeda	<i>N,N,N,N</i> -tetramethylethylenediamine
TMIMA	tris(1-methylimidazol-2-yl)methylamine
Tol	<i>o</i> -toluic acid
TPA, tmpa	tris(2-pyridylmethyl)amine
TPP	tetraphenylporphyrin

9. Note Added after ASAP Posting

After this article was posted ASAP on 1/3/2004, a change was made in the next-to-last paragraph of Section 3.1, where the μ -oxo compound reported by Kitajima et al. in ref 59 is a Mn₂(III,III), not a Mn₂(II,II) compound. The correct version was posted 1/19/2004.

10. References

- Wiegardt, K. *Angew. Chem., Int. Ed. Engl.* **1989**, *28*, 1153.
- Law, N. A.; Caudle, M. T.; Pecoraro, V. L. In *Manganese Redox Enzymes and Model Systems: Properties, Structures, and Reactivity*; Pecoraro, V. L., Ed.; Academic Press: San Diego, CA, 1999; Vol. 46.
- Yoder, D. W.; Hwang, J.; Penner-Hahn, J. E. In *Metal Ions in Biological Systems*; Sigel, A., Sigel, H., Eds.; Marcel Dekker: New York, 1999; Vol. 37.
- Christianson, D. W. *Prog. Biophys. Mol. Biol.* **1997**, *67*, 217.
- Vincent, J. B.; Christou, G. *Adv. Chem.* **1989**, *33*, 197.
- Sheptovitsky, Y. G.; Brudvig, G. W. *Biochemistry* **1998**, *37*, 5052.
- Delwiche, E. A. *J. Bacteriol.* **1961**, *81*, 416.
- Johnston, M. A.; Delwiche, E. A. *J. Bacteriol.* **1962**, *83*, 936.
- Johnston, M. A.; Delwiche, E. A. *J. Bacteriol.* **1965**, *90*, 352.
- Kono, Y.; Fridovich, I. *J. Biol. Chem.* **1983**, *258*, 6015.
- Barynin, V. V.; Vagin, A. A.; Melik-Adamyan, V. R.; Grebenko, A. I.; Khangulov, S. V.; Popov, A. N.; Andrianova, M. E.; Vainshtein, B. K. *Dokl. Akad. Nauk S.S.S.R.* **1986**, *288*, 877.
- Allgood, G. S.; Perry, J. J. *J. Bacteriol.* **1986**, *168*, 563.
- Phucharoen, K.; Takenaka, Y.; Shinozawa, T. *DNA Sequence* **2001**, *12*, 413.

- (14) Kagawa, M.; Murakoshi, N.; Mizobata, T.; Kawata, Y.; Nagai, J. *FASEB J.* **1997**, *11*, A1138.
- (15) Robbe-Saule, V.; Coynault, C.; Ibanez-Ruiz, M.; Hermant, D.; Norel, F. *Mol. Microbiol.* **2001**, *39*, 15335.
- (16) Amo, T.; Atomi, H.; Imanaka, T. *J. Bacteriol.* **2002**, *184*, 3305.
- (17) Barynin, V. V.; Grebenko, A. I. *Dokl. Akad. Nauk S.S.S.R.* **1986**, *286*, 461.
- (18) Penner-Hahn, J. E. In *Manganese Redox Enzymes*; Pecoraro, V. L., Ed.; VCH Publishers: New York, 1992.
- (19) Waldo, G. S.; Penner-Hahn, J. E. *Biochemistry* **1995**, *34*, 1507.
- (20) Khangulov, S. V.; Barynin, V. V.; Voevodskaya, N. V.; Grebenko, A. I. *Biochim. Biophys. Acta* **1990**, *1020*, 305.
- (21) Waldo, G. S.; Fronko, R. M.; Penner-Hahn, J. E. *Biochemistry* **1991**, *30*, 10486.
- (22) Khangulov, S. V.; Goldfeld, M. G.; Gerasimenko, V. V.; Andreeva, N. E.; Barynin, V. V.; Grebenko, A. I. *J. Inorg. Biochem.* **1990**, *40*, 279.
- (23) Khangulov, S. V.; Barynin, V. V.; Antonyuk-Barynina, S. V. *Biochim. Biophys. Acta* **1990**, *1020*, 25.
- (24) Gelasco, A.; Bensiak, S.; Pecoraro, V. L. *Inorg. Chem.* **1998**, *37*, 3301.
- (25) Kono, Y.; Fridovich, I. *J. Biol. Chem.* **1983**, *258*, 13646.
- (26) Nagata, T.; Ikawa, Y.; Maruyama, K. *J. Chem. Soc., Chem. Commun.* **1994**, 471.
- (27) Waldo, G. S.; Penner-Hahn, J. E. *Biochemistry* **1995**, *34*, 1507.
- (28) Meier, A. E.; Whittaker, M. M.; Whittaker, J. W. *Biochemistry* **1996**, *35*, 348.
- (29) Antonyuk, S. V.; Melik-Adamyan, V. R.; Popov, A. N.; Lamzin, V. S.; Hempstead, P. D.; Harrison, P. M.; Artymyuk, P. J.; Barynin, V. V. *Cryst. Rep.* **2000**, *45*, 111.
- (30) Barynin, V. V.; Hempstead, P. D.; Vagin, A. A.; Antonyuk, S. V.; Melik-Adamyan, V. R.; Lamzin, V. S.; Harrison, P. M.; Artymyuk, P. J. *J. Inorg. Biochem.* **1997**, *67*, 196.
- (31) Barynin, V. V.; Whittaker, M. M.; Antonyuk, S. V.; Lamzin, V. S.; Harrison, P. M.; Artymyuk, P. J.; Whittaker, J. W. *Structure* **2001**, *9*, 725.
- (32) Wallar, B. J.; Lipscomb, J. D. *Chem. Rev.* **1996**, *96*, 2625.
- (33) Whittaker, M. M.; Barynin, V. V.; Antonyuk, S. V.; Whittaker, J. W. *Biochemistry* **1999**, *38*, 9126.
- (34) Whittaker, M. M.; Barynin, V. V.; Igarashi, T.; Whittaker, J. W. *Eur. J. Biochem.* **2003**, *270*, 1102.
- (35) Khangulov, S. V.; Pessiki, P. J.; Barynin, V. V.; Ash, D. E.; Dismukes, G. C. *Biochemistry* **1995**, *34*, 2015.
- (36) Dismukes, G. C. *Chem. Rev.* **1996**, *96*, 2909.
- (37) Haddy, A.; Waldo, G. S.; Sands, R. H.; Penner-Hahn, J. E. *Inorg. Chem.* **1994**, *33*, 2677.
- (38) Stemmler, T. L.; Sossong, T. M., Jr.; Goldstein, J. I.; Ash, D. E.; Elgren, T. E.; Kurtz, D. M., Jr.; Penner-Hahn, J. E. *Biochemistry* **1997**, *36*, 9847.
- (39) Stemmler, T. L.; Sturgeon, B. E.; Randall, D. W.; Britt, R. D.; Penner-Hahn, J. E. *J. Am. Chem. Soc.* **1997**, *119*, 9215.
- (40) Zheng, M.; Khangulov, S.; Dismukes, G. C.; Barynin, V. *Inorg. Chem.* **1994**, *33*, 382.
- (41) Schafer, K.-O.; Bittl, R.; Lenzian, F.; Barynin, V.; Weyhermuller, T.; Wieghardt, K.; Lubitz, W. *J. Phys. Chem. B* **2003**, *107*, 1242.
- (42) Khangulov, S.; Sivaraja, M.; Barynin, V. V.; Dismukes, G. C. *Biochemistry* **1993**, *32*, 4912.
- (43) Brunold, T. C.; Gamelin, D. R.; Stemmler, T. L.; Mandal, S. K.; Armstrong, W. H.; Penner-Hahn, J. E.; Solomon, E. I. *J. Am. Chem. Soc.* **1998**, *120*, 8724.
- (44) Gamelin, D. R.; Kirk, M. L.; Stemmler, T. L.; Pal, S.; Armstrong, W. H.; Penner-Hahn, J. E.; Solomon, E. I. *J. Am. Chem. Soc.* **1994**, *116*, 2392.
- (45) Khangulov, S. V.; Barynin, V. V.; Voevodskaya, N. V.; Grebenko, A. I. *Biochim. Biophys. Acta* **1990**, *1020*, 305.
- (46) Jacquamet, L.; Michaud-Soret, I.; Debaecker-Petit, N.; Barynin, V. V.; Zimmermann, J. L.; Latour, J. M. *Angew. Chem., Int. Ed.* **1997**, *36*, 1626.
- (47) Le Pape, L.; Perret, E.; Michaud-Soret, I.; Latour, J.-M. *J. Biol. Inorg. Chem.* **2002**, *7*, 445.
- (48) Michaud-Soret, I.; Jacquamet, L.; Debaecker-Petit, N.; Le Pape, L.; Barynin, V.; Latour, J.-M. *Inorg. Chem.* **1998**, *37*, 3874.
- (49) Algood, G. S.; Perry, J. J. *J. Bacteriol.* **1986**, *168*, 563.
- (50) Antonyuk, S. V.; Melik-Adamyan, V. R.; Popov, A. N.; Lamzin, V. S.; Hempstead, P. D.; Harrison, P. M.; Artymyuk, P. J.; Barynin, V. V. *Structure* **2000**, *45*, 111.
- (51) Regan, L. *Annu. Rev. Biophys. Biomol. Struct.* **1993**, *22*, 257.
- (52) Pecoraro, V. L.; Baldwin, M. J.; Gelasco, A. *Chem. Rev.* **1994**, *94*, 807.
- (53) Tetard, D.; Rabion, A.; Verlhac, J.-B.; Guilhem, J. J. *J. Chem. Soc., Chem. Commun.* **1995**, 531.
- (54) Horner, O.; Anxolabehere-Mallart, E.; Charlot, M.-F.; Tcheratanov, L.; Guilhem, J.; Mattioli, T. A.; Boussac, A.; Girerd, J.-J. *Inorg. Chem.* **1999**, *38*, 1222.
- (55) Cheng, B.; Cukiernik, F.; Fries, P. H.; Marchon, J.-C.; Scheidt, W. R. *Inorg. Chem.* **1995**, *34*, 4627.
- (56) Cheng, B.; Fries, P. H.; Marchon, J.-C.; Scheidt, W. R. *Inorg. Chem.* **1996**, *35*, 1024.
- (57) Schardt, B. C.; Hollander, F. J.; Hill, C. L. *J. Chem. Soc., Chem. Commun.* **1981**, 765.
- (58) Kipke, C. A.; Scott, M. J.; Gohdes, J. W.; Armstrong, W. H. *Inorg. Chem.* **1990**, *29*, 2193.
- (59) Kitajima, N.; Osawa, M.; Tanaka, M.; Moro-oka, Y. *J. Am. Chem. Soc.* **1991**, *113*, 8952.
- (60) Larson, E.; Haddy, A.; Kirk, M. L.; Sands, R. H.; Hatfield, W. E.; Pecoraro, V. L. *J. Am. Chem. Soc.* **1992**, *114*, 6263.
- (61) Kitajima, N.; Singh, U. P.; Amagai, H.; Osawa, M.; Moro-oka, Y. *J. Am. Chem. Soc.* **1991**, *113*, 7757.
- (62) Glerup, J.; Goodson, P. A.; Hazell, A.; Hodgson, D. J.; McKenzie, C. J.; Michelson, K.; Rychlewska, U.; Toftlund, H. *Inorg. Chem.* **1994**, *33*, 4105.
- (63) Goodson, P. A.; Glerup, J.; Hodgson, D. J.; Michelson, K.; Pedersen, E. *Inorg. Chem.* **1990**, *29*, 503.
- (64) Jensen, A. F.; Su, Z.; Hansen, N. K.; Larsen, F. K. *Inorg. Chem.* **1995**, *34*, 4244.
- (65) Manchanda, R.; Brudvig, G. W.; de Gala, S.; Crabtree, R. H. *Inorg. Chem.* **1994**, *33*, 5157.
- (66) Manchanda, R.; Thorp, H. H.; Brudvig, G. W.; Crabtree, R. H. *Inorg. Chem.* **1992**, *31*, 4040.
- (67) Triller, M. U.; Hsieh, W.-Y.; Pecoraro, V. L.; Rempel, A.; Krebs, B. *Inorg. Chem.* **2002**, *41*, 5544.
- (68) Manchanda, R.; Brudvig, G. W.; Crabtree, R. H. *Coord. Chem. Rev.* **1995**, *144*, 1.
- (69) Carroll, J. M.; Norton, J. R. *J. Am. Chem. Soc.* **1992**, *114*, 8744.
- (70) Larson, E.; Lah, M. S.; Li, X.; Bonadies, J. A.; Pecoraro, V. L. *Inorg. Chem.* **1992**, *31*, 373.
- (71) Gohdes, J. W.; Armstrong, W. H. *Inorg. Chem.* **1992**, *31*, 368.
- (72) Baldwin, M. J.; Stemmler, T. L.; Riggs-Gelasco, P. J.; Kirk, M. L.; Penner-Hahn, J. E.; Pecoraro, V. L. *J. Am. Chem. Soc.* **1994**, *116*, 11349.
- (73) Larson, E. J.; Riggs, P. J.; Penner-Hahn, J. E.; Pecoraro, V. L. *J. Chem. Soc., Chem. Commun.* **1992**, 102.
- (74) Larson, E. J.; Pecoraro, V. L. *J. Am. Chem. Soc.* **1991**, *113*, 3810.
- (75) Baldwin, M. J.; Gelasco, A.; Pecoraro, V. L. *Photosynth. Res.* **1993**, *38*, 303.
- (76) Baffert, C.; Collomb, M.-N.; Deronzier, A.; Pecaut, J.; Limburg, J.; Crabtree, R. H.; Brudvig, G. W. *Inorg. Chem.* **2002**, *41*, 1404.
- (77) Zhang, J.-J.; Luo, Q.-H.; Duan, C.-Y.; Wang, Z.-L.; Mei, Y.-H. *J. Inorg. Biochem.* **2001**, *86*, 573.
- (78) Zhang, J.-J.; Tang, Y.-Y.; Luo, Q.-H.; Duan, C.-Y.; Wang, Z.-L.; Mei, Y.-H. *Polyhedron* **2001**, *20*, 2285.
- (79) Caudle, M. T.; Pecoraro, V. L. *Inorg. Chem.* **2000**, *39*, 5831.
- (80) Torayama, H.; Nishide, T.; Asada, H.; Fujiwara, M.; Matsushita, T. *Polyhedron* **1998**, *17*, 105.
- (81) Perret, E.; Le Pape, L.; Michaud, S., I.; Whittaker, J. W.; Latour, J.-M. *J. Inorg. Biochem.* **1999**, *74*, 201.
- (82) Arulsamy, N.; Glerup, J.; Hazell, A.; Hodgson, D. J.; McKenzie, C. J.; Toftlund, H. *Inorg. Chem.* **1994**, *33*, 3023.
- (83) Bertocello, K.; Fallon, G. D.; Murray, K. S. *Polyhedron* **1990**, *9*, 2867.
- (84) Pessiki, P. J.; Khangulov, S. V.; Ho, D. M.; Dismukes, G. C. *J. Am. Chem. Soc.* **1994**, *116*, 891.
- (85) Oberhausen, K. J.; O'Brien, R. J.; Richardson, J. F.; Buchanan, R. M.; Costa, R.; Latour, J.-M.; Tsai, H.-L.; Hendrickson, D. N. *Inorg. Chem.* **1993**, *32*, 4561.
- (86) Tanase, T.; Lippard, S. J. *Inorg. Chem.* **1995**, *34*, 4682.
- (87) Sheats, J. E.; Czernuszewicz, R. S.; Dismukes, G. C.; Rheingold, A. L.; Petrouleas, V.; Stubbe, J.; Armstrong, W. H.; Beer, R. H.; Lippard, S. J. *J. Am. Chem. Soc.* **1987**, *109*, 1435.
- (88) Yu, S.-B.; Lippard, S. J.; Schwelky, I.; Bino, A. *Inorg. Chem.* **1992**, *31*, 3502.
- (89) Wieghardt, K.; Bossek, U.; Ventur, D.; Weiss, J. *J. Chem. Soc., Chem. Commun.* **1985**, 347.
- (90) Kitajima, N.; Komatsuzaki, H.; Hikichi, S.; Osawa, M.; Moro-oka, Y. *J. Am. Chem. Soc.* **1994**, *116*, 11596.
- (91) Reddy, K. R.; Rajasekharan, M. V.; Padhye, S.; Dahan, F.; Tuchagues, J.-P. *Inorg. Chem.* **1994**, *33*, 428.
- (92) Romero, I.; Dubois, L.; Collomb, M.-N.; Deronzier, A.; Latour, J.-M.; Pecaut, J. *Inorg. Chem.* **2002**, *41*, 1795.
- (93) Bossek, U.; Saher, M.; Weyhermuller, T.; Wieghardt, K. *J. Chem. Soc., Chem. Commun.* **1992**, 1780.
- (94) Palopoli, C.; Gonzalez-Sierra, M.; Robles, G.; Dahan, F.; Tuchagues, J.-P.; Signorella, S. *J. Chem. Soc., Dalton Trans.* **2002**, 3813.
- (95) Sakiyama, H.; Tamaki, H.; Kodera, M.; Matsumoto, N.; Okawa, H. *J. Chem. Soc., Dalton Trans.* **1993**, 591.
- (96) Sakiyama, H.; Okawa, H.; Isobe, R. *J. Chem. Soc., Chem. Commun.* **1993**, 882.
- (97) Rardin, R. L.; Tolman, W. B.; Lippard, S. J. *New J. Chem.* **1991**, *15*, 417.
- (98) Baldwin, M. J.; Kampf, J. W.; Pecoraro, V. L. *J. Chem. Soc., Chem. Commun.* **1993**, 1741.
- (99) Rardin, R. L.; Poganiuch, P.; Bino, A.; Goldberg, D. P.; Tolman, W. B.; Liu, S.; Lippard, S. J. *J. Am. Chem. Soc.* **1992**, *114*, 5240.
- (100) Menage, S.; Vitols, S. E.; Bergerat, P.; Codjovi, E.; Kahn, O.; Girerd, J.-J.; Guillot, M.; Solans, X.; Calvet, T. *Inorg. Chem.* **1991**, *30*, 2666.

- (101) Kessissoglou, D. P.; Kirk, M. L.; Bender, C. A.; Lah, M. S.; Pecoraro, V. L. *J. Chem. Soc., Chem. Commun.* **1989**, 84.
- (102) Ye, B.-H.; Mak, T.; Williams, I. D.; Li, X.-Y. *J. Chem. Soc., Chem. Commun.* **1997**, 1813.
- (103) Dubois, L.; Xiang, D. F.; Tan, X. S.; Pecaut, J.; Jones, P.; Baudron, S.; Le Pape, L.; Latour, J.-M.; Baffert, C.; Chardon-Noblat, S.; Collomb, M.-N.; Deronzier, A. *Inorg. Chem.* **2003**, 42, 750.
- (104) Dave, B. C.; Czernuszewicz, R. S. *Inorg. Chim. Acta* **1998**, 281, 25.
- (105) Horner, O.; Girerd, J.-J.; Philouze, C.; Tchertanov, L. *Inorg. Chim. Acta* **1999**, 290, 139.
- (106) Kawamori, A.; Mino, H.; Matsukawa, T. *Proceedings of the XIth International Congress on Photosynthesis*, Budapest, 1998; p 72.
- (107) Matsukawa, T.; Mino, H.; Yoneda, D.; Kawamori, A. *Biochemistry* **1999**, 38, 4072.
- (108) Britt, R. D.; Peloquin, J. M.; Campbell, K. A. *Annu. Rev. Biophys. Biomol. Struct.* **2000**, 29, 463.
- (109) Force, D. A.; Randall, D. W.; Lorigan, G. A.; Clemens, K. L.; Britt, R. D. *J. Am. Chem. Soc.* **1998**, 120, 13321.
- (110) Randall, D. W.; Gelasco, A.; Caudle, M. T.; Pecoraro, V. L.; Britt, R. D. *J. Am. Chem. Soc.* **1997**, 119, 4481.
- (111) Peloquin, J. M.; Campbell, K. A.; Randall, D. W.; Evanchik, M. A.; Pecoraro, V. L.; Armstrong, W. H.; Britt, R. D. *J. Am. Chem. Soc.* **2000**, 122, 10926.
- (112) Peloquin, J. M.; Britt, R. D. *Biochim. Biophys. Acta* **2001**, 1503, 96.
- (113) Munck, E.; Popescu, C. V. *Hyperfine Interact.* **2000**, 126, 59.
- (114) Neese, F. *Curr. Opin. Chem. Biol.* **2003**, 7, 125.
- (115) Bill, E.; Beckman, U.; Wieghardt, K. *Hyperfine Interact.* **2002**, 144, 183–198.
- (116) Bertini, I.; Capozzi, F.; Luchinat, C. *Paramag. Res. Metallobiol.* **2003**, 858, 272.
- (117) Penner-Hahn, J. E. *Coord. Chem. Rev.* **1999**, 190–192, 1101.
- (118) Riggs-Gelasco, P. Ph.D. Dissertation, University of Michigan, Ann Arbor, 1995.
- (119) Hsieh, W.-Y. Ph.D. Dissertation, University of Michigan, Ann Arbor, 2002.
- (120) Yoder, D. W. Ph.D. Dissertation, University of Michigan, Ann Arbor, 2002.
- (121) Alexiou, M.; Dendrinou-Samara, C.; Karagianni, A.; Biswas, S.; Zaleski, C. M.; Kampf, J. W.; Yoder, D. W.; Penner-Hahn, J. E.; Pecoraro, V. L.; Kessissoglou, D. P. *Inorg. Chem.* **2003**, 42, 2185.
- (122) Caudle, M. T.; Riggs-Gelasco, P.; Gelasco, A. K.; Penner-Hahn, J. E.; Pecoraro, V. L. *Inorg. Chem.* **1996**, 35, 3577.
- (123) Gelasco, A.; Kirk, M. L.; Kampf, J. W.; Pecoraro, V. L. *Inorg. Chem.* **1997**, 36, 1829.
- (124) Bonadies, J. A.; Kirk, M. L.; Lah, M. S.; Kessissoglou, D. P.; Hatfield, W. E.; Pecoraro, V. L. *Inorg. Chem.* **1989**, 28, 2037.
- (125) Bertonecchio, K.; Fallon, G. D.; Murray, K. S.; Tiekink, E. R. T. *Inorg. Chem.* **1991**, 30, 3562.
- (126) Kessissoglou, D. P.; Butler, W. M.; Pecoraro, V. L. *Inorg. Chem.* **1987**, 26, 495.
- (127) Yu, S. B.; Wang, C. P.; Day, E. P.; Holm, R. H. *Inorg. Chem.* **1991**, 30, 4067.
- (128) Rajendiran, T. M.; Caudle, M. T.; Kirk, M. L.; Setyawati, I.; Kampf, J. W.; Pecoraro, V. L. *J. Biol. Inorg. Chem.* **2003**, 8, 283.
- (129) Law, N. A.; Kampf, J. W.; Pecoraro, V. L. *Inorg. Chim. Acta* **2000**, 297, 252.
- (130) Wieghardt, K.; Bossek, U.; Nuber, B.; Weiss, J.; Bonvoisin, J.; Corbella, M.; Vitols, S. E.; Girerd, J. J. *J. Am. Chem. Soc.* **1988**, 110, 7398.
- (131) Baldwin, M. J.; Law, N. A.; Stemmler, T. L.; Kampf, J. W.; Penner-Hahn, J. E.; Pecoraro, V. L. *Inorg. Chem.* **1999**, 38, 4801.
- (132) Wieghardt, K.; Bossek, U.; Gebert, W. *Angew. Chem., Int. Ed. Engl.* **1983**, 22, 328.
- (133) Geisselman, A.; Klufers, P.; Pilawa, B. *Angew. Chem., Int. Ed.* **1998**, 37, 1119.
- (134) Rajendiran, T. M.; Kirk, M. L.; Setyawati, I.; Caudle, M. T.; Kampf, J. W.; Pecoraro, V. L. *J. Chem. Soc., Chem. Commun.* **2003**, 824.
- (135) Caudle, M. T.; Kampf, J. W.; Kirk, M. L.; Rasmussen, P. G.; Pecoraro, V. L. *J. Am. Chem. Soc.* **1997**, 119, 9297.
- (136) Mathur, P.; Crowder, M.; Dismukes, G. C. *J. Am. Chem. Soc.* **1987**, 109, 5227.
- (137) Blanchard, S.; Blondin, G.; Riviere, E.; Nierlich, M.; Girerd, J.-J. *Inorg. Chem.*, in press.
- (138) Blanchard, S.; Blain, G.; Riviere, E.; Nierlich, M.; Blondin, G. *Chem. Eur. J.*, in press.
- (139) More, C. B., V.; Asso, M.; Fournel, A.; Roger, G.; Guigliarelli, B.; Bertrand, P. *Biospectroscopy* **1999**, 5, S3–S18 (Suppl. S).
- (140) Sossong, T. M., Jr.; Khangulov, S. V.; Cavalli, R. C.; Soprano, D. R.; Dismukes, G. C.; Ash, D. E. *J. Biol. Inorg. Chem.* **1997**, 2, 433.
- (141) Naruta, Y.; Sasayama, M.; Sasaki, T. *Angew. Chem., Int. Ed. Engl.* **1994**, 33, 1839.
- (142) Naruta, Y.; Maruyama, K. *J. Am. Chem. Soc.* **1991**, 113, 3595.
- (143) Balasubramanian, P. N.; Schmidt, E. S.; Bruice, T. C. *J. Am. Chem. Soc.* **1987**, 109, 7865.
- (144) Balasubramanian, P. N.; Sinha, A.; Bruice, T. C. *J. Am. Chem. Soc.* **1987**, 109, 1456.
- (145) Khangulov, S. V.; Andreeva, N. E.; Gerasimenko, V. V.; Gol'dfel'd, M. G.; Barynin, V.; Grebenko, A. I. *Z. Fiz. Khim.* **1994**, 64.
- (146) Naruta, Y.; Sasayama, M. *J. Chem. Soc., Chem. Commun.* **1994**, 2667.
- (147) Naruta, Y.; Sasayama, M.-a.; Ichihara, K. *J. Mol. Catal. A* **1997**, 117, 115.
- (148) Chang, C. J.; Chang, L. L.; Nocera, D. G. *J. Am. Chem. Soc.* **2003**, 125, 1866.
- (149) Stibrany, R. T.; Gorun, S. M. *Angew. Chem., Int. Ed. Engl.* **1990**, 29, 1156.
- (150) Gelasco, A.; Askenas, A.; Pecoraro, V. L. *Inorg. Chem.* **1996**, 35, 1419.
- (151) Gelasco, A. K. Ph.D. Dissertation, University of Michigan, Ann Arbor, 1995.
- (152) Bhula, R.; Gainsford, G. J.; Weatherburn, D. C. *J. Am. Chem. Soc.* **1988**, 110, 7550.
- (153) Dube, C. E.; Wright, D. W.; Pal, S.; Bonitatebus, J., P. J.; Armstrong, W. H. *J. Am. Chem. Soc.* **1998**, 120, 3704.
- (154) Dube, C. E.; Wright, D. W.; Armstrong, W. H. *Angew. Chem., Int. Ed.* **2000**, 39, 2169.
- (155) Boelrijk, A. E. M.; Dismukes, G. C. *Inorg. Chem.* **2000**, 39, 3020.
- (156) Boelrijk, A. E. M.; Khangulov, S. V.; Dismukes, G. C. *Inorg. Chem.* **2000**, 39, 3009.
- (157) Pessiki, P. J.; Dismukes, G. C. *J. Am. Chem. Soc.* **1994**, 116, 898.
- (158) Delroisse, M.; Rabion, A.; Chardac, F.; Tetard, D.; Verlhac, J.-B.; Fraisse, L.; Seris, J.-L. *J. Chem. Soc., Chem. Commun.* **1995**, 949.
- (159) Higuchi, C.; Sakiyama, H.; Okawa, H.; Isobe, R.; Fenton, D. E. *J. Chem. Soc., Dalton Trans.* **1994**, 1097.
- (160) Aono, T.; Wada, H.; Yonemura, M.; Ohba, M.; Okawa, H.; Fenton, D. E. *J. Chem. Soc., Dalton Trans.* **1997**, 9, 1527.
- (161) Sasaki, Y.; Akamatsu, T.; Tsuchiya, K.; Ohba, S.; Sakamoto, M.; Nishida, Y. *Polyhedron* **1998**, 17, 235.
- (162) Higuchi, C.; Sakiyama, H.; Okawa, H.; Fenton, D. E. *J. Chem. Soc., Dalton Trans.* **1995**, 4015.
- (163) Nishida, Y.; Akamatsu, T.; Kazuyoshi, T.; Sakamoto, M. *Polyhedron* **1994**, 13, 2251.
- (164) Romero, I.; Collomb, M.-N.; Deronzier, A.; Llobet, A.; Perret, E.; Pecaut, J.; Le Pape, L.; Latour, J.-M. *Eur. J. Inorg. Chem.* **2001**, 69.
- (165) Larson, E. J.; Pecoraro, V. L. *J. Am. Chem. Soc.* **1991**, 113, 7809.
- (166) Bossek, U.; Weyhermüller, T.; Wieghardt, K.; Nuber, B.; Weiss, J. *J. Am. Chem. Soc.* **1990**, 112, 6387.
- (167) Hill, R. B.; Raleigh, D. P.; Lombardi, A.; DeGrado, W. F. *Acc. Chem. Res.* **2000**, 33, 745.
- (168) Lu, Y.; Valentine, J. S. *Curr. Opin. Struct. Biol.* **1997**, 7, 485.
- (169) Lu, Y.; Berry, S. M.; Pfister, T. D. *Chem. Rev.* **2001**, 101, 3047.
- (170) Ghadiri, M. R.; Case, M. A. *Angew. Chem., Int. Ed. Engl.* **1993**, 32, 1594.
- (171) Suzuki, K.; Hiroaki, H.; Kohda, D.; Nakamura, H.; Tanaka, T. *J. Am. Chem. Soc.* **1998**, 120, 13008.
- (172) Farrer, B. T.; McClure, C. P.; Penner-Hahn, J. E.; Pecoraro, V. L. *Inorg. Chem.* **2000**, 39, 5422.
- (173) Diekmann, G. R.; McRorie, D. K.; Tierney, D. L.; Utschig, L. M.; Singer, C. P.; O'Halloran, T. V.; Penner-Hahn, J. E.; DeGrado, W. F.; Pecoraro, V. L. *J. Am. Chem. Soc.* **1997**, 119, 6195.
- (174) Klemba, M.; Regan, L. *Biochemistry* **1995**, 34, 10094.
- (175) Regan, L.; Clarke, N. D. *Biochemistry* **1990**, 29, 10878.
- (176) Marsh, E. N. G.; DeGrado, W. F. *Proc. Natl. Acad. Sci. U.S.A.* **2002**, 99, 5150.
- (177) Summa, C. M.; Rosenblatt, M. M.; Hong, J.-K.; Lear, J. D.; DeGrado, W. F. *J. Mol. Biol.* **2002**, 321, 923.
- (178) Schnepf, R.; Horth, P.; Bill, E.; Wieghardt, K.; Hildebrandt, P.; Haehnel, W. *J. Am. Chem. Soc.* **2001**, 123, 2186.
- (179) Daugherty, R. G.; Wasowicz, T.; Gibney, B. R.; DeRose, V. J. *Inorg. Chem.* **2002**, 41, 2623.
- (180) Hellinga, H. W. *J. Am. Chem. Soc.* **1998**, 120, 10055.
- (181) Kennedy, M. L.; Gibney, B. R. *J. Am. Chem. Soc.* **2002**, 124, 6826.
- (182) Mulholland, S. E.; Gibney, B. R.; Rabanal, F.; Dutton, P. L. *J. Am. Chem. Soc.* **1998**, 120, 10296.
- (183) Benson, D. E.; Wisz, M. S.; Liu, W. T.; Hellinga, H. W. *Biochemistry* **1998**, 37, 7070.
- (184) Reedy, C. J.; Kennedy, M. L.; Gibney, B. R. *J. Chem. Soc., Chem. Commun.* **2003**, 570.
- (185) Arnold, P. A.; Benson, D. R.; Brink, D. J.; Hendrich, M. P.; Jas, G. S.; Kennedy, M. L.; Petasis, D. T.; Wang, M. X. *Inorg. Chem.* **1997**, 36, 5306.
- (186) Pasternak, A.; Kaplan, J.; Lear, J. D.; DeGrado, W. F. *Protein Sci.* **2001**, 10, 958.
- (187) Di Costanzo, L.; Wade, H.; Geremia, S.; Randaccio, L.; Pavone, V.; DeGrado, W. F.; Lombardi, A. *J. Am. Chem. Soc.* **2001**, 123, 12749.
- (188) Wu, F.-J.; Kurtz, D. M.; Hagen, K. S.; Nyman, P. D.; Debrunner, P. G.; Vankai, V. A. *Inorg. Chem.* **1990**, 29, 5174.

- (189) Suzuki, M.; Senda, H.; Kobayashi, Y.; Oshio, H.; Uehara, A. *Chem. Lett.* **1988**, 1763.
- (190) Stebler, M.; Ludi, A.; Burgi, H.-B. *Inorg. Chem.* **1986**, *25*, 4743.
- (191) Howard, T.; Telsler, J.; DeRose, V. J. *Inorg. Chem.* **2000**, *39*, 3379.
- (192) Delfs, C. D.; Stranger, R. *Inorg. Chem.* **2001**, *40*, 3061.
- (193) Pal, S.; Chan, M. K.; Armstrong, W. H. *J. Am. Chem. Soc.* **1992**, *114*, 6398.
- (194) Corbella, M.; Costa, R.; Ribas, J.; Fries, P. H.; Latour, J.-M.; Ohrstrom, L.; Solans, X.; Rodriguez, V. *Inorg. Chem.* **1996**, *35*, 1857.
- (195) Vincent, J. B.; Tsai, H.-L.; Blackman, A. G.; Wang, S.; Boyd, P. D. W.; Folting, K.; Huffman, J. C.; Lobkovsky, E. B.; Hendrickson, D. N.; Christou, G. *J. Am. Chem. Soc.* **1993**, *115*, 12353.
- (196) Bhaduri, S.; Tasiopoulos, A.; Bolcar, M.; Abboud, K. A.; Streib, W. E.; Christou, G. *Inorg. Chem.* **2003**, *42*, 1483.
- (197) Dave, B. C.; Czernusiewicz, R. S.; Bond, M. R.; Carrano, C. J. *Inorg. Chem.* **1993**, *32*, 3593.
- (198) Wiegardt, K.; Bossek, U.; Bonvoisin, J.; Beauvillain, P.; Girerd, J.-J.; Nuber, B.; Weiss, J.; Heinze, J. *Angew. Chem., Int. Ed. Engl.* **1986**, *25*, 1030.
- (199) Goodson, P. A.; Oki, A. R.; Glerup, J.; Hodgson, D. J. *J. Am. Chem. Soc.* **1990**, *112*, 6248.
- (200) Owen, J. Electron Paramagnetic Resonance. *Sci. Prog.* **1965**, *53*, (212), 645.
- (201) Harris, E. A. *J. Phys. C5* **1972**.
- (202) Coles, B. A.; Orton, J. W.; Owen, J. *Phys. Rev. Lett.* **1960**, *4*, 116.
- (203) Harris, E. A.; Owen, J. *Phys. Rev. Lett.* **1963**, *11*, 9.
- (204) Heming, M.; Lehmann, G.; Mosebach, H.; Siegel, E. *Solid State Commun.* **1982**, *44*, 543.
- (205) Flassbeck, C.; Weighardt, K.; Bill, E.; Butzlaff, C.; Trautwein, A. X.; Nuber, B.; Weiss, J. *Inorg. Chem.* **1992**, *31*, 21.
- (206) Mikuriya, M.; Adachi, F.; Iwasawa, H.; Handa, M.; Koikawa, M.; Okawa, H. *Inorg. Chim. Acta* **1991**, *179*, 305.
- (207) Schake, A. R.; Vincent, J. B.; Li, Q.; Boyd, P. D. W. *Inorg. Chem.* **1989**, *28*, 1915.
- (208) Hodgson, D. J.; Schwartz, B. J.; Sorrell, T. N. *Inorg. Chem.* **1989**, *28*, 2226.
- (209) Nishida, Y. *Chem. Lett.* **1987**, 2151.
- (210) Mabad, B.; Cassoux, P.; Tuchagues, J.-P.; Hendrickson, D. N. *Inorg. Chem.* **1986**, *25*, 1420.
- (211) Chang, H.-R.; Larsen, S. K.; Boyd, P. D. W.; Pierpont, C. G.; Hendrickson, D. N. *J. Am. Chem. Soc.* **1988**, *110*, 4565.
- (212) Lambert, S. L.; Hendrickson, D. N. *Inorg. Chem.* **1979**, *18*, 2683.
- (213) Downard, A. J.; McKee, V.; Tandon, S. *Inorg. Chim. Acta* **1990**, *173*, 181.
- (214) Antanaitis, B. C.; Brown, R. D., III; Chasteen, N. D.; Freedman, J. H.; Koenig, S. H.; Lilienthal, H. R.; Peisach, J.; Brewer, C. F. *Biochemistry* **1987**, *26*, 7932.
- (215) Menage, S. Ph.D. Dissertation, University of Paris-Sud, 1988.
- (216) Suzuki, M.; Mikuriya, M.; Murata, S.; Uehara, A.; Oshio, H.; Kida, S.; Saito, K. *Bull. Chem. Soc. Jpn* **1987**, *60*, 4305–4312.
- (217) Suzuki, M.; Murata, S.; Uehara, A.; Kida, S. *Chem. Lett.* **1987**, 281.
- (218) Gultneh, Y.; Farooq, A.; Liu, S.; Karlin, K. D.; Zubieta, J. *Inorg. Chem.* **1992**, *31*, 3607.
- (219) Mikuriya, M.; Kawasaki, Y.; Tokii, T.; Yanai, S.; Kawamori, A. *Inorg. Chim. Acta* **1989**, *156*, 21.
- (220) Caneschi, A.; Ferraro, F.; Gatteschi, D.; Melandria, M. C.; Rey, P.; Sessoli, R. *Angew. Chem., Int. Ed. Engl.* **1989**, *28*, 1365.
- (221) Bossek, U.; Wiegardt, K. *Inorg. Chim. Acta* **1989**, *165*, 123.
- (222) Que, L. J.; True, A. E. In *Progress in Inorganic Chemistry*; Lippard, S. J., Ed.; John Wiley & Sons: New York, 1990; Vol. 38.
- (223) Shank, M.; Barynin, V.; Dismukes, G. C. *Biochemistry* **1994**, *33*, 15433.
- (224) Allgood, G. S.; Perry, J. J. *J. Bacteriol.* **1986**, *168*, 563.
- (225) Rush, J. D.; Maskos, Z. *Inorg. Chem.* **1990**, *29*, 897.
- (226) Gelasco, A.; Pecoraro, V. L. *J. Am. Chem. Soc.* **1993**, *115*, 7928.
- (227) Horwitz, C. P.; Winslow, P. J.; Warden, J. T.; Lisek, C. A. *Inorg. Chem.* **1993**, *32*, 82.
- (228) Devereux, M.; McCann, M.; Casey, M. T.; Curran, M.; Ferguson, G.; Cardin, C.; Convery, M.; Quillet, V. *J. Chem. Soc., Dalton Trans.* **1995**, 771.
- (229) Gelasco, A.; Bensiek, S.; Pecoraro, V. L. *Inorg. Chem.* **1998**, *37*, 3301.
- (230) Armstrong, W. H.; et al. *Chem. Rev.*, submitted.

CR020627V